Inaugural - Dissertation

zur Erlangung der Doktorwürde der

Naturwissenschaftlich-Mathematischen Gesamtfakultät der

Ruprecht-Karls-Universität

Heidelberg

Development and Application of Quantum Chemical Methods for the Description of Molecules Under Mechanical Stress

vorgelegt von

Tim Stauch, Master of Science Chemie

aus Hanau

im Juli 2016

Gutachter:

Prof. Dr. Andreas Dreuw

PD Dr. Markus Pernpointner

Datum der mündlichen Prüfung: 25. Oktober 2016

Meiner Familie

„Der Grund und Boden, auf dem alle unsere Erkenntnisse und Wissenschaften ruhen, ist das Unerklärliche.“

Arthur Schopenhauer

Abstract

In mechanochemistry, forces are used to initiate chemical reactions. Although mechanochemical reactions have been conducted for millennia, a fundamental understanding of the relevant processes at the molecular level is still unavailable. Nevertheless, mechanochemistry is a lively field with an extraordinarily wide range of applications. Several approaches to apply forces to single molecules are commonly used today. One such approach is Single-Molecule Force Spectroscopy, where forces are transmitted from the cantilever of an Atomic Force Microscope to a macromolecule that is anchored to a glass surface. Moving the cantilever away from the surface exerts a pulling force on the molecule. In another class of mechanochemical experiments, ultrasound baths are used to rupture polymers mechanically or to transduce forces to a mechanically susceptible moiety. This capability of ultrasound baths is due to the collapse of cavitational bubbles in the liquids, which generates tensile forces. Furthermore, ball milling or grinding techniques can be used to crush solids, thereby applying forces to molecules. This procedure can be applied to make and break covalent bonds. Due to the lack of solvent, mechanochemical synthesis in a ball mill shows enormous potential as a sustainable and environment-friendly alternative to thermochemistry.

Despite this rich body and long history of experimental mechanochemical procedures, the underlying processes are not well understood at the molecular level. However, such a comprehension is desperately needed for the optimization of mechanochemical syntheses. The use of quantum chemical methods to describe mechanochemical processes, which is called *quantum mechanochemistry*, has proven to be of tremendous value in understanding mechanochemistry at its most fundamental level. Quantum chemical methods for the description of molecules under external forces afford predictions on force-induced changes in molecular geometry, reactivity and spectroscopic properties. Moreover, force analysis tools are available that can be used to identify the mechanically relevant degrees of freedom in a molecule or its force-bearing scaffold, thereby rationalizing mechanochemical reactivity.

During my PhD work, I have developed the JEDI (**J**udgement of **E**nergy **DI**stribution) analysis, which is a quantum chemical force analysis tool for the distribution of stress energy in a mechanically deformed molecule. Based on the harmonic approximation, an energy is calculated for each bond, bending and torsion in a molecule, thus allowing the

identification of the mechanically most strained regions in a molecule as well as the rationalization of mechanochemical processes. When a molecule is stretched, some internal modes store more energy than others. This leads to particularly large displacements of certain modes and to the preconditioning of selected bonds for rupture. Using the JEDI analysis I investigated the mechanochemical properties of polymer strands that are tangled into knots. In analogy to ropes, polymer strands are weakened by the ubiquitous overhand knot by approximately 50% and the point of bond rupture is located at the "entry" or "exit" of the knot. The JEDI analysis revealed the reason for this behavior. Upon stretching, most stress energy is stored in the torsions of the curved part of the knot and only a remarkably small amount of energy is used to stretch the bonds that ultimately break. This observation leads to the physical picture that the knot "chokes off" the chain in its immediate vicinity. In this process, the torsions act as work funnels that effectively localize the mechanical energy in the knot, thus preconditioning the covalent bonds at its entry and exit for bond rupture.

Besides the description of mechanical deformation in the ground state, the JEDI analysis can be used in the electronically excited state to quantify the energy gained by relaxation on the excited state potential energy surface (PES). For this, the harmonic approximation needs to be applicable on the excited state PES of interest. The physical process that is described by the excited state JEDI analysis is fundamentally different from the ground state variant. While in the ground state JEDI analysis the distribution of stress energy in a mechanically deformed molecule is analyzed, i.e. energy is expended for deformation, the excited state JEDI analysis quantifies the energy gained by the relaxation of each internal mode upon relaxation on the excited state PES, i.e. energy becomes available. With the excited state JEDI analysis, the mechanical efficiency of molecular photoswitches can be calculated. The spatial extension of a photoswitch that undergoes, e.g., *cis-trans*-photoisomerization, changes significantly during this process and forces are exerted on the environment. However, other internal modes of the photoswitch that do not contribute to the change in spatial extension change as a side effect of the relaxation on the excited state PES and a certain amount of energy is wasted on them. This effect limits the mechanical efficiency of photoswitches. Using the excited state JEDI analysis, I investigated the mechanical efficiency of the stiff-stilbene photoswitch, which had been used in an experiment in literature to accelerate the electrocyclic ring opening of cyclobutene by photoisomerization. I found that the mechanical efficiency of stiff-stilbene is much too low to account for the observed enhancement of the reaction. A much more reasonable physical explanation is that excess energy from absorption of a photon is dissipated as heat, which accelerates the rupture of the thermally labile bond in cyclobutene.

Furthermore, I used the JEDI analysis to investigate methods for the stabilization of strained hydrocarbons. Angle-strained cycloalkynes with a ring size smaller than eight carbon atoms are highly unstable under normal laboratory conditions, since the C≡C−C bond angles deviate substantially from linearity. Applying an external force in an appropriate direction partially linearizes these bond angles, thus leading to a stabilization of the cycloalkyne. Incorporating cycloheptyne into a macrocycle with stiff-stilbene, however, does not lead to a significant stabilization, since the mechanical efficiency of stiff-stilbene is low. Coupling cycloheptyne to another strained hydrocarbon, on the other hand, stabilizes the molecule tremendously. In particular, cycloheptyne was coupled to a strained cyclophane in a condensed macrocycle and I found that appropriate linking leads to a loss of strain in both hydrocarbons.

In addition to the development of the JEDI force analysis tool, I used existing quantum mechanochemical methods to develop molecular force probes. This class of molecules can be incorporated into larger systems like polymers and proteins and can be used to monitor forces acting in different regions of the macromolecules in real-time via force-induced changes in the spectroscopic signals of the force probes. I found that the reduction of point group symmetry upon mechanical deformation of the molecular force probe is a profitable feature, since electronically excited states that are degenerate in the unperturbed state can split up upon application of an external force. This effect can lead to the generation of new peaks in the spectrum, thus allowing the precise identification of the force probe signal. Additionally, I incorporated molecular force probes into the backbone of proteins without disturbing their natural fold. The formation of hydrogen bonds between the force probe and neighboring strands in a β-sheet preserves the secondary and tertiary structure of the protein and allows the identification of the pulling direction. The application of forces along and perpendicular to the backbone yields pronounced and clearly distinguishable signals of the force probes in the infrared and Raman spectra. Advantageously, the intensities of these signals are proportional to the external force at selected points of the spectrum, which makes the molecules "force rulers". The signals of the force probes can be intensified and shifted to a transparent window in the protein spectrum by isotopic substitution.

Zusammenfassung

Chemische Reaktionen werden traditionell durch Wärme, Licht oder Elektrizität initiiert. Die benötigte Aktivierungsenergie kann jedoch auch durch mechanische Kraft aufgewendet werden. Obwohl dieser Zweig der Chemie, der auch als Mechanochemie bezeichnet wird, auf eine jahrtausendealte Geschichte zurückblickt, sind die zugrunde liegenden Prozesse auf molekularer Ebene noch nicht hinreichend untersucht. Nichtsdestotrotz ist die Mechanochemie ein hochaktuelles Forschungsgebiet mit vielfältigen Anwendungsbereichen. Experimentell steht eine Vielzahl von Möglichkeiten zur Verfügung, um Kraft auf einzelne Moleküle auszuüben. So werden beispielsweise in der Einzelmolekül-Kraftspektroskopie mechanische Kräfte auf ein Molekül übertragen, welches zwischen der Messnadel eines Rasterkraftmikroskops und einer Glasscheibe eingespannt ist. Sobald sich die Messnadel senkrecht von der Glasscheibe entfernt, wird das eingespannte Molekül einer Zugkraft ausgesetzt. Eine weitere Möglichkeit, Kräfte auf einzelne Moleküle auszuüben, besteht in der Benutzung von Ultraschallbädern. Die periodische Entstehung und der Zusammenbruch mikroskopischer Bläschen in einem Ultraschallbad erzeugt Zugkräfte, welche stark genug sind, um vielfältige chemische Transformationen zu aktivieren und sogar Polymere zu zerreißen. In einer anderen Klasse von mechanochemischen Experimenten werden Feststoffe in Kugelmühlen oder mittels Mörser und Pistill zerkleinert, wobei Moleküle ebenfalls Kräften ausgesetzt werden. Dieser Zweig der Mechanochemie ist bereits sehr alt und kann heute unter anderem dazu verwendet werden, kovalente Bindungen zu knüpfen und zu brechen. Der weitgehende Verzicht auf Lösemittel in diesen Experimenten demonstriert das enorme Potenzial der Mechanochemie als nachhaltige und umweltfreundliche Alternative zur Thermochemie.

Trotz der großen Vielfalt an mechanochemischen Experimenten sind die zugrunde liegenden Prozesse auf molekularer Ebene noch weitgehend unerforscht. Solch ein grundlegendes Verständnis ist allerdings die Voraussetzung für die Optimierung mechanochemischer Synthesen. Die *Quanten-Mechanochemie*, in der quantenchemische Methoden zur Beschreibung mechanochemischer Prozesse verwendet werden, hat sich als äußerst hilfreich für das molekulare Verständnis von Mechanochemie erwiesen. Quantenchemische Methoden für die Beschreibung von Molekülen unter externen Kräften ermöglichen die Berechnung der deformierten Molekülgeometrie, der kraftinduzierten Änderungen der Reaktivität sowie der spektroskopischen Eigenschaften. Desweiteren erlauben computergestützte Kraftanalysen die Identifikation der mechanisch relevanten Freiheitsgrade eines

Moleküls, was sich als grundlegend für das Verständnis mechanochemischer Reaktivität erwiesen hat.

Im Rahmen meiner Doktorarbeit habe ich die JEDI (engl. **J**udgement of **E**nergy **DI**stribution, dt. Beurteilung der Energieverteilung) Analyse entwickelt, die ein quantenchemisches Analysewerkzeug für die Verteilung mechanischer Energie in deformierten Molekülen ist. Auf Basis der harmonischen Näherung wird für jede Bindung, jeden Bindungswinkel und jeden Diederwinkel in einem Molekül ein Energiewert berechnet. Diese Prozedur erlaubt die Identifikation der mechanisch am stärksten beanspruchten Regionen eines Moleküls und trägt zum Verständnis unterschiedlichster mechanochemischer Prozesse bei. Wenn ein Molekül gestreckt wird, speichern einige interne Moden mehr Energie als andere, was zu einer stärkeren Auslenkung und zur Vorkonditionierung für einen Bindungsbruch führen kann. Ich habe mit der JEDI Analyse beispielsweise die mechanochemischen Eigenschaften von verknoteten Polymersträngen untersucht. Wie im Fall makroskopischer Seile wird die mechanische Widerstandsfähigkeit von Polymersträngen durch einen einfachen Knoten um etwa 50% verringert und der Bruch erfolgt stets am „Eingang" oder „Ausgang" des Knotens. Durch die JEDI Analyse konnte ich zeigen, dass beim Strecken die meiste mechanische Energie in den Torsionen entlang des gekrümmten Teils des Knotens gespeichert wird, wohingegen lediglich ein geringer Teil der Energie diejenigen Bindungen streckt, die am Ende reißen. Dieser Effekt kann physikalisch so interpretiert werden, dass der Knoten die Polymerkette in seiner unmittelbaren Umgebung abschnürt. Die Torsionen fungieren dabei als „Energietrichter", welche die mechanische Energie in der Region des Knotens lokalisieren und die kovalenten Bindungen an dessen Eingang und Ausgang für den Bindungsbruch vorkonditionieren.

Neben der Beschreibung mechanischer Deformationen im Grundzustand kann die JEDI Analyse im elektronisch angeregten Zustand verwendet werden, um die Energie, die während der Relaxation auf der Potenzialhyperfläche des angeregten Zustands frei wird, zu quantifizieren. Wie im Grundzustand ist die Voraussetzung hierfür, dass die harmonische Näherung auf der relevanten Potenzialhyperfläche anwendbar ist. Der physikalische Prozess, der durch die JEDI Analyse im angeregten Zustand beschrieben wird, ist jedoch völlig unterschiedlich zur Grundzustandsvariante. Während im Grundzustand die Energieverteilung in einem mechanisch deformierten Molekül berechnet wird, d.h. Energie wird für die Deformation aufgewendet, wird in der JEDI Analyse im angeregten Zustand jene Energie quantifiziert, die durch die Relaxation auf der Potenzialhyperfläche frei wird, d.h. Energie wird der Umgebung zur Verfügung gestellt. Mithilfe der JEDI Analyse im angeregten Zustand kann die mechanische Effizienz molekularer Photoschalter berechnet werden. Durch die Änderung der räumlichen Ausdehnung eines Photoschalters

während einer photochemischen *cis-trans*-Isomerisierung werden Kräfte auf die Umgebung ausgeübt. Während der Relaxation auf der Potenzialhyperfläche ändern sich jedoch auch andere interne Koordinaten des Photoschalters, welche nicht direkt zur Änderung der räumlichen Ausdehnung beitragen. Dadurch wird ein gewisser Anteil an Energie verbraucht, sodass die mechanische Effizienz eines Photoschalters begrenzt ist. Mithilfe der JEDI Analyse im angeregten Zustand habe ich die mechanische Effizienz des Stiff-Stilben Photoschalters untersucht, welcher in einem literaturbekannten Experiment dazu verwendet wurde, die elektrozyklische Ringöffnung von Cyclobuten zu beschleunigen. Ich konnte zeigen, dass die mechanische Effizienz von Stiff-Stilben bei weitem zu gering ist, als dass der rein mechanische Einfluss des Photoschalters für die beobachtete Beschleunigung der Reaktion verantwortlich sein könnte. Eine physikalisch sinnvollere Erklärung besteht darin, dass sich überschüssige Energie aus der Absorption des Photons als Wärme im Makrozyklus verteilt, was zur Beschleunigung des Bruchs der thermisch labilen Bindung in Cyclobuten führt.

Desweiteren habe ich die JEDI Analyse für die Untersuchung von Methoden zur Stabilisierung gespannter Kohlenwasserstoffe verwendet. Cycloalkine, deren Ringe aus weniger als acht Kohlenstoffatomen bestehen, sind unter Normalbedingungen instabil, da die C≡C−C Bindungswinkel deutlich von der Linearität abweichen. Das Anlegen einer geeigneten externen Kraft führt zur partiellen Linearisierung dieser Bindungswinkel und zur Stabilisierung der Cycloalkine. Die Kopplung von Cycloheptin und Stiff-Stilben führt jedoch nur zu einer unwesentlichen Stabilisierung von Cycloheptin, da die mechanische Effizienz von Stiff-Stilben sehr gering ist. Die Kopplung von Cycloheptin zu anderen gespannten Kohlenwasserstoffen kann das Molekül jedoch deutlich stabilisieren. Im speziellen Fall der Anbindung von Cycloheptin an ein gespanntes Cyclophan fand ich heraus, dass eine geeignete Verknüpfung die Spannung beider Kohlenwasserstoffe deutlich verringert.

Weiterhin habe ich im Rahmen meiner Doktorarbeit existierende quantenchemische Methoden verwendet, um molekulare Kraftsonden zu entwickeln. Diese Klasse von Molekülen kann in größere Systeme wie Polymere und Proteine eingebaut werden und erlaubt die Beobachtung von Kräften in verschiedenen Regionen der Makromoleküle in Echtzeit durch kraftinduzierte Änderungen in den spektroskopischen Signalen der Kraftsonden. Ich konnte zeigen, dass die Verringerung der Punktgruppensymmetrie der Kraftsonde beim Anlegen einer externen Kraft eine nützliche Eigenschaft ist, da energetisch entartete elektronisch angeregte Zustände durch externe Kraft aufspalten können. Dieser Effekt kann zur Entstehung neuer Signale im Spektrum führen, was die eindeutige Zuordnung des Signals der Kraftsonde ermöglicht. Ferner habe ich Kraftsonden

in das Rückgrat von Proteinen eingebaut, ohne deren natürliche räumliche Struktur zu beeinflussen. Die Ausbildung von Wasserstoffbrückenbindungen zwischen der Kraftsonde und benachbarten Strängen eines β-Faltblatts erhält die Sekundär- und Tertiärstruktur des Proteins und ermöglicht die Identifikation der Richtung, in welche die externe Kraft wirkt. Das Anlegen einer Kraft entlang und senkrecht zum Proteinrückgrat führt zu starken und klar unterscheidbaren Signalen der Kraftsonden in den Infrarot- und Raman-Spektren. Die Intensitäten dieser Signale sind an ausgewählten Stellen des Spektrums proportional zur externen Kraft, sodass die Moleküle als „Kraftlineale" bezeichnet werden können. Die Signale der Kraftsonden können durch isotopische Substitution intensiviert und in ein transparentes Fenster im Proteinspektrum verschoben werden.

Contents

Abbreviations

AFM   Atomic Force Microscopy

AIMD   *Ab Initio* Molecular Dynamics

BBP   Bond Breaking Point

BOMD   Born-Oppenheimer Molecular Dynamics

COGEF   COnstrained Geometries Simulate an External Force

CPMD   Car-Parrinello Molecular Dynamics

DFT   Density Functional Theory

EBT   Extended Bell Theory

EFEI   External Force is Explicitly Included

EGO   Enforced Geometry Optimization

EVB   Empirical Valence Bond

FDA   Force Distribution Analysis

FMPES   Force-Modified Potential Energy Surface

JEDI   Judgement of Energy DIstribution

MD   Molecular Dynamics

NTO   Natural Transition Orbital

PES   Potential Energy Surface

QMDFF   Quantum Mechanically Derived Force Field

RBS   Rigid Bond Stretching

RS   Reactant State

SMFS   Single-Molecule Force Spectroscopy

TDDFT   Time-Dependent Density Functional Theory

TS   Transition State

Chapter 1

Introduction

„Ist es der Sinn, der alles wirkt und schafft? Es sollte stehn: Im Anfang war die Kraft!"

Johann Wolfgang von Goethe: Faust. Der Tragödie erster Teil

Please note that the content of this Chapter is based on an invited review by Prof. Dr. Andreas Dreuw and myself, which has been submitted for publication in *Chemical Reviews*.

1.1 Using forces to initiate chemical reactions

To initiate a chemical reaction, chemists typically resort to the use of heat, light or electricity to provide the required activation energy. Another, less well-known method of triggering a chemical reaction is the use of mechanical force. This research area is termed "mechanochemistry" and its origins date back to prehistoric times: The mortar and pestle have been used as early as the stone age.[1] The mechanical force that is applied to the material during the grinding process can not only be used for crushing solids, but also for the initiation of chemical processes. The first written documentation of a mechanochemical experiment dates back to 315 B.C., when Theophrastus of Eresus, a student of Aristotle and his successor as the head of the Lyceum, noted in his book

1

"On stones" that the grinding of cinnabar in a copper mortar with a copper pestle in the presence of vinegar yields mercury:[1,2]

$$HgS + Cu \rightarrow Hg + CuS$$
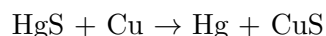
Although the mortar and pestle were standard instruments in the laboratories of the alchemists, few details on mechanochemical reactions were documented until the 19th century.[1] One can only assume that scientists predominantly thought of the mortar and pestle as a mere tool to grind solids and were not fully aware of the mechanochemical reactions they were initiating. It was not until 1919 that the term "mechanochemistry" found its way into textbooks.[3] In Ostwald's *Handbuch der Allgemeinen Chemie*,[4] mechanochemistry was established as the fourth of the chemical subclasses, in addition to thermochemistry, photochemistry and electrochemistry. More information on the history of mechanochemistry can be found in ref. 1.

Today, mechanochemistry is a lively field with an extraordinarily wide range of applications.[5] In its *Gold Book*, the IUPAC defines a mechanochemical reaction as a "[c]hemical reaction that is induced by the direct absorption of mechanical energy" and proceeds to give a few examples for the sources of this mechanical energy. Several approaches to apply forces to single molecules are commonly used today, which will be briefly introduced below. The main advantage of using mechanical force to initiate chemical reactions is its vectorial nature, which (at least in principle) allows to conduct experiments in a much more controlled way than by standard thermochemistry.

1.2   Experimental and quantum mechanochemistry

While mechanochemical experiments have been conducted for eons, the systematic description of mechanochemical processes with quantum chemical methods has lagged far behind for a long time. In fact, the field of "quantum mechanochemistry" is not even two decades old. In quantum mechanochemistry, quantum chemical methods are used for the description of mechanochemical processes at the molecular level, providing an in-depth understanding of the influence of forces on molecules and materials. Such a

comprehension is desperately needed, since mechanochemistry is still a largely alchemistic discipline, despite the long history of the field. However, we are currently witnessing an unprecedented gain in understanding of mechanochemical processes and quantum mechanochemistry has made the key contribution to this important development. The quantum chemical description of mechanically deformed molecules, which has been conducted systematically since the turn of the millennium, and, above all, the development of computational force analysis tools throughout the past five to ten years has paved the way for a more efficient use of mechanical force in academic and industrial laboratories. Computational methods for the calculation of geometries, energies, transition states, reaction rates etc. for molecules on the force-modified potential energy surface (FMPES) are introduced in Chapter 2. Force analysis tools, which allow the identification of the mechanically relevant degrees of freedom and the "force-bearing scaffold" of a molecule, are discussed in Chapter 2.6.

A fundamental problem in understanding and designing efficient mechanochemical experiments is the length gap. Typically, forces are transmitted from a macroscopic system to single molecules and methods have been developed that enable such a transmission in a controlled way. One efficient way of applying forces to a single molecule is by conducting Single-Molecule Force Spectroscopy (SMFS) experiments.[2,6–16] For this, the Atomic Force Microscope (AFM) is the most commonly used technique. In a typical AFM experiment, a macromolecule (e.g. a protein) is anchored between an AFM tip and a glass surface.[2] The rupture of covalent bonds or the unfolding of secondary structure domains during stretching of a protein can be monitored by the force-versus-extension curves generated in these experiments. This approach has been used extensively to measure the mechanical response of biological systems. In a groundbreaking contribution, Rief and co-workers measured the mechanochemical properties of titin, which is a crucial component of muscles and hence is an important research subject in mechanobiology.[17] Titin consists of repetitive immunoglobulin domains, each of which is folded into a seven-stranded β-barrel. Unfolding titin yields a sawtooth-like force-versus-extension curve with a periodicity between 25 and 28 nm and maximum forces between 150 and 300 pN. It was shown that the individual immunoglobulin domains unfold successively and that the weakest domain unfolds first, because rupture forces increase in each unfolding step. Despite this remarkable success, the interpretation of force-versus-extension curves is far

from straightforward and depends, e.g., on the stiffness of the cantilever.[18] Moreover, in most AFM studies the point of bond rupture cannot be identified uniquely. In many cases it is not clear whether a bond in the main chain of the macromolecule breaks or whether rupture occurs instead at one of the bonds connecting the macromolecule to the AFM tip or the glass surface. Here, quantum mechanochemistry can tremendously aid in the interpretation of the experiments by determining the geometry of the stretched molecule and the energetics during stretching as well as by identifying the mechanically relevant degrees of freedom in the macromolecule via force analyses.

An alternative approach to apply mechanical forces to single molecules is the use of ultrasound baths, an approach that is known as *sonochemistry*. While ultrasound baths have traditionally been applied for purposes like cleaning, efficient mixing and solid activation, a mechanical component has been identified, which can be used to trigger various chemical processes.[19,20] The propagation of an ultrasonic wave through a liquid generates small cavitational bubbles.[21–23] Upon collapse, the gas entrapped within these cavities is highly compressed, so that, besides tensile forces, pressures of several hundred atmospheres and temperatures of several thousand Kelvin are generated.[20,21] Chemical reactions like bond rupture occur at the bubble interface or inside the bubbles, given that reagents are sufficiently volatile.[24] Applications of ultrasound baths in chemical synthesis are diverse and include the switching of a reaction mechanism from an aromatic electrophilic to an aliphatic nucleophilic substitution[25] and the apparent circumvention of the Woodward-Hoffmann rules.[26] Furthermore, using ultrasound it was possible to trap a diradical transition state,[27] to induce Bergman cyclizations[28] and to conduct disulfide metathesis reactions.[29] Mechanisms and applications of sonochemistry have been reviewed several times.[20,30–33] The advantages of conducting mechanochemical syntheses in ultrasound baths include the simplicity, energy-efficiency and wide applicability of the approach as well as the possibility to conduct reactions at low ambient temperatures.[20,21] However, as described above, the processes in an ultrasound bath are complex and not purely mechanochemical. They involve several length and time scales in addition to elevated pressures and temperatures. Hence, a systematic optimization of sonochemical reactions based on a thorough understanding of the underlying processes is hardly possible until the present day. For the same reasons, the quantum chemical modeling of sonochemical reactions is a challenging task. Nevertheless, remarkable progress

has been made recently in understanding the transduction of mechanical forces through polymers, the activation of mechanophores (molecules that react to mechanical stress by significant structural changes) and chemical reactivity in an ultrasound bath.[34,35]

Ball milling and grinding techniques are another widely-used method to transmit mechanical energy to molecules. The impact of balls in a ball mill and the grinding of a pestle in a mortar generate forces that can be used both for crushing solids and for the initiation of chemical reactions. A solvent-free two-step mechanochemical synthesis of tetra-substituted porphyrins, for example, was presented recently.[36] This application involves grinding with a mortar and pestle as well as treatment in a ball mill and is an example of a mechanochemical carbon-carbon bond formation. As such, it nicely demonstrates the power of mechanochemical synthesis as a cheap, simple, energy-efficient, and typically solvent-free synthetic route and its potential as a sustainable and environment-friendly alternative to thermochemistry. Ball milling and grinding techniques as well as their applications for various purposes have been reviewed recently.[5,37–39] However, even today scientists in this field mostly resort to rules of thumb when it comes to designing and optimizing syntheses conducted in a ball mill or with mortar and pestle. This deficiency is due to a lack of understanding of the mechanochemical processes at the molecular level and the coupling to the macroscopic experimental setups. As will be shown in Chapters 2 and 2.6, quantum mechanochemical methods provide a molecular understanding of mechanochemistry and are potentially suited for optimizing ball milling and grinding experiments.

Mechanochemistry is not limited to observing the effect of external mechanical forces on molecules. A suitably chosen molecule can itself apply forces to its environment and this concept is exploited in molecular machines and nanomechanical devices. These systems are typically powered by light, which induces a structural change in a photoswitch.[40] Advantageously, light is an abundant resource and the reaction time of the photoswitches to the external stimulus usually lies within the picosecond range. The change in spatial extension of the photoswitch upon photoisomerization generates forces that can be used to perform mechanical work in the chemical environment. Based on this approach, Hugel and co-workers have designed a single-molecule opto-mechanical device,[40] in which azobenzene[41,42] is used as the molecular actuator. While related opto-mechanical devices

are based on unidirectional rotational motion,[43,44] the *cis-trans*-photoisomerization of azobenzene offers the advantages of a relatively high yield, reversibility and a significant change in spatial extension. In their study, Hugel and co-workers anchored a polymer of approximately 47 azobenzene units between an AFM tip and a glass surface.[40] Optical pumping at 365 nm was used to induce excited state photoisomerization of the azobenzene molecules, resulting in a difference in spatial extension of the polymer of approximately 6 nm. With this setup, the authors were able to exert a force of 200 pN to the AFM tip. Other groups exploited the mechanical work performed by azobenzene to induce structural changes in peptides,[45–53] DNA,[54–56] and synthetic foldamers.[57–59] Photoswitches from the spiropyran family were also shown to be applicable in this context.[60,61] Quantum mechanochemistry makes the key contribution to our understanding of the mechanical effects during photoswitching by allowing the calculation of the efficiency of the energy conversion and transmission process (cf. Chapters 3.3 and 4.2). This knowledge paves the way for an optimization of molecular machines by increasing the amount of mechanical work they can perform.

Of course, quantum mechanochemical methods can be used in their own right, without any coupling to experiments. While the conclusions drawn from an experiment are necessarily limited to the molecule under investigation, general concepts can be derived by quantum mechanochemical theory and calculations of molecules on the FMPES. This is a key strength of quantum mechanochemistry and the primary reason why a systematic optimization of many mechanochemical processes has become possible during the past two decades.

The rest of this thesis is structured as follows. The major theoretical concepts and computational methods to describe molecules under external forces are discussed in Chapter 2. The JEDI (**J**udgement of **E**nergy **DI**stribution) analysis, which is a quantum chemical force analysis tool developed in the course of my PhD work, is introduced in Chapter 3. Several applications of the JEDI analysis are discussed in Chapter 4. In Chapter 5, molecular force probes that were developed with the help of quantum mechanochemical methods are introduced. Chapter 6 concludes this thesis with a brief summary and an outlook.

Chapter 2

Theory and computational methods

The aim of this Chapter is to introduce the most important theoretical concepts of mechanochemistry and the computational methods that can be used to calculate the geometry, energy, spectroscopic properties, and reactivity of molecules under external forces. In Chapter 2.1, the influence of force on the potential energy surface is discussed. In Chapters 2.2 and 2.3, two widely used methods to calculate the geometry of mechanically deformed molecules, i.e. the COGEF and the EFEI method, as well as related approaches are described. Dynamic calculations of mechanically strained molecules (Chapter 2.4) as well as Bell theory (Chapter 2.5) are briefly introduced as well. Finally, several mechanochemical force analysis tools that have been developed within the past few years are discussed in Chapter 2.6. Please note that the content of this Chapter is based on an invited review by Prof. Dr. Andreas Dreuw and myself, which has been submitted for publication in *Chemical Reviews*.

2.1   The influence of force on the potential energy surface

If an external force acts on a molecule, the potential energy surface (PES) is affected in a way that either enhances or suppresses chemical reactivity. This effect has been
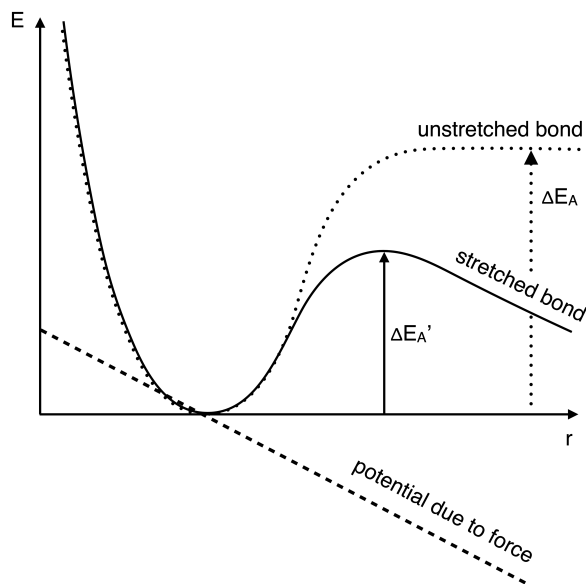
FIGURE 2.1: Schematic representation of a force-deformed potential energy curve of a covalent bond that is modeled by a Morse potential in its relaxed state (dotted line). In the absence of force, an activation energy ΔE_A is needed to rupture the bond. The application of a force is modeled by the addition of a falling linear potential (dashed line). In the resulting force-modified potential energy curve (solid line), the activation energy $\Delta E_A{}'$ is smaller than in the case of the unstretched bond. The scheme is adapted from ref. 62.

described by Kauzmann and Eyring already in 1940. The authors investigated the effect of a constant external pulling force, which can be modeled as a linear, falling potential, on a bond with a Morse-type potential.[62] If a bond does not undergo any vibrations, a dissociation energy of magnitude ΔE_A must be supplied to break it (dotted line in Figure 2.1). This activation energy can, however, be reduced by an external force, the extent of which of course depends on the magnitude of the external force (solid line in Figure 2.1). In the case of a single bond that is stretched by a constant stretching force F_0, the resulting deformed PES $V_F(r)$ can be calculated via

$$V_F(r) = V_{\text{ab initio}}(r) - F_0 \Delta r \ , \tag{2.1}$$

where a linear potential involving F_0 and the displacement Δr is subtracted from the total energy $V_{\text{ab initio}}(r)$. These considerations constitute the basis for several quantum mechanochemical methods for the calculation of mechanically deformed molecules (cf. Chapter 2.3).

An important consequence of this observation is that a stretched bond has a finite lifetime, with larger pulling forces typically leading to shorter lifetimes.[2,9,63] This was also shown by Freund, who developed a one-dimensional energy landscape model in which a large number of identical bonds are subjected to an imposed constraint.[64] While the probability of bond dissociation without external force is extremely small for a strong bond that is modeled by a steep potential, the survival probability decreases rapidly with external force. This demonstrates that mechanochemical bond rupture is a statistical process.

2.2   The COGEF method

The application of a mechanical force to a molecule results in a change of the nuclear configuration. Conversely, if a deformed molecular geometry is generated, the force needed to induce this change mechanically can be calculated as the nuclear gradient of the energy at this geometry. This realization led to the development of the computational COGEF (**CO**nstrained **G**eometries simulate **E**xternal **F**orce) method.[63] While the relation between changes in a structural parameter and mechanical force had been realized before,[65] the term *COGEF* was coined by Beyer in 2000. In a typical COGEF calculation, the distance r between two atoms that shall be subjected to an external force is fixed and an otherwise relaxed geometry optimization is carried out. For this calculation, standard Density Functional Theory (DFT) or wave function based methods can be used. Varying r within a range of values simulates an isometric pulling scenario and generates the COGEF potential.

A typical pulling scenario is shown in Figure 2.2, where the stretching of the propane molecule is simulated by incrementing the distance r between the terminal carbon atoms over a desired range. Increasing r leads to an elongation of the two carbon-carbon bonds of the molecule. Generally, the bond breaking point (BBP) can be determined by finding the inflection point of the COGEF potential, because this is the point of maximum force, provided the computational method used for the calculation of the COGEF potential still converges at these large bond elongations. Similarly, decreasing the distance between the terminal carbon atoms simulates a compressive force. It is important to note that
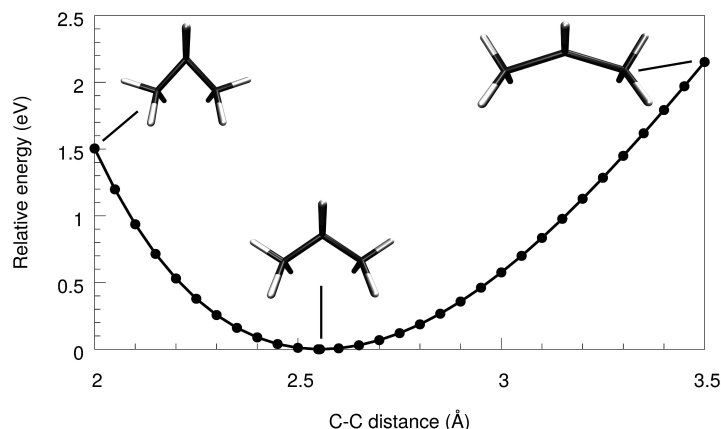
FIGURE 2.2: COGEF potential of the propane molecule, calculated at the B3LYP[66,67]/cc-pVDZ[68] level of theory. The distance between the terminal carbon atoms was varied between 2 and 3.5 Å. The equilibrium geometry, in which the distance between the terminal carbon atoms amounts to 2.554 Å, as well as the geometries at 2 and 3.5 Å are included.

several internal modes of propane besides the carbon-carbon bonds, i.e. various bond angles and dihedral angles, change if the distance between the terminal carbon atoms is varied, so that it is not appropriate to think of the COGEF method as a procedure for bond stretching alone. The distribution of stress energy among the different internal modes can be calculated with the JEDI analysis (cf. Chapter 2.6).

Typically, the rupture of strong and short bonds requires large forces (Table 2.1). For the dissociation of the Si–Si bond, for example, much lower forces (3.28 nN) are needed than for the rupture of the C–C bond (6.92 nN) in an analogous molecule.[63] Moreover, the rupture forces depend critically on the chemical environment: The O–H bond in H_2O ruptures at a higher force (9.77 nN) than in the HOCl molecule (9.18 nN). For the selection of a COGEF coordinate it should be kept in mind that the choice of a different coordinate r changes the rupture force in a nontrivial manner. Hence, great care should be exercised, so that the COGEF coordinate indeed models the mechanochemical process of interest.

The calculation of bond rupture forces via the COGEF method is an extraordinarily helpful tool to judge the mechanochemical strength of a molecule and to identify the point of bond rupture. COGEF calculations have been applied extensively since the introduction of the approach around the turn of the millennium and it is evident that the COGEF method has played a vital role in shaping the field of quantum

mechanochemistry. However, the COGEF method is a static quantum chemical approach that by its nature does not include thermal oscillations (cf. Chapter 2.4). Therefore, bond rupture forces calculated with the COGEF method are typically much too large compared with experiments. The main strength of the COGEF method is its simplicity. The constrained geometry optimizations and calculations of the nuclear gradient that are needed to generate the COGEF potential and to calculate the bond rupture force are implemented in every major quantum chemistry program package.

Obviously, COGEF rupture forces depend on the computational method that is used in the geometry optimizations. In the original paper it was found that the rupture forces can differ by more than 5% when a different basis set is chosen. However, benchmarking studies on the ability of computational methods to accurately predict bond rupture forces and distances are rare. In a study by Iozzi and co-workers, a set of diatomic and polyatomic molecules was mechanically deformed using the COGEF approach and a closely related method, which the authors call *Rigid Bond Stretching* (RBS).[70] Both the COGEF and the RBS method use constrained geometries to simulate mechanical deformation. However, in the RBS approach single point calculations are carried out instead of constrained geometry optimizations. Thus, the RBS method simulates infinitely fast deformation, whereas infinitely slow deformation is described by the COGEF approach. A well-known problem in computational chemistry is the inability of single-determinant methods to describe static correlation at large bond separations. Such systems have strong multi-reference character and single-determinant methods

Bond type	Molecule	F_{max} (nN)
H–H	H_2	8.31
H–F	HF	10.79
Cl–Cl	Cl_2	4.60
O=O	O_2	14.89
N≡N	N_2	26.27
C–C	$H_3CCH_2CH_3$	6.92
Si–Si	$H_3SiSiH_2SiH_3$	3.28
O–H	H_2O	9.77
O–H	HOCl	9.18

TABLE 2.1: Rupture forces F_{max} in nN of different bonds in various molecules calculated at the B3LYP[66,67]/D95(d,p)[69] level of theory via the static COGEF approach. The values were taken from ref. 63.

fail to capture this effect. Although Kohn-Sham DFT[71,72] in principle describes the dissociation correctly, the approximations to the exchange-correlation functionals make DFT functionals also error-prone in the description of long bond elongations.

Iozzi and co-workers found that all of the investigated molecules remain single-reference systems up to the bond breaking point. This remarkable conclusion was drawn by calculating the norm of the vector containing the singles amplitude T1 in a coupled-cluster calculation (T1 diagnostic), which is a measure of the multi-reference character of a system.[73] This result is of outstanding importance for the field of quantum mechanochemistry, as it generally allows the accurate prediction of bond rupture forces and geometries by computationally cheap single-reference methods.

The authors benchmarked several computational methods against the "gold standard" CCSD(T)[74–76]/aug-cc-pVQZ[77] level of theory. It was found that Hartree-Fock (HF) overestimates rupture elongation by approximately 20% and rupture force by approximately 30%, which is consistent with the well-known overbinding property of HF. For the same reason, Local Density Approximation (LDA) DFT functionals overestimate these values as well. CASSCF overcompensates this effect, resulting in an underestimation of rupture elongation and force. The NEVPT2[78,79] method yields remarkably reliable results that differ by only one or two percent from the CCSD(T) results. However, the cost of the NEVPT2 method for the calculation of larger systems makes the use of computationally less expensive methods desirable. In this regard it was found that General Gradient Approximation (GGA) DFT functionals deliver reliable results. In particular, PBE[80,81] and BLYP[66,82] overestimate rupture elongation and underestimate rupture force by approximately 5% each. Hence, these functionals are a cheap alternative to the costly CCSD(T) method. The very popular functionals B3LYP[66,67] and CAM-B3LYP[83], in turn, consistently overestimate rupture force and elongation in diatomic molecules. However, this property strongly depends on the system size: In polyatomic molecules, B3LYP was found to deliver the best results, while CAM-B3LYP performed poorly.

In another quantum mechanochemical benchmarking study by Kedziora and co-workers, a test set of small molecules was stretched using the COGEF approach.[84] The CCSD[74,75] method as well as a number of DFT functionals were tested, including the

double-hybrid functional B2PLYP.[85] It was found that static correlation is not significant until the bond breaking point, which agrees well with the earlier benchmarking study by Iozzi and co-workers. Of the single-reference methods, unrestricted GGA functionals were shown to perform best. In particular, the functionals N12[86], OLYP[66,87] and PBE[80,81] deliver especially reliable results. Methods with scaled exchange, however, often perform poorly. Interestingly, G4 dissociation energies[88] are much better reproduced by DFT using the small double-zeta basis set cc-pVDZ[68] than by using the larger triple-zeta basis set cc-pVTZ.

The aforementioned studies came to the conclusion that computationally inexpensive single-reference methods can be used in the description of mechanochemical processes, at least until the point of bond rupture. However, great care should be exercised in the choice of computational method in quantum mechanochemistry, because the summarized studies were necessarily limited to small sets of molecules. Moreover, the number of DFT functionals and wave function based methods tested in these studies was limited and the basis set dependence was only investigated coarsely. Therefore, further studies on larger test sets are needed, in which more computational methods and basis sets are tested. Until a comprehensive overview of the accuracy of computational methods for describing mechanochemical processes is available, the combination of method and basis set has to be chosen very carefully.

2.3 Approaches that consider the force explicitly

As an alternative to the simulation of external forces via constrained geometries, force can also be considered explicitly, thus allowing the simulation of isotensional stretching. A popular approach that considers the force explicitly is the EFEI (**E**xternal **F**orce is **E**xplicitly **I**ncluded) method, which was introduced by Ribas-Arino and co-workers in 2009[89]. The EFEI method enables the investigation of the molecular distortion on the FMPES directly instead of indirectly by imposing distance constraints. In principle, the EFEI method yields the exact distortion of the molecular structure at a given external force acting along a specific vector. This affords calculations of reactant and transition state geometries and activation energies of mechanochemical reactions.

In the EFEI method, a minimization of the expression

$$V_{\mathrm{EFEI}}(r, F_0) = V_{\mathrm{ab\ initio}}(r) - F_0 \cdot q(r) \tag{2.2}$$

with respect to the molecular geometry r is carried out. F_0 is the constant external force, $V_{\mathrm{ab\ initio}}(r)$ is the Born-Oppenheimer PES and $q(r)$ is a structural parameter. In practice, a geometry optimization of a system under the influence of an external force is carried out by adding a constant to the gradient along the vector connecting two atoms. The geometry optimization under external force converges when the external force and the internal restoring force of the molecule cancel out, provided that the external force is smaller than the rupture force. The advantage of applying the force along a vector connecting two atoms is that overall translations and rotations of the molecule are ruled out. However, it has to be kept in mind that the direction of the force vector generally changes in every step of the geometry optimization. Using the EFEI approach it was found that forces between 3.1 and 6.5 nN that are applied to the methyl groups of *cis*-1,2-dimethylbenzocyclobutene activate the mechanically induced disrotatory ring-opening, which is forbidden thermodynamically.[89] Above the threshold of 6.5 nN, the molecule dissociates. These findings demonstrate that different pathways can be activated by different forces.

A disadvantage of the EFEI approach in comparison to the COGEF method is that it is not automatically featured in every major quantum chemical program package. The implementation, however, is straightforward: A user-defined constant force is added to the nuclear gradient along the vector connecting two user-defined atoms. If this additional gradient points outward, mechanical pulling is simulated, while in the opposite case the molecule is compressed. In previous literature,[89–91] the EFEI method was interfaced with the Turbomole[92] program package or, alternatively, a modified version of Gaussian09[93] was used. The results reported in this thesis were acquired using my own implementation of the EFEI method in the Q-Chem[94] program package, which is publicly available in versions 4.3 and newer. The EFEI implementation in Q-Chem allows geometry optimizations and *ab initio* Molecular Dynamics (AIMD) simulations in the ground and excited state under the influence of a constant external force using

various DFT functionals and wave function based methods. In the case of an AIMD simulation, the force is applied constantly by modifying the gradient as described above in every AIMD time step.

In most cases, but not always,[95] it was found that the differences between the results obtained with the COGEF and EFEI methods are only subtle, leading to the notion that the two methods provide different points of view on the same mechanochemical process. In fact, it was shown that the EFEI potential is the Legendre transform of the COGEF potential at stationarity.[89] The close connection between the EFEI and COGEF methods was also found by Wolinski and Baker, who presented an approach that is analogous to the EFEI method.[96] Their approach was reported at the same time as the EFEI method and was called EGO/N (**E**nforced **G**eometry **O**ptimization, N = **N**uclei) in a subsequent publication.[97] The authors point out that geometry optimization techniques in which the force is considered explicitly only deliver stable structures until the bond rupture force is reached. After the BBP, the molecular fragments are pulled further apart and the geometry optimization fails to converge. The COGEF method, on the contrary, can also be used to calculate the molecular geometry after the bond is ruptured. Wolinski and Baker apply the EGO/N method to study conformational transitions of the pyranose ring and identify several previously unknown isomers of azobenzene ($C_{12}H_{10}N_2$), some of which are at least metastable. The capability of the EGO method to investigate structural isomerism is based on the formation of new bonds and was later used to generate and study different isomers of stilbene.[98]

Wolinski and Baker later proposed an extension of their method, which considers the influence of an external force not only on the nuclei (as in EFEI and EGO/N), but also on the electrons.[97] In particular, the effect of force on the 1s core electrons was included in the EGO approach, because these electrons are considered by the authors to be rigidly connected to the nucleus. This extended approach is called EGO/NE (NE = **N**uclei and some **E**lectrons). The authors argue that the EGO/N method, which describes only the influence of force on the nuclei, is a zeroth-order approach, as it does not explicitly include the interaction of an AFM tip with the attached molecule. Theories that are used to describe AFM experiments should therefore involve an explicit treatment of the electron density. Hence, it is reasonable to assume that this neglect of electronic

treatment is at least partially responsible for the systematic overestimation of AFM rupture forces by zeroth-order approaches like the EGO/N and the EFEI method. While thermal oscillations are certainly another key factor in this regard (cf. Chapter 2.4), Bader pointed out that electrons cannot be neglected in the interpretation of AFM experiments.[99]

An explicit treatment of the effect of force on electrons in the EGO/NE approach is achieved by introducing an external force in the Hamiltonian in analogy to an external electric field. In contrast to traditionally used external electric fields in the Hamiltonian, however, this field acts on the nuclei and electrons in the same and not in the opposite direction. In this treatment, the authors chose to only include those 1s electrons that, in the AO basis, are assigned to the atom that is subjected to the force, since these electrons are considered to be "rigidly attached" to the nucleus. Although this choice gives rise to a strong basis set dependence, the EGO/NE method was found to be remarkably robust. The EGO/NE method yields the same structural changes as the EGO/N method, but the forces needed to induce these changes are usually smaller by a factor of 3. The EGO/N method yields forces between 1667 and 3893 pN for pyranose ring transitions, for example. The EGO/NE method, by contrast, yields values between 499 and 1206 pN, which is remarkably close to the AFM experiment, where forces between 300 and 1500 pN are observed. In addition, it is possible to generate force-extension curves that reflect conformational transitions and that can be used for direct comparison with AFM experiments.

Wolinski and Baker point out that the number of electrons that are subjected to an external force in the EGO/NE method is limited to two, which is an obvious weakness of the method. They speculate that the factor of 3 by which the force is diminished in comparison to the EGO/N method could originate from the number of particles. If three times the particles are subjected to the same force, then only one third of the total force is needed to induce structural changes. Thus, it is still unclear whether the EGO/NE method is indeed a computationally cheap alternative to dynamic calculations (cf. Chapter 2.4), which achieve a much better agreement with experiments in comparison to static quantum mechanochemical calculations by including thermal effects.

At the same time as the EFEI method and the EGO approach, Ong and co-workers presented another analogous approach, which was termed FMPES (**F**orce-**M**odified **P**otential **E**nergy **S**urface).[100] The FMPES can be constructed via

$$V_{\text{FMPES}}(r) = V_{\text{ab initio}}(r) + \sum_{i}^{N_{\text{attach}}} F_0(||r_i^{\text{fix}} - r_i|| - ||r_i^{\text{fix}} - r_i^0||) \ . \qquad (2.3)$$

Here, the force-induced change in the Born-Oppenheimer PES $V_{\text{ab initio}}(r)$ is calculated by adding up contributions from each *attachment point* (AP), which is the point in the molecule where the external force is applied. As before, F_0 denotes the constant external force. r_i^0 and r_i are the initial and current positions of the AP, respectively, and r_i^{fix} is the invariant position of the *pulling point* (PP). A PP is a point in space towards which the force is directed. As can be easily seen, each of the N_{attach} AP-PP pairs i contributes a term of the type $F_0 \Delta r$ to the total energy. The consideration of APs and PPs constitutes a subtle difference to the the EFEI and the EGO methods. An extensive discussion of the particularities of each of these pulling setups can be found in ref. 101.

Knowledge of the FMPES was used to rationalize the pathways in a paradigmatic mechanochemical reaction, in which the Woodward-Hoffmann rules are apparently circumvented.[100] The Woodward-Hoffmann rules are based on orbital symmetry and state that electrocyclic reactions are thermally allowed if they proceed via conrotatory pathways, whereas photochemically induced reactions preferentially proceed in a disrotatory manner.[102–104] However, it could be shown that this set of rules can be circumvented in the case of the mechanically induced ring opening of cyclobutene. Ong and co-workers, for example, demonstrated that a tremendous lowering of the activation energy barrier of the thermally forbidden disrotatory pathway and its preference over the allowed conrotatory pathway can be achieved by mechanical force, provided that an appropriate pulling coordinate is chosen. Different computational studies on this and related reactions have been reviewed recently.[101]

The concept of the FMPES has aroused considerable interest in the past. Recently, a method to locate transition states (TS) on the FMPES was reported, which avoids the guess of the TS structure that is typically necessary in computational TS searches.[105]

Moreover, a further generalization of the FMPES concept was introduced by Subramanian and co-workers,[106] who point out that in most theoretical descriptions of the FMPES the external force is considered to be a constant. However, the inclusion of a spatially varying force is necessary for the description of the transmission of macroscopically uniform stress to the atomic level. Furthermore, in SMFS experiments the constant force approximation is only applicable in the limiting case of "soft" handles that apply force to the molecule. Hence, the authors introduce the G-FMPES ("Generalized" FMPES) formalism, which is valid for both constant and spatially varying external load. The G-FMPES is calculated via

$$
V_{\text{G-FMPES}}(r) = V_{\text{ab initio}}(r) + \int_{s=r}^{s=r_{\text{ref}}} F_{\text{ext}}(s)ds \ , \tag{2.4}
$$

where $F_{\text{ext}}(s)$ is a spatially varying external force. r and r_{ref} denote the desired and the reference configuration, respectively. The potential in Equation 2.4 reduces to the EFEI, EGO or FMPES potentials in the limit of a constant external force. The G-FMPES approach describes not only the shift of stationary points upon mechanical deformation, but also modifications in the curvature of the PES. The reason is that the Hessian also changes tremendously if the external force is spatially varying. However, the G-FMPES approach does not allow for the introduction of new minima in the PES upon application of force. More sophisticated and computationally expensive methods have to be used to describe these effects. In their study, the authors apply pseudo-hydrostatic pressure instead of considering mechanical deformation like pulling explicitly, and the relation between these two scenarios remains unclear. Nevertheless, using the G-FMPES approach the authors show that compressive stress increases the rotational barrier in ethane and a conformational barrier in a derivate of triazine. Based on these results, they speculate that compressive pressure intensifies steric effects and forces molecules into more compact conformations.

If a molecule is attached to a glass surface and an AFM cantilever exerts a stretching force of 2 nN on the molecule, then a force of the same magnitude, but opposite direction has to act on the other side of the molecule so that its overall translation and rotation in the mechanical equilibrium is zero. Similarly, if two atoms in a molecule are stretched

apart by forces of 2 nN applied to each of these atoms along the connecting vector between them, the molecule dose not move or rotate. Throughout this thesis, a scenario in which 2 nN are acting on each of the atoms is referred to as a total force of 2 nN pulling the atoms apart.

2.4   Thermal effects and dynamic calculations

As shown in Chapter 2.1, mechanical force deforms the PES in such a way that the activation energy for bond rupture is changed. In the simple case of a covalent bond, a stretching force reduces this energy barrier and the lifetime of the bond. In addition, consideration of a simple Morse potential shows that the temperature also has a significant impact on the rupture force of a bond. At room temperature, the available thermal energy amounts to approximately 0.6 kcal/mol[9], which, in the case of a bond that is sufficiently weakened by a mechanical force, can be enough to overcome the activation energy barrier for bond rupture. Physically, the thermal oscillations in a molecule periodically lead to stretching and compression of bonds. Bond rupture is most likely to occur at the moment of highest amplitude, even if the applied force is lower than the bond rupture force, which is usually calculated as the force needed to rupture a bond at 0K in static quantum chemical calculations.

The influence of temperature on mechanical bond rupture has been documented in literature. Lo and co-workers, for example, measured the biotin-avidin bond rupture forces at six different temperatures between 13 and 37°C in an AFM setup.[107] More than 200 individual measurements were carried out at each temperature and it was found that the unbinding force decreases by a factor of 5 within this temperature range. Although this experiment probed only one type of non-covalent interaction, similar behaviors are expected in other systems and the results can be assumed to be general in a qualitative sense. Measurements of the unbinding forces of complementary DNA strands at different temperatures between 6 and 36°C, for example, confirm that unbinding forces decrease with increasing temperature.[108]

For an accurate computational description of thermal effects and their influence on mechanical bond rupture, static quantum chemical calculations are of limited usefulness. Thermal oscillations can, however, be included explicitly in dynamic calculations at finite temperatures, e.g. by conducting *ab initio* Molecular Dynamics (AIMD) simulations. In contrast to classical Molecular Dynamics (MD) simulations, AIMD methods do not rely on any pre-defined force field. Instead, the potential is calculated "on the fly" using quantum chemical methods. The propagation of the system in time, however, is achieved using standard algorithms from MD. A clear advantage of AIMD over MD methods is that no parameterization of a force field is necessary, so that AIMD simulations are not limited to systems that closely resemble the one for which the force field was parameterized. Moreover, the quantum chemical background of AIMD calculations allows the simulation of bond rupture and bond formation events occurring during (mechanochemical) reactions. Therefore, it is possible to investigate the relation between force and bond lifetime as well as the influence of thermal oscillations on mechanochemical properties. However, these useful features of AIMD simulations do not come without a cost. The need to perform quantum chemical calculations in every time step generally limits the utility of the approach to small or medium-sized systems and moderate time scales. Hence, simulations of large proteins over a prolonged time via AIMD methods are computationally not feasible.

AIMD simulations have found a plethora of applications in the context of mechanochemistry. The rupture process of ethylthiolate (CH_3CH_2S) on a gold surface, for example, was simulated at 300 K with the Car-Parrinello MD (CPMD) method,[109] which is a variant of AIMD.[110] Krüger and co-workers prepared a relaxed initial configuration and subsequently constrained the terminal carbon atom of ethylthiolate to different values in steps of 0.2 Å, resulting in an isometric approach of pulling the molecule away from the surface perpendicularly. The forces were converged in every step, thus imitating a very slow process. It was found that perpendicular pulling results in the successive formation of a monoatomic, diatomic and triatomic gold bridge. Interestingly, the S−Au bond remains intact and a gold triangle is formed after rupture. The authors attributed this effect to the stabilization of the S−Au bond by the formation of the gold wire. The calculated rupture force amounts to 1.2 nN, suggesting again that lower forces are needed for bond rupture in dynamic calculations than in static quantum chemical calculations. This is a

useful property that makes CPMD simulations valuable complements to experiments in related systems.[111,112] A detailed derivation of the CPMD method and a comparison to other flavors of AIMD can be found in ref. 113. The interested reader is referred to refs. 114 and 115 for a comprehensive overview of mechanochemical applications of AIMD simulations.

2.5   Bell theory

The calculations of mechanochemical pathways, rupture forces and deformed geometries of molecules under an external force via the COGEF, the EFEI, the FMPES or the EGO approach usually necessitate a considerable number of geometry optimizations. Depending on the system size and the computational method that is used in these calculations, the full characterization of the FMPES can become computationally expensive. Hence, a number of approximations have been introduced that drastically reduce the computational cost by conducting all necessary calculations at zero force. This family of methods originates from a work by Bell that describes the adhesion of cells.[116] Bell Theory has primarily found use in the calculation of the change in activation energy of a reaction upon application of an external force. It is assumed that the activation energy barrier depends linearly on the applied force. To a first order approximation, the rate of a chemical reaction with an applied external force can be calculated as

$$k(F_0, T) = A \cdot \exp\left(\frac{\Delta G^{\ddagger}(0) - F_0\Delta q}{RT}\right) . \tag{2.5}$$

In this ansatz, the reaction rate depends exponentially on the constant external force F_0, demonstrating that chemical reactions are extremely sensitive to force. $\Delta G^{\ddagger}(0)$ is the activation energy of the reaction at zero force, A is the Arrhenius pre-exponential factor and Δq is a structural parameter that has to be chosen properly. Hence, the activation energy barrier of a mechanochemical reaction is described by Bell theory via

$$\Delta G^{\ddagger}(F_0) = \Delta G^{\ddagger}(0) - F_0\Delta q , \tag{2.6}$$

demonstrating that the change in activation energy in Bell theory is proportional to the external force.

Tian and co-workers evaluated the accuracies of different models for the calculation of the change in free energy of activation of the ring opening reactions of cyclobutene and dibromocyclopropane mechanophores. [117] It was found that, while Bell theory yields qualitatively correct results, $\Delta G^\ddagger$ is consistently underestimated in those cases where the transition state is distorted towards the reactant geometry. This is a general limitation of the simple Bell model: The term Δq in Equations 2.5 and 2.6 is itself force-dependent, which is not captured by Bell theory.

Another important property of Bell theory was revealed in a study by Kucharski and co-workers, who calculated changes in the activation enthalpy in S_N2 reactions via Equation 2.6. [118] In this study, the non-bonded separation $H_3C\cdots O_{MS}$ in EtOMs (Ms = SO_2Me) was taken as q, because this non-bonded coordinate captures both the elongation of a bond and the displacement of bond angles, which constitute crucial structural parameters for the investigated reaction. Although it is a covalent bond that breaks in these reactions, the authors argued that this single bond coordinate fails to capture the essential part of the structural changes occurring in the reaction, so that a non-bonded separation was chosen. This view is confirmed by the observation that the elongation of the scissile bond considerably overestimates the force-induced acceleration of the reaction, whereas the non-bonded separation yields accurate results. These findings demonstrate that the predictions afforded by Bell theory strongly depend on the choice of the coordinate q. While the need to properly choose q has been acknowledged in literature, [119,120] it is often assumed that the same coordinate q can be used for all reactions of the same mechanism. As pointed out before, [121] a clear theoretical or empirical justification to use a simple internal coordinate of the reactant for q is simply non-existent. As a result, it may prove difficult to find a coordinate that accurately predicts accelerations of a given reaction by mechanical force.

While the problem of choosing an appropriate structural parameter is still unsolved, the missing force-dependence of the Δq term has been addressed in the so-called *Extended Bell Theory* (EBT). [122] Basic Bell Theory predicts a linear, first-order dependence of the activation energy on the external force, which was extended to a second-order treatment

in EBT by Konda and co-workers. In EBT, the change in activation energy upon application of an external force can be calculated as

$$\Delta\Delta G^{\ddagger} = -F_0 \Delta q - \Delta\chi F_0^2/2 \; , \qquad (2.7)$$

which originates from a second-order perturbative treatment of the FMPES. In EBT, the additional term that is quadratic in the force includes the mechanical compliance $\Delta\chi$ of the molecule. $\Delta\chi$ can be considered an inverse force constant and is a measure how readily a molecule responds to mechanical stress by deformation. The truncation of the Taylor series at second instead of first order, however, necessitates the calculation of the Hessian, which is used in the calculation of the mechanical compliance. Nevertheless, EBT is significantly less expensive than the full characterization of the FMPES by the COGEF or EFEI method. Kucharski and co-workers compared EBT with basic Bell theory and found that the second-order correction leads to a drastic improvement in the description of force-induced changes in structure and activation energy in comparison to the first-order treatment. Simple Bell theory was only found to deliver reliable results in the treatment of stiff molecules, since in these cases Δq is small. Moreover, it was found that stretching forces between two atoms accelerate a mechanochemical reaction if the distance between these two atoms increases in the TS. This result demonstrates the power of calculations on zero-force structures in describing mechanochemical reactions.

A basic assumption of EBT is that the PES can be approximated as quadratic in the vicinity of the reactant and transition state (TS), which can hardly be guaranteed in general. Additionally, the quadratic approximation indicates that EBT is also limited to sufficiently low forces, because the activation energy barrier disappears at the bond breaking point and the harmonic approximation breaks down. Analogous observations were made by Bailey and Mosey,[123] who found a semi-quantitative agreement of the EBT reaction barriers with quantum chemical reference data and a significant improvement over basic Bell theory. The authors point out that sufficiently large forces can alter the reaction pathway, which is not described by the second-order treatment in EBT. A third-order expansion, however, is impractical form a computational point of view,

since the third order tensor of the derivatives of the energy with respect to nuclear displacement would need to be calculated.

Bailey and Mosey point out a method to calculate the molecular distortion upon application of an external force by using the EBT approximation instead of the COGEF or EFEI method. The force can be calculated via

$$\vec{F} = \mathbf{H}_{\text{int}} \overrightarrow{\Delta q} \,, \tag{2.8}$$

where $\mathbf{H}_{\text{int}}$ is the Hessian in internal coordinates. Hence, the molecular distortion can be calculated via

$$\overrightarrow{\Delta q} = \mathbf{C} \vec{F} \,, \tag{2.9}$$

where $\mathbf{C} = \mathbf{H}_{\text{int}}^{-1}$ is the compliance matrix.[124,125] Within the quadratic approximation, this procedure yields the molecular distortion and constitutes a computationally less expensive alternative to COGEF or EFEI calculations at sufficiently low forces.

The change in character of the critical points of the FMPES has been addressed explicitly by Konda and co-workers.[126] Their method acknowledges the possibility of switching to an alternative reaction mechanism or to a barrierless process upon application of large forces. The evolution of any given critical point of the PES, i.e. the reactant state (RS) and TS, can be tracked automatically. Moreover, mechanical instabilities, which occur when a critical point ceases to exist at a certain force, are tracked as well. The inclusion of these effects is a significant improvement over Bell theory or EBT, where such situations cannot be described. The method is based on catastrophe theory[127] and allows predictions by considering different types of catastrophes. In the *fold-catastrophe* scenario, in which only one parameter (the force) is varied and the FMPES does not feature any special symmetries, two critical points may coalesce with one another. In the *cusp-catastrophe* scenario, which can emerge if the FMPES has certain symmetries, two equivalent critical points may merge with a third one. As in the case of EBT, a constant force and a locally quadratic PES is assumed and the equation

$$r(F) = r(0) + \int_0^F \mathbf{H}^{-1}[r(F')] \overrightarrow{l} \, dF' \tag{2.10}$$

is propagated numerically to generate the displacement $r(F)$. In Equation 2.10, $r(0)$ is an RS or TS at zero force, F is the absolute value of the force and $\overrightarrow{l}$ is a vector specifying its direction. As before, $\mathbf{H}^{-1}$ is the inverse of the Hessian. The reaction barrier is then calculated as

$$\Delta G(F)^{\ddagger} = V[r_{\mathrm{TS}}(F)] - V[r_{\mathrm{RS}}(F)] - Fl[r_{\mathrm{TS}}(F) - r_{\mathrm{RS}}(F)] \ . \tag{2.11}$$

Like EBT, the advantage of the method is that it requires only a single TS search at zero force. As an example for a fold-catastrophe scenario, the authors present the electrocyclic ring-opening of *trans*-1,2-dimethylbenzocyclobutene. In this example, increasing the stretching force F between the carbon atoms of the methyl groups causes the energy barrier between RS and TS to disappear. This can be monitored conveniently by tracking the eigenvalues of the Hessians during this process. As the catastrophe point is approached, one negative eigenvalue of the TS Hessian approaches zero from below and one positive eigenvalue of the RS Hessian approaches zero from above. In general, this tracking of Hessian eigenvalues allows the identification of mechanical instabilities in various catastrophe scenarios, which cannot be described by EBT. In principle, the integration of Equation 2.10 can be conducted in large force steps far away from an instability. Adaptive integration schemes can ensure that the force steps become smaller in the vicinity of an instability, thus reducing the computational demand.

When a molecule is stretched, one intuitively expects that the energy pumped into the system by the mechanical force accelerates chemical transformations. In fact, most work using Bell and related theories is based on this assumption. A bond that is weakened by an external force is called a *slip bond*. However, during recent years much work has been devoted to identifying bonds that are either insensitive to mechanical load[128] or that apparently get stronger by an external force.[112,129–131] This type of bond is commonly referred to as a *catch bond* and can lead to a deceleration of chemical reactions by mechanical force. This effect can be triggered if competing reaction channels are

activated by different forces or when local deformations or large-scale conformational changes occur.[91,129] Additionally, it was found that an increase in steric strain due to an external force can lead to a decrease in the reaction rate. Steric strain can be quantified by the empirical Taft equation.[132,133] Kuprička and co-workers combined the Taft equation with classic Bell theory, resulting in the Bell-Taft approach.[91] In this model, the activation energy of a reaction under external force is calculated via

$$\Delta G^{\ddagger}_{\text{Bell-Taft}}(F_0) = \Delta G^{\ddagger}(0) - F_0 \Delta q - 2.303 RT \psi' \nu'_x \, , \qquad (2.12)$$

where the first two terms originate from basic Bell theory. The factor 2.303 stems from the conversion between the natural and the decadic logarithm, ψ' is a dimensionless empirical parameter and Taft's conformation-dependent parameter ν'_x is calculated via

$$\nu'_x(\alpha) = \nu'_{x0} + \eta \cos(\alpha) \, . \qquad (2.13)$$

Here, ν'_{x0} is another empirical parameter. The dimensionless parameter η describes the increase in steric strain due to a change in the torsion angle α and was obtained by a fitting procedure. The carbon atoms in a model system of polyethylene glycol (PEG) were stretched isotensionally and the changes in activation energies of several substitution reactions were calculated with Bell Theory, EBT and the Bell-Taft approach. In the case of ethyl propyl ether reacting with ethoxide, for example, an initial increase in the activation barrier for forces up to 500 pN was observed. This behavior can only be qualitatively reproduced by the Bell-Taft approach, whereas the Bell model and EBT predict a decrease in activation energies even at the lowest forces. The observed decrease in activation energy at larger forces is predicted by all three tested models. Hence, the Bell-Taft model is a useful complement to EBT that can be applied in those cases where force induces strain, thereby leading to a deceleration of the mechanochemical reaction at low forces.

The simplicity and modest computational demand of the Bell model and its extensions is reflected in the continuous use and steady advancement of the theory. Makarov,

for example, included quantum-chemical tunneling effects in Bell theory, resulting in the Quantum Bell formula.[134] While the calculation of reaction rates and structural deformations of mechanochemical reactions at zero force is extremely attractive from a computational point of view, it has to be kept in mind that still no unique way of choosing the structural parameter q that is used in Bell theory and its variants is available. Choosing a different coordinate q often changes the results dramatically. Hence, Bell theory remains a computationally inexpensive approximation to explicit calculations of the FMPES.

2.6 Force analysis tools

The computational methods introduced so far provide access to geometries, minimum energy pathways and reaction rates of molecules that are deformed by an external force. Therefore, they constitute the basis of quantum mechanochemistry and lend fundamental insights into mechanochemical processes at the molecular level. However, the question which part of a molecule is mechanochemically most susceptible represents a serious challenge for methods like COGEF and EFEI. Answering this question would allow the identification of the mechanochemically most relevant degrees of freedom in a molecule (or the "force-bearing scaffold"), thus affording accurate predictions about and rationalizations of the bond that is ruptured if a molecule is overstretched. Such insights would be highly valuable in the design of stress-responsive materials, molecular machines and photoswitches that can be used to trigger structural changes in their environment. Moreover, the identification of mechanochemically relevant degrees of freedom in a molecule can be used in experimental mechanochemistry to design and optimize reactions that yield a desired product as well as in mechanobiology to understand allosteric signaling pathways and structural changes in proteins. For this purpose, mechanochemical force analysis tools have been developed, which answer the following questions: Where is the stress energy stored in a mechanically deformed molecule? Which bonds, angles and torsions of the molecule are particularly stressed and why? Do these effects influence the properties of the molecule to such an extent that force-induced chemical transformations are possible? In this Chapter, several force analysis tools developed within the past few years are introduced. This will set the stage for an in-depth discussion of the JEDI

analysis, which is a quantum chemical force analysis tool that I have developed during my PhD work (cf. Chapter 3).

2.6.1   Force analysis tools using only one coordinate of interest

Many force analysis tools focus on the magnitude of force or the amount of stress energy in only one or very few coordinates of interest, i.e. the capability of the rest of the molecule to bear mechanical stress is ignored. Due to its simplicity, this ansatz has been applied extensively in the past. Koo and co-workers, for example, used this approach for determining the key factors for the activation of cyclobutane-based mechanophores embedded in a polymer.[135] Activation of these mechanophores by carbon-carbon bond rupture generates fluorescence, which can be used to identify damage precursors in polymers. For this investigation, a hybrid MD approach was used, which combined the classical Merck Molecular Force Field (MMFF)[136,137] and the Reactive Force Field (ReaxFF).[138] The carbon-carbon bond lengths of the cyclobutane moieties were chosen as the coordinates of interest. This choice is certainly reasonable in that mechanical stretching of one of these covalent bonds leads to rupture of the cyclobutane moiety at sufficiently high forces. Local force analysis revealed that the amplitude of the force indeed contributes to the deformation of the carbon-carbon bonds. However, for different cyclobutane moieties the results differ dramatically and fail to account for mechanophore activation under mechanical stress, since in some cases unphysically large forces are observed that unexpectedly do not trigger bond breaking. Hence, the authors conducted a local work analysis by calculating $E = \int \vec{F} \cdot d\vec{L}$, which yielded a much better description of mechanical deformation and mechanophore activation. This demonstrates the usefulness of both a one-dimensional model of mechanical activation (provided the coordinate of interest can easily be identified) and an analysis of stress energy as an alternative to local force analysis.

An alternative approach has been used by Huang and co-workers for describing the ring-opening of cyclobutene upon excited state *cis→trans*-isomerization of 1-(1-indanyliden)indan, commonly referred to as stiff-stilbene.[139] Due to the tremendous

change in spatial extension during isomerization, stiff-stilbene exerts forces on its environment. It is reasonable to assume that sufficiently large forces generated by stiff-stilbene play a crucial role in the ring opening of cyclobutene. Although thermal effects were found to play a more significant role in this process (Chapter 4.2), it is insightful to calculate the force stiff-stilbene can apply to cyclobutene. Huang and co-workers chose the distance between the C6 and the C6' atom in stiff-stilbene as the coordinate of interest, since these atoms are attached to the cyclobutene moiety via linkers and their separation increases tremendously during isomerization. The strain was estimated by fragmenting the macrocycle and calculating the restoring force via the energy gradient. Using this ansatz, a maximum force of 700 pN was found to be generated by stiff-stilbene.

Force analyses using only one coordinate of interest have found various applications, including the activation of dibromocyclopropane mechanophores by stiff-stilbene,[140] analysis of bond cleavage at the Si(100)-SiO$_2$ interface[141] and estimations of the strain in a hindered aryl-aryl bond.[142] As in the case of Bell theory and related models (Chapter 2.5), however, choosing the coordinate that is used in the local force or work analysis is not a trivial task.[143] As a result, scientists have to rely on their mechanochemical intuition to judge which coordinate is interesting for describing a given mechanochemical process. Clearly, different results are obtained for different coordinates, and it is impossible to judge how much force or stress energy is "wasted" on other coordinates that are not included in the analysis. In the case of the cyclobutane moiety discussed above,[135] the choice of using the distance between two carbon atoms in the cyclobutane ring is intuitive. However, for the interpretation of the results it has to be kept in mind that, e.g., bond angle deformations are not explicitly included in the model. Thus, bendings are not considered to be reservoirs of stress energy and it is not possible to calculate the total stress in the cyclobutane ring. While a restriction of the force analysis to the discussion of a single coordinate of interest makes the procedure straightforward, the capability of the rest of the molecule to bear force or stress energy is neglected. Moreover, the elongation of the scissile bond was often shown to be an inadequate coordinate for describing mechanical activation even in small systems.[144–146] As in Bell theory, general rules for choosing an appropriate coordinate are unavailable, so that great care has to be exercised in defining a coordinate and interpreting the results.

2.6.2   Internal forces

An analysis tool based on the quantification of internal forces was introduced by Avdoshenko and co-workers.[147] In this approach, the molecular distortion upon application of an external force is calculated to first order according to $\overrightarrow{\Delta q} = \mathbf{C}\overrightarrow{F}$ (Equation 2.9) and the discussion is limited to the weak force regime, where the distortion is small. The authors calculate the energy E stored in a mechanically strained molecule to lowest order via

$$E = \sum_{i<j} \int_{\mathrm{RS}}^{\mathrm{TS}} F_{ij} dR_{ij} \; , \qquad\qquad (2.14)$$

where F_{ij} is the force between atoms i and j and R_{ij} is the vector connecting these atoms. The total work in the stressed molecule is then generated by simply adding up the contributions of each two-body interaction. For this, a set of $3N - 6$ interatomic distances (either covalent bonds or non-bonded terms) is defined and the distribution of forces along these connecting lines is analyzed. The approach focuses on interatomic distances and bond angles or torsions are not included. If the mechanochemical process of interest is well localized, only a small number of terms contribute significantly to Equation 2.14. The set of interatomic distances is generated by first specifying those coordinates that are judged as particularly important for the mechanochemistry of the system and subsequently adding new coordinates in a random manner. In each step, a check for dependencies is carried out and redundant coordinates are removed. A consequence of this procedure is that the result depends critically on the coordinates that are included, since there is no unique way of specifying the coordinate system. Also, the force distribution pattern does not necessarily have the same symmetry as the molecule and apparently unphysical results can be obtained in that internal forces may propagate far into the unloaded part of the system. Since the results of the force analysis depend on the choice of included coordinates, the same bond may appear stretched or relaxed, depending on which coordinate system is used. Although the sensitivity of force distribution to changes in the coordinate system is less dramatic in larger molecules, the authors conclude that internal forces afford only limited insight into mechanochemical

processes. An in-depth discussion of the sensitivity of force analysis tools on the choice
of included coordinates can be found in Chapter 3.1.5.

2.6.3   Compliance constants

How strong is a covalent bond? This fundamental question in mechanochemistry is not
easy to answer, since the strength of a covalent bond is not a uniquely defined concept.
Nevertheless, the concept of bond strength is often used qualitatively to explain the
molecular deformation upon application of a force and the location of rupture in a large
molecule. Different approaches have traditionally been used to quantify covalent bond
strength. One commonly used method is the calculation of bond dissociation enthalpies,
but this quantity depends crucially on the singlet-triplet gaps of the fragments that
are formed after dissociation.[148] The bond dissociation enthalpy of a carbon-carbon
double bond, for example, varies over 400 kJ/mol in different substituted olefins.[149]
Although it is clear that the chemical environment influences the strength of a given
bond, a more stable approach for calculating this quantity is desirable. Another obvious
approach is the calculation of force constants, which are given as the eigenvalues of
the Hessian matrix. Hence, they are only rigorously defined for normal modes and an
exact calculation for a redundant set of internal coordinates is not possible. Typically,
normal modes are delocalized over large parts of the molecule. This property makes the
interpretation of force constants as quantifiers of covalent bond strength problematic,
although approaches for the localization of normal modes have been proposed.[150]

However, the elements of the Hessian are intuitively related to bond strength. In the
case of a covalent bond that is approximated by a harmonic potential, the only element
of the Hessian is the force constant, which can be calculated as the second derivative of
the energy with respect to bond length. A strong, stiff bond is characterized by a narrow
potential and a large force constant. However, the interpretation of the elements of the
Hessian of larger molecules in the context of mechanochemistry is problematic because
of the rigidity of these quantities.[148,151] This means that the rest of the molecule is
constrained to zero displacement upon deformation of a single coordinate and off-diagonal
couplings are excluded. In molecules, on the other hand, the displacement of an internal

coordinate typically causes the displacement of other coordinates as well, which leads to the generation of additional forces on the PES. Therefore, the rigidity of the elements of the Hessian makes interpretations of mechanochemical processes and bond strengths based on these quantities alone problematic. Brandhorst and Grunenberg argue that the interpretation of force constants is based on the assumption that the atoms are connected via harmonic Hookean springs.[148] Although this assumption is typically made in force fields, the authors reject this scenario, since the bonding situation is always considered too strong.

Instead, Brandhorst and Grunenberg advocate the use of compliance constants, which are the elements of the compliance matrix,[124,125] as estimators of bond strength. The compliance matrix is given as

$$\mathbf{C} = \mathbf{H}_q^{-1} \; , \tag{2.15}$$

where $\mathbf{H}_q^{-1}$ is the inverse Hessian matrix in non-redundant internal coordinates. A crucial advantage of interpreting the compliance constants as quantifiers of bond strength is that they are "relaxed" instead of "rigid", meaning that all other forces in the molecule are allowed to relax.[148] Moreover, the elements of $\mathbf{C}$ are independent of the choice of coordinate system.[152,153] Both properties constitute significant advantages over force constants. The coupling between the elements of $\mathbf{C}$ is usually weak, demonstrating that compliance constants are a local property and suggesting that they may be more transferable than force constants.[148]

For the interpretation of compliance constants in the context of mechanochemistry it is necessary to note that strong bonds have a small compliance constant.[148] Furthermore, it is possible to not only quantify covalent bond strength but also to judge the strength of long-range interactions. Brandhorst and Grunenberg have calculated compliance constants for fullerene C_{60},[154] which demonstrate that vicinal interactions are stronger and have smaller compliance constants than long-range interactions. Interestingly, a proportionality between compliance constants and distance was found in C_{60}. In another example, compliance constants were used to reassess the traditional notion that a short

bond is automatically a strong bond. In a bimetallic gallium complex, a remarkably short gallium-gallium bond with a very high compliance constant was found.[154,155] This indicates a fairly weak bond and leads to the physical interpretation that the gallium-gallium bond is compressed precisely because it is so weak. Compressing a weak bond to maximize other favorable interactions in the complex is energetically most favorable.

The above examples demonstrate that compliance constants can be used for quantifying the strength of chemical bonds, which is a crucial feature of force analyses. In addition to describing bond strength at stationary points of the PES, compliance constants are also available at nonstationary points.[156] This makes them potentially applicable in geometry optimizations, where coordinate interdependency and coupling is a well-known problem. As the coupling between compliance constants is weak, the perspective of using the elements of the inverse Hessian in geometry optimizations is promising. Furthermore, the initial guess needed for pseudo-Newton-Raphson techniques could be facilitated by compliance matrices because of their potential transferability. It would be very interesting to use compliance constants in the geometry optimizations involved in the COGEF and EFEI methods, since the calculation of force-induced molecular deformation would deliver the information needed for a force analysis as a byproduct.

2.6.4   Force analyses from Molecular Dynamics simulations

During recent years, remarkable progress has been made in the development of force analysis tools based on Molecular Dynamics (MD) simulations. MD simulations use classical force fields that typically neglect quantum effects, which enables the treatment of large systems like proteins or polymers. A prime example of force analysis tools from the realm of Molecular Dynamics is the Force Distribution Analysis (FDA). This approach has been used to investigate the mechanochemical properties of proteins and to identify the mechanisms of long-range communication.[157] In the latter case, many proteins fail to undergo visible conformational changes, leading to the notion that molecular geometry alone is insufficient to quantify mechanical stress in these systems. This effect is often compared to Newton's cradle, where the balls in the middle transmit energy despite not

being displaced themselves. Therefore, FDA aims at identifying the molecular framework for strain propagation in MD simulations by calculating changes in pairwise forces via

$$\Delta F_{ij} = F_{ij}^{\text{pert}} - F_{ij}^{\text{ref}} \; , \tag{2.16}$$

where F_{ij}^{pert} denotes the force between the atoms i and j in the mechanically strained state of the protein and F_{ij}^{ref} denotes the corresponding force in the relaxed state.[157] Conducting this calculation for every pair of atoms generates an N x N matrix, where N equals the number of atoms. This procedure is advantageous in that forces are calculated automatically during an MD simulation. The use of pairwise forces allows to conduct FDA in equilibrium, since, in contrast to forces on single atoms, pairwise forces do not converge to zero under equilibrium conditions. Furthermore, bonds can be considered explicitly by using pairwise forces, whereas angles and dihedrals have to be approximated as forces acting in an appropriate direction.[157] A limitation of the FDA approach is that it does not converge in cases with high conformational flexibility or when large-scale conformational changes occur.[158] Hence, the investigation of intrinsically disordered proteins or force analyses of simulations near the melting point are not viable with FDA.

FDA was used to determine the optimal length of β-sheets, which are highly resistant to mechanical force and therefore are the primary building blocks of stress-bearing proteins.[159,160] In most proteins, average β-sheet strands are four or five residues long, whereas the strands in spider silk are twice as long. FDA was used to quantify the gain in rupture force per residue and it was found that strain is deflected vertically to other strands via hydrogen bonds. Around the eighth residue, however, forces in the hydrogen bonds were found to decay to almost zero. Hence, the optimal length of β-sheets in mechanically resilient proteins is eight residues, since the incorporation of additional residues does not lead to a significant gain in mechanical resistance.

Further applications of FDA include the investigation of allosteric pathways,[161–166] protein unfolding[167] and the mechanochemical properties of proteins[157,168,169] and silk fiber[170,171]. In many cases, the resulting mechanical networks were found to be sparse and anisotropic and forces were deflected into the protein core.[157] Moreover, the

upper speed limit of mechanical signal transfer in a model protein was calculated to be 50 Å ps^{-1}.[172] Recently, time-resolved FDA (TRFDA) was introduced, which allows the monitoring of pairwise forces during conformational changes.[173–175]

Another method that can potentially be used in the context of mechanochemistry was presented by Grimme.[176] A black-box method for the generation of a molecule-specific force field entirely from quantum mechanical reference data was introduced, which is called QMDFF (Quantum Mechanically Derived Force Field). In this approach, quantum chemical calculations provide the equilibrium structure, Hessian, partial charges and covalent bond orders for the automatic generation of a force field that is not transferable between molecules. While the lack of transferability necessitates the renewed generation of the force field every time a new system is investigated, this procedure assures that a QMDFF is specifically tailored for the system of interest. This can be considered an advantage over conventional force fields, where transferability between similar but different systems is more or less assumed. Despite the increased computational demand, systems with up to a thousand atoms can be calculated on a desktop computer. The total energy E of the QMDFF can be written as

$$E = E_{\mathrm{e,QM}} + E_{\mathrm{intra}} + E_{\mathrm{NCI}} \; , \tag{2.17}$$

where $E_{\mathrm{e,QM}}$ is the quantum mechanical energy of the reference structure in equilibrium and E_{NCI} consists of the intra- and intermolecular noncovalent interactions. The bonded force field energy E_{intra} is calculated via

$$E_{\mathrm{intra}} = \sum_{\mathrm{bonds}} V_{\mathrm{str}}^{12} + \sum_{1,3} V_{\mathrm{str}}^{13} + \sum_{\mathrm{bend}} V_{\mathrm{bend}} + \sum_{\mathrm{torsion}} V_{\mathrm{tors}} + \sum_{\mathrm{inversion}} V_{\mathrm{inv}} \; . \tag{2.18}$$

The sums runs over all bonds, 1,3-interactions with two bonds in between, bending and torsion terms as well as inversion angles (out-of-plane terms). The V terms are the corresponding potential functions, which are described in detail in ref. 176. QMDFF performs remarkably well in the calculation of geometries, vibrational frequencies, conformational

energies, noncovalent and supramolecular interactions as well as atomization energies. QMDFF is fully anharmonic and allows dissociation, thus suggesting its use in the investigation of mechanical stress in deformed molecules. For example, the atomization energy and the dissociation coordinate of fullerene C_{60} were calculated. Although the simulation of a mechanochemical process is not the main intention in this example, the remarkable accuracy of QMDFF in modeling dissociation events emphasizes its potential usefulness in calculating mechanochemical properties of large molecules.

Recently, an extension of the QMDFF approach was presented,[177] in which the recombination of bonds is allowed by combining QMDFF with the Empirical Valence Bond (EVB) method by Warshel.[178] In this hybrid method, two or more force fields are on the diagonal of a matrix and suitable coupling elements are added as off-diagonal terms. The resulting method is called EVB-QMDFF and allows the simulation of both bond rupture and reformation processes. It is obvious that the EVB-QMDFF method is potentially very useful in describing mechanochemical reactions and analyzing forces and stress energies throughout the entire reaction coordinate.

Finally, it is worth noting that, in principle, the energy in each internal coordinate can be readily obtained in an MD simulation through its displacement. Bonds and bendings, for example, are defined in a force field as Hookean springs with parameterized force constants and, like in classical mechanics, the displacement of these springs yields the potential energies stored in these coordinates. This approach is remarkably simple and has been used in the calculation of the energy stored in selected coordinates.[179]

2.6.5　Other force analysis tools

Smalø and Uggerud developed an analysis to answer the question which bond in a linear polymer chain is ruptured by an external force.[180] This question is a key problem in mechanochemistry and is not straightforward to answer, since all bonds and angles are displaced if a polymer chain is stretched. Hence, the amount of energy that is pumped into the system considerably exceeds the energy needed to rupture a single, isolated bond. The authors use results from COGEF calculations to divide the total stretching energy into individual bond contributions, each of which has a component parallel and

one perpendicular to the bond. This allows the calculation of a term that stretches the bond and a term that bends the angle. The total energy can be divided into these contributions via

$$E = \int F dl = \sum_i \int F \cos^2 \alpha_{i,i+1} dr_{i,i+1,x} + \int F \sin^2 \alpha_{i,i+1} dr_{i,i+1,x} = \sum_{i,i+1} \int F dr_{i,i+1,x} \ .$$
(2.19)

Hence, the total energy is calculated by summing up all individual bond contributions, each of which consists of a cos-term for bond stretching and a sin-term for bending. The method was developed for linear polymers without rings that are stretched end-to-end. As a result, torsions are neglected and forces are only considered between neighboring atoms. Despite its conceptional simplicity, the approach is a valuable tool for describing the successive unfolding, bond and angle displacements and rupture of linear polymers. For example, it was found that it is not necessarily the thermodynamically weakest bond that is ruptured if a polymer is stretched. The dissociation energy, the harmonic force constant and the angle between the bond and the external force are important factors as well. While the observation that it is not straightforward to quantify the strength of a covalent bond agrees with previous literature,[148] other authors have identified the dissociation energy and harmonic force constants as being rather ambiguous quantifiers of bond strength (Chapter 2.6.3).

Smalø and Uggerud have identified three terms that play a role in the bond rupture process if only forces parallel to the bond are considered: (1) The energy stored in the bond, (2) the work done by neighboring bonds and (3) the work needed for the motion from the transition state to the fully separated fragments.[180] Somewhat surprisingly, it was found that the energy stored in a bond that is modeled by a Morse potential is a relatively insignificant term, whereas the energy needed to generate the fully separated fragments becomes the dominant term for large forces. Hence, the intuitive picture that it is sufficient to pump a certain amount of energy into a bond to rupture it mechanically is too simplistic.

The authors investigated a number of hydrocarbons that were used to model polymers and found that the thermodynamically stronger carbon-carbon bonds at the end of the chain are ruptured instead of the bonds in the middle of the chain. The reason for this effect is that the angles at the end of the chain are softer than in the middle, so that the terminal bonds are aligned much better with the external force. However, the authors point out that thermal fluctuations can lead to deviations from this behavior and to bond rupture at much lower forces. Since temperature effects are not included in static COGEF calculations, Born-Oppenheimer MD (BOMD) simulations were carried out in a subsequent study.[181] It was found that a gradually applied external force ruptures one or both terminal bonds, which is in agreement with the static COGEF calculations. Contrarily, a suddenly applied external force leads to bond rupture in the middle of the chain at relatively low forces. This phenomenon can be rationalized by the propagation of two shock waves that are applied to the ends of the chain. Clearly, propagation of the shock waves and constructive interference in the middle of the chain leads to bond rupture at relatively low forces. This physical picture is supported by the observation that bond rupture probability increases and decreases periodically if rupture does not occur within the first cycle. Moreover, an inverse proportionality between the time needed for chain rupture and its length was found for sufficiently large systems. The authors point out that the sudden force scenario is presumably most relevant for sonochemical experiments, where rupture also occurs predominantly in the center of the chain.

Other force analysis tools that shall only briefly be mentioned here include an atomistic finite element approach, in which each atom is described as an elastic joint, each chemical bond is represented by an elastic rod and van der Waals bonds are modeled as non-linear springs.[182] With this approach, relations between the atomistic displacement and the force can be derived. As a result, stress-strain curves can be generated for amorphous polymers. In another very recent work, Newton trajectories were used to find the optimal pulling geometry in a mechanically initiated reaction.[183] It was found that a desired reaction pathway can be selected from a set of competing reaction channels by choosing the appropriate pulling geometry.

Chapter 3

The JEDI analysis

The JEDI (**J**udgement of **E**nergy **DI**stribution) analysis, which I developed in the scope of my PhD work, is a quantum chemical analysis tool for the distribution of stress energy in a mechanically deformed molecule.[184–186] In this Chapter, the theoretical background of the JEDI analysis is established and selected model applications are discussed, which demonstrate the usefulness and the limitations of the JEDI analysis. Further applications of the JEDI analysis can be found in Chapter 4. Please note that parts of this Chapter have already been published by Prof. Dr. Andreas Dreuw and myself in *The Journal of Chemical Physics* **2014**, *140*, 134107, in *The Journal of Chemical Physics* **2015**, *143*, 074118 and in *The Journal of Physical Chemistry Letters* **2016**, *7*, 1298-1302.

3.1   The ground state JEDI analysis

For the purpose of analyzing the distribution of force in a molecule, an obvious ansatz is to calculate the restoring force F_i in the internal mode q_i of a molecule as the negative partial derivative of the potential V with respect to q_i via

$$F_i = -\frac{\partial V}{\partial q_i} \; .$$ (3.1)

However, if F_i is calculated for every primitive internal mode of a molecule, i.e. every bond length, bond angle, dihedral angle etc., this analysis is hardly insightful. The reason is that the outcome of this analysis depends on which coordinates are kept fixed in case more than $3N - 6$ internal coordinates (or $3N - 5$ in the case of linear molecules) are used to describe the molecular structure.[147] In this case, the internal modes are interdependent, meaning that a change in one coordinate potentially leads to a change in other coordinates. The problem that not all internal modes can be varied independently is a result of the redundancy of the coordinate system, since more degrees of freedom are specified than necessary for a complete description of molecular connectivity. In mechanochemistry, the displacement of one coordinate in a redundant coordinate system leads to additional forces in other coordinates. These effects cannot be captured by Equation 3.1, thus leading to physically ambiguous results.

In the following it is shown that the problem of interdependent coordinates can be circumvented by calculating the stress energy stored in each internal coordinate within the harmonic approximation instead of computing the force that is experienced by each mode. The calculation of stress energy has the additional advantage that energy is a scalar and not a vector, which greatly facilitates the interpretation and visualization of the results. Below, different coordinate systems are introduced and the question which of these systems is most suitable for calculating and analyzing the distribution of stress energy is answered.

3.1.1   Force analysis in normal modes

In the harmonic approximation, mechanical stress energy can be assigned to a set of $3N - 6$ ($3N - 5$ in the case of linear molecules) orthonormal modes $\vec{n_i}$. The harmonic stress energy in a molecule can be written as

$$\Delta E_{\text{harm}} = \frac{1}{2} k_{\text{eff}} \left(\overrightarrow{\Delta x} \right)^2 \ ,   \tag{3.2}$$

where $\overrightarrow{\Delta x}$ is the difference vector between the relaxed and the mechanically deformed geometries in Cartesian coordinates and k_{eff} is the effective force constant of the overall

system. Furthermore, assume that a basis M of $3N - 6$ ($3N - 5$ in the case of linear molecules; N = number of atoms) normal modes has been determined,

$$M = \{\overrightarrow{\Delta n_1}, \overrightarrow{\Delta n_2}, ..., \overrightarrow{\Delta n_{3N-6}}\} \; , \tag{3.3}$$

with the basis vectors $\overrightarrow{\Delta n_i}$ fulfilling the orthonormality relation

$$\left\langle \overrightarrow{\Delta n_i} | \overrightarrow{\Delta n_j} \right\rangle = \delta_{ij} \; . \tag{3.4}$$

The displacements in Cartesian coordinates can be written as a linear combination of normal modes:

$$\overrightarrow{\Delta x} = \sum_{i=1}^{3N-6} c_i \overrightarrow{\Delta n_i} \; , \tag{3.5}$$

the coefficients c_i of which can be determined using

$$c_i = \left\langle \overrightarrow{\Delta n_i} | \overrightarrow{\Delta x} \right\rangle \tag{3.6}$$

due to the orthonormality of the set of normal modes. Inserting Equation 3.5 into Equation 3.2 and using the orthonormality relation (Equation 3.4) yields

$$\Delta E_{\mathrm{harm}} = \frac{1}{2} k_{\mathrm{eff}} \left(\sum_{i=1}^{3N-6} c_i \overrightarrow{\Delta n_i} \right)^2 = \frac{1}{2} \sum_{i=1}^{3N-6} k_i c_i^2 \overrightarrow{\Delta n_i}^2 = \frac{1}{2} \sum_{i=1}^{3N-6} k_i c_i^2 \; , \tag{3.7}$$

where the effective force constant, k_{eff}, has been replaced by the force constants of the normal modes k_i. Equation 3.7 can be split up, yielding the energy stored in normal mode i:

$$\Delta E_i = \frac{1}{2} k_i c_i^2 \; . \tag{3.8}$$

Although conceptionally simple and easy to apply, normal modes are often delocalized over large parts of the molecule and thus generally not very insightful for a chemical interpretation of mechanochemistry in terms of individual bonds or angles. While a localization scheme for normal modes has been proposed, which makes use of a unitary transformation into a set of maximally localized modes,[150] another property of normal modes makes their use in mechanochemical force analysis problematic: In contrast to internal coordinates, normal modes constitute a rectilinear coordinate system,[187] since angle bendings, torsions etc. are approximated as linear displacements. In Chapter 3.1.5, the suitability of normal modes for mechanochemical force analyses is discussed and the results are compared to analysis tools in curvilinear coordinates.

In general, Cartesian coordinates are another rectilinear coordinate system. Since the degrees of freedom of translation and rotation are not projected out of the set of $3N$ Cartesian coordinates, the results of a force analysis in Cartesian coordinates depend on the orientation of the molecule in space and on the direction of the external force. Therefore, Cartesian coordinates are neglected in the present discussion, since they exhibit a redundancy that leads to an intrinsic ambiguity of the obtained results.

3.1.2   Force analysis in delocalized internal coordinates

Delocalized internal coordinates constitute a nonredundant set of internal coordinates.[188] In geometry optimizations, they are valuable because of the small coupling between different coordinates. Their generation makes use of Wilson's matrix $\mathbf{B} = dq/dx$, which describes the change of the primitive internal coordinates q due to the change of the Cartesian coordinates x.[187] Delocalized internal coordinates are generated by diagonalizing the matrix $\mathbf{G} = \mathbf{BB}^T$ and constitute the set of those eigenvectors of $\mathbf{G}$ with non-zero eigenvalues.[188] In general, they are expressed as linear combinations of potentially all primitive internal modes (typically bond lengths, bond angles and torsions). These primitive modes are determined by most quantum-chemical program packages

using a well-defined set of rules for the connectivity of the atoms as well as for the bond angles and dihedral angles.

To derive an energy expression for the assignment of mechanical stress energy to nonredundant coordinates, it is assumed that the potential energy of a system is a function of $M = 3N - 6$ nonredundant coordinates q

$$V = V(\vec{q}) \quad \text{with} \quad \vec{q} = (q_1, ..., q_M)^T \ . \tag{3.9}$$

The force at any point $\vec{Q}$ is then given by

$$\vec{F}(\vec{Q}) = -\nabla V(\vec{q})\big|_{\vec{q}=\vec{Q}} \ , \tag{3.10}$$

or equivalently

$$\vec{F_i}(\vec{Q}) = -\frac{\partial V(\vec{q})}{\partial q_i}\bigg|_{\vec{q}=\vec{Q}} \quad \forall \ i = 1, ..., M \ . \tag{3.11}$$

This force is physically meaningful, since $\vec{q}$ is a set of nonredundant coordinates and every coordinate can be treated separately. The energy gained or work required to move the system along some path C from a point $\vec{q_0}$ to a point $\vec{q_1}$ is given by

$$\Delta E = \int_C \vec{F}(\vec{q}) d\vec{q} \ . \tag{3.12}$$

For infinitesimal small paths the integral can be approximated by

$$\Delta E = \vec{F}(\vec{q_0})\vec{\Delta q} \quad \text{with} \quad \vec{\Delta q} = \vec{q_1} - \vec{q_0} \ . \tag{3.13}$$

However, more generally, the above integral has to be solved by finding a representation of the path C as a function of a single variable t (most easily on the interval $[0,1]$)

$$\vec{q} \rightarrow \vec{q}(t) \quad \text{and} \quad d\vec{q} \rightarrow \frac{\partial \vec{q}(t)}{\partial t} dt = \partial_t q dt. \tag{3.14}$$

Given such a representation the integral can be rewritten as

$$\Delta E = \int_0^1 \vec{F}(\vec{q}) \partial_t q \, dt = \sum_i^M \int_0^1 F_i(\vec{q}) \partial_t q_i \, dt = \sum_i^M \Delta E_i \ , \tag{3.15}$$

where ΔE_i can be interpreted as the energy gained along one specific direction q_i

$$\Delta E_i = \int_0^1 F_i(\vec{q}) \partial_t q_i \, dt = \int_0^1 -\frac{\partial V(\vec{z})}{\partial z_i}\bigg|_{\vec{z}=\vec{q}(t)} \partial_t q_i \, dt \ . \tag{3.16}$$

Assuming a linear path between $\vec{q_0}$ and $\vec{q_1}$, the substitution becomes

$$\vec{q}(t) = \vec{q_0} + \partial_t q t \quad \text{with} \quad \frac{\partial \vec{q}(t)}{\partial t} = \partial_t q \tag{3.17}$$

and the energy contribution is obtained as

$$\Delta E_i = \int_0^1 \vec{F_i}(\vec{q_0} + \partial_t q t) \partial_t q_i \, dt = \int_0^1 -\frac{\partial V(\vec{z})}{\partial z_i}\bigg|_{\vec{z}=\vec{q_0}+\partial_t q t} \partial_t q_i \, dt \ . \tag{3.18}$$

Now, assuming a Taylor expansion of $V(\vec{q})$ around $\vec{q_0}$

$$V(\vec{q}) = V(\vec{q_0}) + \nabla V(\vec{z})\big|_{\vec{z}=\vec{q_0}}(\vec{q} - \vec{q_0}) + \frac{1}{2} \sum_{i,j}^M \frac{\partial^2 V(\vec{z})}{\partial z_i \partial z_j}\bigg|_{\vec{z}=\vec{q_0}} (\vec{q_i} - \vec{q_{0,i}})(\vec{q_j} - \vec{q_{0,j}}) + \dots \tag{3.19}$$

is available, the derivative of V becomes

$$\frac{\partial V(\vec{q})}{\partial q_i} = \frac{\partial V(\vec{z})}{\partial z_i}\bigg|_{\vec{z}=\vec{q_0}} + \sum_j^M \frac{\partial^2 V(\vec{z})}{\partial z_i \partial z_j}\bigg|_{\vec{z}=\vec{q_0}} (\vec{q_j} - \vec{q_{0,j}}) \, , \qquad (3.20)$$

where only terms up to second order have been taken into account. This expression can now be used to compute the energy contribution ΔE_i. Therefore, $\frac{\partial V(\vec{q})}{\partial q_i}$ has to be evaluated at the point $\vec{z} = \vec{q_0} + \partial_t q t$

$$\frac{\partial V(\vec{q})}{\partial q_i}\bigg|_{\vec{q}=\vec{q_0}+\partial_t q t} = \frac{\partial V(\vec{z})}{\partial z_i}\bigg|_{\vec{z}=\vec{q_0}} + \sum_j^M \frac{\partial^2 V(\vec{z})}{\partial z_i \partial z_j}\bigg|_{\vec{z}=\vec{q_0}} \partial_t q_j t \, . \qquad (3.21)$$

Prior to force analysis, a geometry optimization is carried out and the molecule is in a minimum of the potential energy. Hence, the first term on the r.h.s. of Equation 3.21 vanishes. Inserted into the expression of the energy contribution (Equation 3.18) one obtains

$$\Delta E_i = \sum_j^M \int_0^1 -\frac{\partial^2 V(\vec{z})}{\partial z_i \partial z_j}\bigg|_{\vec{z}=\vec{q_0}} \partial_t q_i \partial_t q_j t \, dt = \frac{1}{2}\sum_j^M \frac{\partial^2 V(\vec{z})}{\partial z_i \partial z_j}\bigg|_{\vec{z}=\vec{q_0}} \Delta q_i \Delta q_j \, . \qquad (3.22)$$

The total molecular stress energy, calculated within the harmonic approximation, then reads

$$\Delta E_{\text{harm}} = \sum_i^M \Delta E_i = \frac{1}{2}\sum_{i,j}^M \frac{\partial^2 V(\vec{q})}{\partial q_i \partial q_j}\bigg|_{\vec{q}=\vec{q_0}} \Delta q_i \Delta q_j \, . \qquad (3.23)$$

Equation 3.22 can be used to assign the mechanical stress energy to every single mode in a nonredundant set of internal coordinates.[184,185] To evaluate the suitability of the harmonic approximation for the molecule under investigation, it is useful to compare ΔE_{harm} (Equation 3.23) to the "ab initio stress energy" $\Delta E_{\text{ab initio}}$ or the "Density Functional Theory stress energy" ΔE_{DFT}, which is here defined as the difference in total energies between the deformed and the relaxed molecule. Discrepancies between these quantities are due to anharmonic effects caused by the mechanical deformation

of bonds, angles and torsions, which are not described by force analysis tools based on the harmonic approximation. In this context it is important to note that, in reality, the force constants of the internal modes change as a result of the mechanical deformation, the effects of which are discussed in Chapter 3.1.5.

Natural internal coordinates[189] are another possible choice of nonredundant coordinates. However, the generation of this coordinate system makes use of a set of complicated rules partly based on local pseudosymmetry. Delocalized internal coordinates, in contrast, can be defined in a much more straightforward and well-defined way. Hence, natural internal coordinates are neglected in the present discussion.

For the subsequent discussion of the transformation of the energy expressions from a nonredundant into a redundant set of coordinates, it is convenient to reformulate Equations 3.22 and 3.23 in matrix notation and label them as expressions for delocalized internal coordinates (DICs):

$$
\begin{aligned}
\overrightarrow{\Delta E_i}^{\mathrm{DICs}} &= \frac{1}{2} \Delta q_i^{\mathrm{DICs}} \cdot \mathbf{H}^{\mathrm{DICs}} \cdot \overrightarrow{\Delta q}^{\mathrm{DICs}} \\
&= \frac{1}{2} \Delta q_i^{\mathrm{DICs}} \cdot ((\mathbf{B}^{\mathrm{DICs}})^T)^+ \cdot \mathbf{H}^{\mathrm{cart}} \cdot (\mathbf{B}^{\mathrm{DICs}})^+ \cdot \overrightarrow{\Delta q}^{\mathrm{DICs}}
\end{aligned}
\tag{3.24}
$$

$$
\Delta E_{\mathrm{harm}}^{\mathrm{DICs}} = \frac{1}{2} (\overrightarrow{\Delta q}^{\mathrm{DICs}})^T \cdot ((\mathbf{B}^{\mathrm{DICs}})^T)^+ \cdot \mathbf{H}^{\mathrm{cart}} \cdot (\mathbf{B}^{\mathrm{DICs}})^+ \cdot \overrightarrow{\Delta q}^{\mathrm{DICs}}
\tag{3.25}
$$

Note that an array $\overrightarrow{\Delta E_i}^{\mathrm{DICs}}$, in which the energy in every individual internal coordinate is stored, is generated. The transformations between the Hessian in Cartesian coordinates $\mathbf{H}^{\mathrm{cart}}$ and in delocalized internal coordinates $\mathbf{H}^{\mathrm{DICs}}$ makes use of the generalized inverse of the B-matrix for the delocalized internal coordinates, denoted by $(\mathbf{B}^{\mathrm{DICs}})^+$. The transformations between the Hessians are related to the protocol described by Bakken and Helgaker.[190]

3.1.3   Force analysis in redundant internal coordinates

The JEDI analysis is a variant of the force analysis described above that makes use of a redundant set of internal coordinates. It can be derived without any additional

approximations from the force analysis in delocalized internal coordinates. For this, the matrix $\mathbf{U}$ is used, which consists of the set of nonredundant eigenvectors of $\mathbf{G} = \mathbf{B}\mathbf{B}^T$. $\mathbf{U}$ is a semi-orthogonal matrix, meaning that $\mathbf{U}^T\mathbf{U} = \mathbf{1}$, but $\mathbf{U}\mathbf{U}^T \neq \mathbf{1}$.[191] As a result, all semi-unitary transformations involving a multiplication of $\mathbf{U}$ from the left conserve the Euclidean norm. Hence, it is possible to transform both the displacements in the nonredundant set of delocalized internal coordinates $\overrightarrow{\Delta q}^{\text{DICs}}$ and the corresponding B-matrix $\mathbf{B}^{\text{DICs}}$ into redundant internal coordinates (RICs) via

$$\overrightarrow{\Delta q}^{\text{RICs}} = \mathbf{U} \cdot \overrightarrow{\Delta q}^{\text{DICs}} \quad \text{and} \quad \mathbf{B}^{\text{RICs}} = \mathbf{U} \cdot \mathbf{B}^{\text{DICs}} . \tag{3.26}$$

Using these expressions, the energies can be transformed into the set of redundant internal coordinates:

$$\overrightarrow{\Delta E_i}^{\text{RICs}} = \frac{1}{2}(\mathbf{U} \cdot \overrightarrow{\Delta q}^{\text{DICs}})_i \cdot ((\mathbf{U} \cdot \mathbf{B}^{\text{DICs}})^T)^+ \cdot \mathbf{H}^{\text{cart}} \cdot (\mathbf{U} \cdot \mathbf{B}^{\text{DICs}})^+ \cdot (\mathbf{U} \cdot \overrightarrow{\Delta q}^{\text{DICs}})$$

$$= \frac{1}{2}\Delta q_i^{\text{RICs}} \cdot \mathbf{H}^{\text{RICs}} \cdot \overrightarrow{\Delta q}^{\text{RICs}} \tag{3.27}$$

$$\Delta E_{\text{harm}}^{\text{RICs}} = \frac{1}{2}(\mathbf{U} \cdot \overrightarrow{\Delta q}^{\text{DICs}})^T \cdot ((\mathbf{U} \cdot \mathbf{B}^{\text{DICs}})^T)^+ \cdot \mathbf{H}^{\text{cart}} \cdot (\mathbf{U} \cdot \mathbf{B}^{\text{DICs}})^+ \cdot (\mathbf{U} \cdot \overrightarrow{\Delta q}^{\text{DICs}})$$

$$= \Delta E_{\text{harm}}^{\text{DICs}} \tag{3.28}$$

Because of the semi-unitary nature of the transformation from delocalized to redundant internal coordinates, the harmonic stress energy remains the same and the stress energy can be uniquely assigned to all redundant internal coordinates (Equation 3.27). Hence, redundant internal coordinates can indeed be used in mechanochemical force analysis, since, as was shown here, the correct energy assignment is obtained within the harmonic approximation. The use of the physically ambiguous force in redundant internal co-ordinates (Equation 3.1) is avoided by deriving an energy expression via the force in nonredundant internal coordinates and subsequently transforming the energy into the redundant coordinate system. Profitably, the use of a coordinate system that arbitrarily omits potentially relevant coordinates and that inevitably leads to ambiguous results is avoided.

The above discussion of the semi-unitary transformation from delocalized into redundant internal coordinates demonstrates that Equations 3.22 and 3.23 are also applicable if redundant internal coordinates are used, which is the protocol for the JEDI analysis. For discussing the distribution of stress energy in a mechanically deformed molecule it is useful to differentiate between two different kinds of second derivative terms in Equation 3.22. First, for every internal mode, the equation contains a second derivative with respect to the same internal coordinate, which can be interpreted as the force constant of the appropriate internal mode if there were no redundancies in the set of internal coordinates and no coupling between the different modes. Second, the $M - 1$ mixed second derivatives need to be considered. These terms can be interpreted as the coupling terms between the modes by means of which redundancies are accounted for. If the coupling between two modes is strong, these terms can become relatively large. However, in some cases the coupling terms are negative, which can be interpreted as relaxation effects of one mode if another coordinate is displaced.

The JEDI analysis requires three pieces of input: (1) The geometry of the relaxed molecule, generated by standard quantum chemical geometry optimization techniques, (2) the Hessian at the relaxed geometry, calculated in a standard frequency calculation and (3) a mechanically deformed geometry, generated by the COGEF, EFEI or RBS (single point) calculation (cf. Chapter 2). From this information, it is possible to conduct the necessary matrix transformations and multiplications. Further details on the implementation and on the generation of color-coded molecular structures for a visualization of the results of the JEDI analysis can be found in Chapter 3.4.

3.1.4   Force analysis in Z-matrix coordinates

Similarly, transformations from delocalized internal coordinates to other coordinate systems can be found. For this purpose, the definition of the transformation matrix $\mathbf{U}$ is critical. Another possible coordinate system, which is routinely used in the definition of molecular connectivity, is the Z-matrix. The Z-matrix typically consists of $N - 1$ bonds, $N - 2$ bond angles and $N - 3$ dihedral angles, resulting in a nonredundant set of $3N - 6$ internal coordinates. However, the choice of coordinates to be included in the

Z-matrix is typically ambiguous. Hence, there is no unique transformation matrix that converts delocalized internal coordinates to Z-matrix coordinates. This also applies to many other nonredundant sets of internal modes, e.g. coordinate systems made up solely of interatomic distances, which have been used previously.[147] While a force analysis in Z-matrix coordinates is still possible, the consequences of the ambiguity in the definition of the Z-matrix for force analysis is discussed in detail below.

3.1.5   Model calculations

In the following, the distribution of stress energy in several mechanically deformed molecules using the analysis tools introduced above is analyzed. First, the rigid stretching of the oxygen-oxygen bond in hydrogen peroxide is discussed, since it is clear *a priori* that all stress energy is stored in this single bond and it is insightful to investigate the capabilities of the force analyses in different coordinate systems to reproduce this result. Subsequently, a carbon-carbon-hydrogen angle bending in ethene is considered, because the same motion can be described by another bond angle (hydrogen-carbon-hydrogen). Hence, there is a redundancy between these two bond angles and stress energy is distributed among the two of them. Comparing the performances of the different force analyses gives insight into the advantages and limitations of each coordinate system and into the question how redundancies are treated. Furthermore, the stretching of two carbon-carbon bonds on opposite sides of benzene is discussed. In this case, stress energy is split evenly between these two bonds. This example was chosen to highlight the ambiguity in the definition of Z-matrix coordinates, which typically do not include all bonds in cyclic molecules. The impact of this property on the validity of the results of the force analysis is further elaborated on in the discussion of stretched pentacene.

All calculations reported in this Chapter were carried out using the Q-Chem 4.3 program package.[94] Forces were applied to the molecules via the EFEI method (cf. Section 2.3). As an exception, the molecular geometries of hydrogen peroxide and ethene were deformed and single point calculations were carried out. Unless specified otherwise, the EFEI and single point calculations as well as the calculations of the Hessians were performed with Density Functional Theory (DFT) at the BLYP[66,82]/6-31G(d)[192]

level of theory. Usually, the results of force analyses in general and of the JEDI analysis in particular depend on the level of theory, which makes benchmarking necessary. Here, however, the focus lies on the comparison of different coordinate systems. Hence, one has to take care that the same level of theory is used for every set of coordinates. The primitive and delocalized internal coordinates were generated by Q-Chem. Details on the generation of the color-coded molecular structures are given in Chapter 3.4.

Hydrogen peroxide. At the BLYP/6-31G(d) level of theory, the equilibrium oxygen-oxygen distance of hydrogen peroxide amounts to 1.49 Å. This distance was stretched to 1.6 Å and a single point calculation was carried out. As a result, the distance between the two hydrogen atoms increases as well. Although this example involves an "unphysical" deformation in the sense that it cannot be simulated in experiments (e.g. AFM), it is an illustrative starting point in the present investigation, since the stretching of the oxygen-oxygen bond length is a purely rectilinear deformation. Moreover, all internal modes (three bond lengths, two bond angles and one dihedral angle) constitute a nonredundant set of $3N - 6 = 6$ coordinates and it is clear from the outset that 100% of the mechanochemical energy is stored in the stretched oxygen-oxygen bond.

In this case, all investigated coordinate systems (normal modes, delocalized internal, redundant internal and Z-matrix coordinates) yield the same harmonic stress energy of 3.38 kcal/mol, i.e. an overestimation of the DFT energy difference by 20.9%. As has been discussed above, this discrepancy is due to the anharmonicity of the bond stretching potential. The perfect agreement between all tested coordinate systems can be rationalized by the rectilinear nature of the oxygen-oxygen bond stretching, which causes the normal mode analysis to deliver the same results as the (potentially) curvilinear force analyses using internal coordinates. However, the decomposition of the harmonic stress energy into the individual modes differs between the coordinate systems. In the normal mode analysis, 85.3% of the stress energy is stored in a mode that can be described as an oxygen-oxygen stretching mode with the hydrogen atoms staying in place (O−O stretch, Figure 3.1), and 14.5% is stored in the linearized oxygen-oxygen-hydrogen angle bending mode (Normal mode B). Although this linear combination of modes is inconvenient for chemical interpretation, it is needed to describe the structural deformation brought about

O-O stretch   Symmetric O-O-H bend
85.3%   14.5%
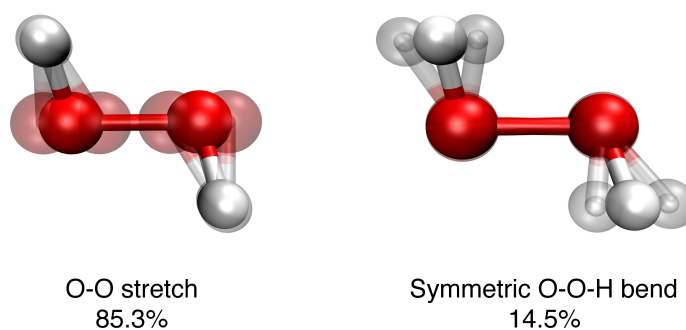
FIGURE 3.1: Visualization of the normal mode displacements that are needed to describe bond stretching in hydrogen peroxide. Displaced structures are glassy to distinguish them from the equilibrium structure. The percentages of stress energy stored in each mode are included.

by the stretching of the oxygen-oxygen bond alone in the manner described above and indeed, the normal mode analysis yields the correct stress energy.

The force analysis in delocalized internal modes yields an even more complicated linear combination of mechanically relevant coordinates (Table 3.1). The stress energy is assigned to four of the six delocalized internal modes and these modes themselves are linear combinations of internal coordinates. A detailed discussion is both cumbersome and superfluous, since this energy distribution can be exactly mapped onto the redundant internal coordinates (cf. Chapter 3.1.3). It turns out that, in the case of both the JEDI analysis, which uses redundant internal coordinates, and the force analysis in Z-matrix coordinates, all stress energy is stored in the oxygen-oxygen bond. This result was expected, since the oxygen-oxygen bond is the only internal coordinate that changes

TABLE 3.1: Contributions of each primitive internal mode to each of the six delocalized internal coordinates (DICs) in hydrogen peroxide and the percentages of stress energy (ΔE_i) stored in each DIC. The pairs of oxygen-hydrogen bond lengths and oxygen-oxygen-hydrogen bond angles are distinguished by superscripts.

Primitive mode coefficient	DIC 1	DIC 2	DIC 3	DIC 4	DIC 5	DIC 6
$c(BL_{O-O})$	0.417	0.000	-0.177	0.000	-0.458	0.765
$c(BL^1_{O-H})$	0.219	0.094	-0.152	0.701	0.618	0.216
$c(BL^2_{O-H})$	0.219	-0.094	-0.152	-0.701	0.618	0.216
$c(BA^1_{O-O-H})$	0.579	0.701	-0.081	-0.094	-0.089	-0.388
$c(BA^2_{O-O-H})$	0.579	-0.701	-0.081	0.094	-0.089	-0.388
$c(DA_{H-O-O-H})$	0.246	0.000	0.954	0.000	0.096	0.145
ΔE_i	29.2%	0.0%	3.9%	0.0%	23.7%	43.2%

A

B
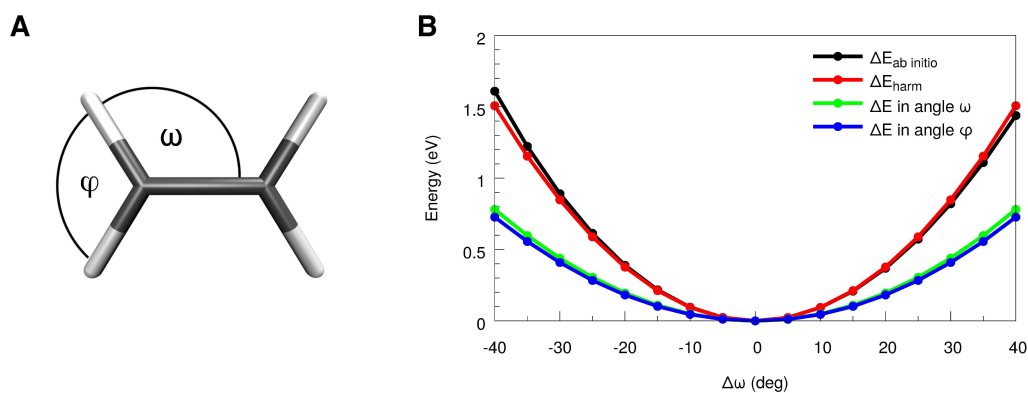
FIGURE 3.2: A) A carbon-carbon-hydrogen bond angle of ethene was displaced by $\Delta\omega = -\Delta\varphi = 25°$ and the distribution of stress energy was investigated using different coordinate systems. B) Energy contributions along the angle bending coordinate shown in A), calculated with the JEDI analysis at the RI-MP2[193–196]/cc-pVTZ[68] level of theory with the RI-MP2-cc-pVTZ[197] auxiliary basis set.

when hydrogen peroxide is stretched in the manner discussed here. Moreover, the internal coordinates of hydrogen peroxide do not contain any redundancies, so that the molecular connectivity can be uniquely defined via a Z-matrix that uses all primitive internal coordinates.

Ethene. As a second model example, a carbon-carbon-hydrogen bond angle of ethene was changed by $\Delta\omega = -\Delta\varphi = 25°$ (Figure 3.2A) and a single point calculation was carried out. As in the case of hydrogen peroxide, this deformation highlights the differences between the coordinate systems and is not intended to relate to any experiments directly. In contrast to the bond stretching in hydrogen peroxide, the angle bending in ethene is a curvilinear deformation and the molecular structure involves redundant internal coordinates.

The harmonic approximation, on which all force analyses considered here are based, causes the analyses using curvilinear internal modes, i.e. the JEDI analysis in redundant internal as well as the analyses in delocalized internal and Z-matrix coordinates, to overestimate the DFT stress energy by 2.9%. In contrast, the normal mode analysis overestimates this quantity by 17.9%. The reason for this discrepancy is that the normal mode analysis has difficulties in representing the curvilinear angle bending deformation and compensates this by extensive linear combinations of rectilinear normal mode displacements. Hence, if the displacements in the internal coordinates caused by

molecular deformations are predominantly curvilinear, normal modes should not be used to analyze the distribution of mechanical stress in these systems.

In analogy to the previous example of H_2O_2, delocalized internal coordinates again yield a complicated set of mechanically relevant modes, each of which itself is a linear combination of primitive internal coordinates. The larger a molecule, the more delocalized internal coordinates have to be taken into account and the situation becomes increasingly complicated and less insightful. Hence, in the following, the discussion focuses on the JEDI analysis in redundant internal coordinates and on the force analysis in Z-matrix coordinates. Due to redundancies in the set of internal coordinates, an interesting difference between these two force analyses can be observed: if all primitive internal modes are included in the force analysis, which is the protocol for the JEDI analysis, 52% of the stress energy is stored in the angle ω and 48% is attributed to φ, demonstrating that different angles have different "stiffnesses". If the force analysis in Z-matrix coordinates is carried out, however, the Z-matrix typically does not comprise all bond angles in the molecular plane. Depending on which angle is included in the Z-matrix (ω or φ), 100% of the stress energy is stored in this particular angle and any information concerning the other, undefined angle is lost.

If the JEDI analysis is used to investigate the distribution of stress energy, the ratio of the energies stored in the different bond angles is the same in each point of the deformation coordinate (Figure 3.2B), since the Hessian of the relaxed molecule is used. Here, a possible extension of the basic JEDI approach may be discussed. Instead of using the Hessian of the relaxed molecule, the Hessian of an intermediate structure ($\vec{q_k} \neq \vec{q_0}$), which is potentially better suited for the description of the energy landscape at larger displacements, could be used to determine the distribution of stress energy at a given deformed geometry. Thus, a "stepwise" harmonicity would be achieved, potentially refining the results. However, this approach would lead to a drastic complication of the method, since Hessian matrices would have to be calculated at a number of different points of the deformation coordinate, thus intensifying the computational demands of the approach significantly. While it is certainly possible to evaluate the Hessian at a lower level of theory, this introduces an additional approximation with unpredictable accuracy. Therefore, it is not advisable to follow this more expensive approach. Instead, the use of

the original JEDI analysis is recommended, since valuable insights can be gained in most chemically relevant cases if displacements in internal coordinates are small.

Benzene. To expand on the problem of the ambiguous definition of internal coordinates via the Z-matrix, it is illustrative to consider the force analysis of benzene, in which two opposite carbon-carbon bonds were stretched by forces of 1250 pN each in opposite directions via the EFEI approach. Although the rest of the molecule was allowed to relax freely, angle deformations are negligible and the only significant molecular deformations are those of the bonds that are stretched. As a result, only three normal modes are needed to account for the major part of the stress energy and the normal mode analysis overestimates the DFT stress energy by only 8.3%. In comparison, force analyses using curvilinear coordinates overestimate the DFT stress energy by 8.2%. Therefore, if the displacements of curvilinear modes caused by the mechanical deformation of a molecule are not too large and a small number of normal modes are available that represent the deformation adequately, the normal mode analysis typically delivers useful results.

Nevertheless, the linear combination of normal modes makes this analysis less intuitive and less meaningful than an analysis in internal coordinates. If the JEDI analysis is carried out, 50% of the stress energy is stored in each of the stretched bonds, demonstrating that the contribution of other modes is negligible (Figure 3.3). The results of the Z-matrix force analysis, however, depend crucially on the internal coordinates specified in the Z-matrix that is used. If one of the stretched carbon-carbon bonds is not included in the Z-matrix (Z-matrix 1), 100% of the stress energy is stored in the remaining stretched bond. If, on the other hand, both stretched bonds are included and another, relaxed bond is omitted in the definition of the Z-matrix (Z-matrix 2), the results are the same as for the JEDI analysis and mechanical stress is divided evenly among the two stretched bonds. The effect that the results of the force analysis using Z-matrix coordinates depend on the definition of the Z-matrix makes this coordinate system problematic for the description of molecules that include rings.

An interesting effect can be observed upon closer inspection of the results of Z-matrix 1: The $C-C-C$ bond angles next to the missing bond store 13% of the stress energy, which is compensated by -13% of stress energy stored in the other two $C-C-C$
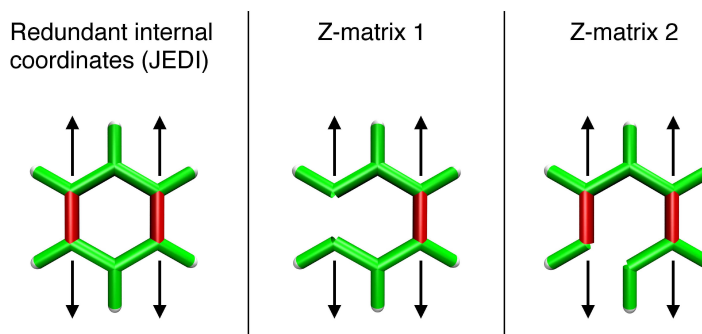
FIGURE 3.3: Force analyses of benzene, in which two opposite carbon-carbon bonds were stretched by forces of 1250 pN each, by following the JEDI protocol or by using two different Z-matrices. Bonds that store a high amount of stress energy are red, whereas relaxed bonds are green.

bond angles. In the JEDI analysis, minor negative energy values can be interpreted as relaxation effects of the internal modes. In the present case, however, the displacements of the bond angle modes is very small, so that the effect of the bond angle contributions is clearly unphysical and an artifact of the harmonic force analysis in Z-matrix coordinates. The reason is that, if certain coordinates are missing, the elements of the Hessian in internal coordinates and the summation carried out in the calculation of the energy stored in a certain mode (Equations 3.22 and 3.27) are asymmetric. In particular, the terms involving the mixed derivatives (the coupling elements) of the Hessian lead to the effect described here.

Pentacene. Finally, forces of 1250 pN were applied to two pairs of carbon atoms on opposite sides of pentacene, so that the molecule was stretched along its axis (Figure 3.4). The normal mode analysis performs surprisingly well. While the force analyses based on curvilinear coordinates overestimate the DFT stress energy by 6.0%, the normal mode analysis only overestimates it by 5.6%, because the molecular deformation can be reproduced to 86% by the symmetric stretching normal mode. This emphasizes the previous observation that a normal mode analysis performs well if only a small number of modes are needed to describe the molecular deformation, given that curvilinear deformations in each mode are sufficiently small.

The results for the JEDI analysis are shown in Figure 3.4. In contrast to the previous examples, the bendings now store significant amounts of stress energy (39%), although the displacements in each of the bond angle coordinates are small enough for the normal
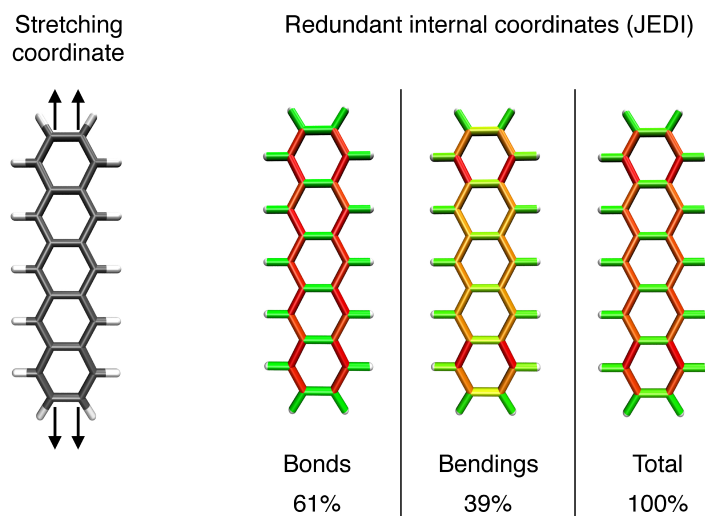
FIGURE 3.4: Stretching coordinate and JEDI analysis of pentacene, in which two pairs of carbon atoms on opposite sides of the molecule were pulled apart by forces of 1250 pN each.

mode analysis to deliver reasonable results. Mechanical stress energy is rather evenly distributed along the molecular axis, thus mirroring the stretching coordinate. Minor variations can only be observed in the internal coordinates of the terminal ring, because these modes are different from the coordinates in the middle of the molecule.

For comparison with the JEDI analysis, two different Z-matrices were used and again the outcome strongly depends on the choice of applied Z-matrix (Figure 3.5). In molecules that involve rings, Z-matrices typically do not include all bonds in the ring. In Z-matrix 1, this leads to mechanical stress only localized on one side of the molecular axis. Although half of the carbon-carbon bonds on the other side of the molecular axis are included, the omitted coupling to the modes that are not included seemingly leads to a relaxation of these bonds. In Z-matrix 2, most carbon-carbon bonds along the molecular axis are included while most bonds perpendicular to the stretching coordinate are neglected. This leads to the confusing result that mechanical stress is mostly localized at one end of the molecule. On comparison of the two Z-matrices, it can be observed that bonds can appear both relaxed and stretched, depending on which Z-matrix is used. Hence, the results of the force analysis in Z-matrix coordinates strongly depends on the definition of the Z-matrix. Considering this, it is unclear whether it is even possible to find a Z-matrix that delivers physically meaningful results in this case. Irrespective
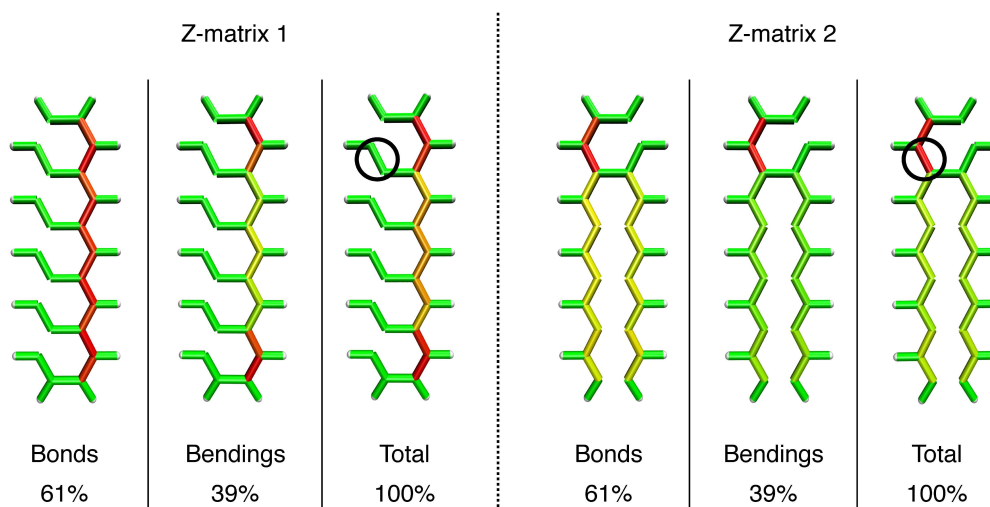
FIGURE 3.5: Force analysis of stretched pentacene using two different Z-matrices. Depending on the definition of the Z-matrix, the same bond can appear either mechanically stressed or relaxed (mark).

of the chosen Z-matrix, however, the sum of stress energy in all bonds (69%) and all bendings (31%) is the same as in the case of the JEDI analysis.

To summarize these findings, normal modes can constitute a useful set of coordinates for mechanical force analyses, if (1) displacements in curvilinear coordinates (e.g. angle bendings) are not too large upon application of external forces and (2) a small number of normal modes exist that describe the molecular deformation adequately. Z-matrix coordinates are problematic, particularly if the system of interest contains rings, since the results of the force analysis strongly depend on the internal coordinates that are included in the Z-matrix. Arbitrarily omitting mechanically relevant modes or even modes adjacent to them can lead to confusing and unreliable results. A redundant set of internal coordinates was found to deliver chemically intuitive and easily interpretable results in contrast to delocalized internal coordinates, since the latter typically comprise complicated linear combinations of primitive internal modes. Hence, the JEDI analysis using redundant internal modes has some good advantages over force analysis tools that use other coordinate systems, because it delivers reliable and meaningful results in all investigated test molecules.

3.2   The dynamic JEDI analysis

In Chapter 3.1, the JEDI analysis was used to calculate the distribution of stress energy in a molecule that was deformed using the COGEF, the EFEI or the RBS method. These calculations yield a static picture of the deformation process. However, it is also possible to apply the JEDI analysis in *ab initio* Molecular Dynamics (AIMD) simulations. In these dynamic calculations, each time step is considered a deformed geometry. The optimized structure of the molecule is taken as the reference structure, for which the Hessian is calculated. This procedure allows the real-time monitoring of the propagation of stress energy in molecules under external forces at different temperatures. However, it has to be kept in mind that the JEDI analysis is very sensitive to molecular deformation and it is possible that pronounced thermal fluctuations obscure the results of the JEDI analysis.

To demonstrate the gist of the dynamic JEDI analysis, the propagation of stress energy is monitored in two model systems (hydrogen peroxide and benzene). The RI-MP2[193–196] method in combination with the cc-pVDZ[68] basis set and the RI-MP2-cc-pVDZ[197] auxiliary basis set was used as the electronic structure method in the Born-Oppenheimer Molecular Dynamics (BOMD) simulations. While the trajectories were simulated at 298K, the initial nuclear velocities were set to zero to separate the propagation of stress from thermal fluctuations. A total of 3000 time steps for hydrogen peroxide and 30 000 time steps for benzene were calculated with a step width of 10 au (0.242 fs) each.

Hydrogen peroxide. As a first example, a BOMD trajectory was calculated for hydrogen peroxide, in which a constant stretching force of 2.5 nN was applied to the oxygen-oxygen bond (Figure 3.6A). Applying this force, hydrogen peroxide oscillates around a time-averaged oxygen-oxygen distance of 1.55 Å with the lower boundary being the equilibrium distance in the relaxed geometry (1.46 Å). The potential energy stored in the oxygen-oxygen bond, calculated via the JEDI analysis, oscillates in phase with the distance. The dihedral angle stores only small amounts of stress energy, with the largest contributions occurring predominantly in those points in which the potential energy in the oxygen-oxygen bond is minimal. The energy contributions of the oxygen-hydrogen bond
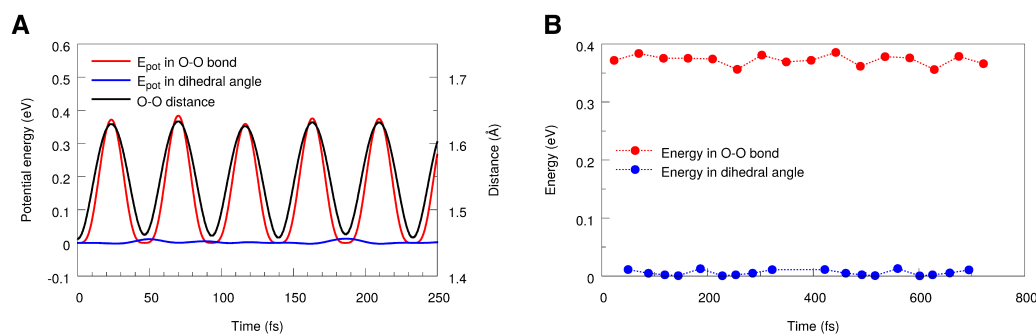
FIGURE 3.6: A) Extract from the BOMD trajectory of hydrogen peroxide with a constant force of 2.5 nN pulling the oxygen atoms apart, calculated at the RI-MP2/cc-pVDZ level of theory with the RI-MP2-cc-pVDZ auxiliary basis set. The potential energy contributions in the oxygen-oxygen bond and in the dihedral angle as well as the oxygen-oxygen bond length are plotted as a function of time. The average oxygen-oxygen distance during the trajectory amounts to 1.55 Å. B) Total energy contributions during the entire simulation.

lengths and of the hydrogen-oxygen-oxygen bond angles are insignificant. However, only the peaks of the temporal progress of the potential energy distribution are of particular interest. The reason is that the kinetic energy in a given mode, which is not calculated in the JEDI analysis, contributes to the total energy in every other point of the trajectory. Hence, considering only the peaks of the potential energy allows to isolate the potential energy from the kinetic energy. As can be deduced from Figure 3.6B, in which the points with maximum potential energy stored in the relevant modes are shown as a function of time, no considerable energy transfer from the oxygen-oxygen bond to the dihedral angle can be observed on the time scale of the simulation. This effect is caused by the constant nature of the force stretching the oxygen-oxygen bond and by the weak couplings between the different modes in hydrogen peroxide.

Benzene. To analyze the energy distribution in an initially stretched molecule that is suddenly allowed to relax freely from its strained geometry, a BOMD trajectory of benzene was calculated, in which two carbon-carbon bonds on opposite sides of the molecule were initially stretched. The equilibrium lengths of the carbon-carbon bonds in benzene amount to 1.4 Å at the RI-MP2/cc-pVDZ level of theory and were initially constrained to 1.7 Å via the COGEF approach. During the trajectory, however, the molecule was allowed to propagate without any constraints or external forces (Figure 3.7A).

The two types of internal modes, in which the major part of the initial stress energy
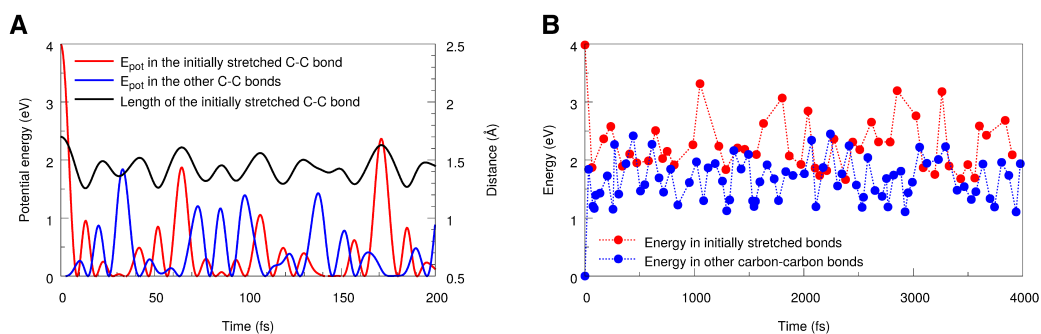
FIGURE 3.7: A) Extract from the BOMD trajectory of benzene, in which the molecule relaxes from a starting geometry with two carbon-carbon bonds on opposite sides of the molecule constrained to 1.7 Å, calculated at the RI-MP2/cc-pVDZ level of theory with the RI-MP2-cc-pVDZ auxiliary basis set. Potential energy contributions in two kinds of internal modes and the length of the initially stretched carbon-carbon bonds are shown as a function of time. B) Total energy contributions during the first 4 ps of the simulation. For clarity, only the highest peaks are included.

is stored, are the bond lengths that were initially stretched as well as the other carbon-carbon bond lengths. Despite the complexity of the distribution of potential energy among these modes, it can be observed that the potential energy stored in the initially stretched bonds is correlated with the corresponding bond lengths, because peaks in the one quantity occur at the same time as in the other quantity (Figure 3.7A). For further discussion, however, the analysis of peak potential energies throughout the trajectory, as carried out for hydrogen peroxide, is helpful (Figure 3.7B). From this analysis it becomes apparent that a significant transfer of potential energy from the initially stretched bonds to the other carbon-carbon bonds takes place within the first 50 fs. This effect can be attributed to the strong coupling between the internal coordinates and to the setup of the calculation: As there is no constraint to the initially stretched bonds, these bond lengths decrease rapidly, converting potential energy to kinetic energy and enabling a transfer of energy to the other degrees of freedom. In the further course of the trajectory, the potential energies show an asymptotic behavior. However, a number of recurrences of high amounts of potential energy stored in the initially stretched bonds can be identified, e.g. at 1051 fs and 1802 fs, which can be attributed to occasionally increased bond lengths. On longer timescales, an even distribution of the initial stress energy among all coupled redundant internal modes in the molecule is expected, which is associated with a smoothing of the energy curve.

In the dynamic JEDI analysis, the kinetic energy is neglected, because an analysis

of the distribution of kinetic energy among redundant internal coordinates is far from straightforward.[187] The calculation of the kinetic energy contributions in internal coordinates involves the inverse of the matrix $\mathbf{G}^m$, which is the mass-weighted form of the matrix $\mathbf{G}=\mathbf{B}\mathbf{B}^T$ (cf. Chapter 3.1.2). If the coordinate system involves redundancies, the matrix $\mathbf{B}$, which establishes the transformation between Cartesian and internal coordinates, contains linear dependencies, thus prohibiting a straightforward inversion of $\mathbf{G}^m$. Nevertheless, as was shown in this Chapter, the JEDI analysis can be used to analyze the distribution and propagation of the potential energy in a molecule under external force as well as the total energy at selected points of the trajectory.

3.3   The excited state JEDI analysis

Chapters 3.1 and 3.2 focused on static and dynamic analyses of the distribution of stress energy in mechanically deformed molecules in their electronic ground state. However, the JEDI analysis can also be applied in the electronically excited state to investigate the mechanical properties of molecular photoswitches, which convert light to mechanical work. This concept holds great promise as an abundant, cheap and sustainable source of energy.[40,43,198–205] In a typical photoswitch, light triggers an isomerization (e.g. a reversible *cis-trans*-isomerization), and, due to the concomitant change in volume or spatial extension of the photoswitch, mechanical forces are applied to the chemical environment. Hence, the light-induced structural changes of the photoswitch can ultimately be exploited for the generation of mechanical work as demonstrated by molecular motors based on unidirectional rotational motion.[43,204] However, the mechanical efficiency of photoswitches is limited and forces generated by photoswitches usually do not exceed a few hundred pN.[114,139,144,145,205–207] The mechanical efficiency of a photoswitch can be defined as the percentage of energy that is released by the motion of the photoswitch in a desired direction during relaxation in the electronically excited state. The mechanical efficiency of a photoswitch is in most cases significantly lower than 100%, since, during photoisomerization, a considerable amount of energy is wasted on other internal modes that do not contribute directly to the switching capability of the photoswitch. This can be, for example, the stretching of a carbon-hydrogen bond as a side effect of the motion along the excited state potential energy surface (PES) during *cis-trans*-isomerization.

Methods to increase the mechanical force the photoswitch can exert and the work it can perform involve molecular modifications of size and stiffness of the linkers connecting the photoswitch to the chemical environment or an enlargement of the spatial dimensions of the photoswitch itself, leading to larger displacements resulting from the isomerization. [144,205]

Considering the remarkable potential of photoswitches to generate mechanical energy from light, it becomes apparent that a better *a priori* understanding of the excited state behavior of photoswitches is desirable. In particular, for the design of improved, "stronger" photoswitches it would be beneficial to determine how much mechanical energy a photoswitch can utilize for the motion into a certain direction. With this information one could judge in advance whether a photoswitch can indeed perform a desired switching function. The JEDI analysis can be used in the electronically excited state to calculate the mechanical efficiency of a photoswitch in the beginning of the photoisomerization. [186] As in the ground state variant, all potentially relevant internal modes that play a role in the excited state isomerization of the photoswitch are considered. The present discussion focuses on photoswitches in which relaxation processes in the excited state lead to a minimum structure on the excited state PES, which limits the quantum yield of the isomerization. In contrast, those highly efficient photoswitches that isomerize quickly by following a barrierless path in the excited state are not discussed here. After a brief account of the theoretical foundations of the excited state JEDI analysis, the method is used to describe the excited state relaxation process of carbon monoxide to demonstrate its gist and potential, since it is clear from the outset that 100% of the energy that is released during this process arises from the change of the carbon-oxygen bond length. Subsequently, the mechanical efficiency of the *p*-coumaric acid photoswitch during the first step of the *cis→trans*-photoisomerization is discussed as one typical representative example.

3.3.1   Theoretical background

To derive an expression for the calculation of the mechanical efficiency of a photoswitch, it is important to note that the JEDI analysis does not involve any assumptions concerning

the electronic state. This means that the JEDI analysis can be used for the description of excited state mechanochemical processes, as long as the excited state PES can be approximated as harmonic and a Hessian for the desired state as well as a difference in geometries $\overrightarrow{\Delta q}$ can be calculated. Moreover, the ground state JEDI analysis is commonly used to describe the distribution of stress energy in a mechanically deformed molecule, i.e. a molecule that is stretched or compressed by an external force. Hence, energy is expended and its distribution among the redundant internal modes of the molecule is analyzed. However, if a molecule is excited by light, the motion along the excited state surface from the Franck-Condon point to, e.g., an energy minimum in the excited state typically constitutes a relaxation and not a forced deformation, i.e. energy is released rather than being expended. This process can also be described by the excited state variant of the JEDI analysis (Figure 3.8). Here, the excited state PES is approximated as harmonic and the Hessian in the minimum of the excited state PES is calculated. The geometry difference used in Equations 3.27 and 3.28 is calculated as the difference between the minima of the excited state and the ground state PES. The harmonic energy difference (ΔE_{harm}, Equation 3.28) can then be interpreted as the total mechanical energy that the photoswitch can release into its environment during isomerization, arising purely from the relaxation of the photoswitch in the excited state. Equation 3.28 can be used to calculate ΔE_i, which is the energy that becomes available due to the motion of the photoswitch in the direction of coordinate i. Dividing ΔE_i by ΔE_{harm} yields the mechanical efficiency of the photoswitch, if i represents the coordinate of interest. In the case of a photochemical *cis-trans*-isomerization, e.g., the coordinate of interest might be the torsion along the central dihedral angle.

Clearly, certain requirements have to be met for the excited state JEDI analysis to be viable. First of all, the excited state PES should not involve any barrier for the process of interest, at least during the initial motion. Neither should the excited state PES be dissociative or lead to a conical intersection on a barrierless path. Rather, relaxation from the Franck-Condon point should lead to a minimum on the excited state PES that can be approximated as harmonic. To estimate the quality of the harmonic approximation, it is useful to compare the harmonic energy difference (Equation 3.28) to the *ab initio* (or TDDFT) energy difference, which is defined in the excited state JEDI analysis as
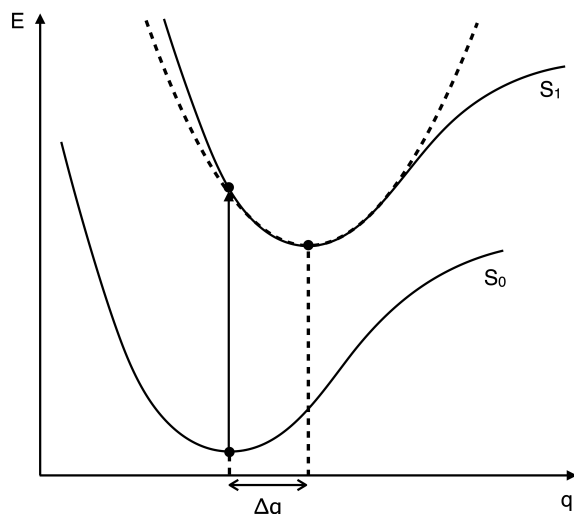
FIGURE 3.8: Schematic representation of the relevant potential energy surfaces (PESs) in the excited state JEDI analysis. The dotted parabola represents the harmonic approximation in the S_1 state. Δq is a displacement in the arbitrary internal coordinate q.

the difference in total energies between the Franck-Condon point and the excited state minimum.

The excited state JEDI analysis only allows statements about processes in the excited state that occur before the minimum on the excited state PES is reached. Any process that occurs after the relaxation to the minimum (e.g. fluorescence or decay through a conical intersection) cannot be described by the excited state JEDI analysis. Furthermore, the maximum energy released by a molecule that is relaxing in its electronically excited state may be significantly higher than the energy calculated with the excited state JEDI analysis, because thermal effects are neglected in this treatment. Thermal vibrations are known to have a destabilizing effect on bonds. [181,208,209] It can be assumed that these oscillations increase the maximum force molecules can exert on their environment upon relaxation in the excited state, since a large part of the energy absorbed via the photon is converted to thermal energy. To capture thermal effects, AIMD simulations in the excited state would need to be performed, which are, however, prohibitively expensive even for small molecules on the relevant time scales. Moreover, during these AIMD trajectories, the energy distribution for the potential and kinetic energy terms would have to be calculated separately. For the kinetic energy, this is far from trivial when redundant internal modes are used as the coordinate system (cf. Chapter 3.2). Therefore,

the present discussion is limited to photochemical processes that arise from relaxation of the internal modes during the motion along the excited state PES.

The calculations of the ground and excited state minima, the excitation energies and the Hessian in the excited state that are reported here were performed with the Q-Chem 4.3 program package[94] using Density Functional Theory (DFT)[71,72] and Time-Dependent DFT (TDDFT)[210] at the B3LYP[66,67]/cc-pVDZ[68] level of theory. As usual, benchmarking against experimental data or more accurate wave function based methods is required for obtaining reliable results. However, the results discussed in this Chapter are considered a first proof-of-principle. Moreover, the calculation of the excited state Hessian with more accurate wave function based methods becomes computationally prohibitive even for medium-sized systems.

3.3.2 Excited state relaxation of carbon monoxide

The excited state relaxation of carbon monoxide is discussed as the first example. In contrast to more complex molecules, it is known *a priori* that 100% of the energy released upon relaxation in the excited state originates from changes in the carbon-oxygen bond length. The electronic structure of the excited states of carbon monoxide has been investigated thoroughly several decades ago.[211,212] At the TDDFT/B3LYP/cc-pVDZ level of theory, the first electronically excited singlet state (S_1) at the Franck-Condon point is characterized by a transition to a π^* orbital, which leads to an elongation of the carbon-oxygen bond upon relaxation in the S_1 state. Scanning the carbon-oxygen bond length reveals that the S_1 state can be approximated as harmonic (Figure 3.9) and the excited state JEDI analysis can be applied. The carbon-oxygen bond length at the Franck-Condon point amounts to 1.13 Å, which is significantly shorter than the bond at the S_1-minimum (1.25 Å). As a result, the harmonic energy difference (Equation 3.28) is 25.7% lower than the DFT energy difference.

Although carbon monoxide is of course not a photoswitch, the energy that is released during the relaxation of the carbon-oxygen bond length amounts to 0.53 eV (DFT energy difference) or 0.39 eV (harmonic energy difference), respectively. This energy becomes available for the environment and could in theory be used to apply forces to the
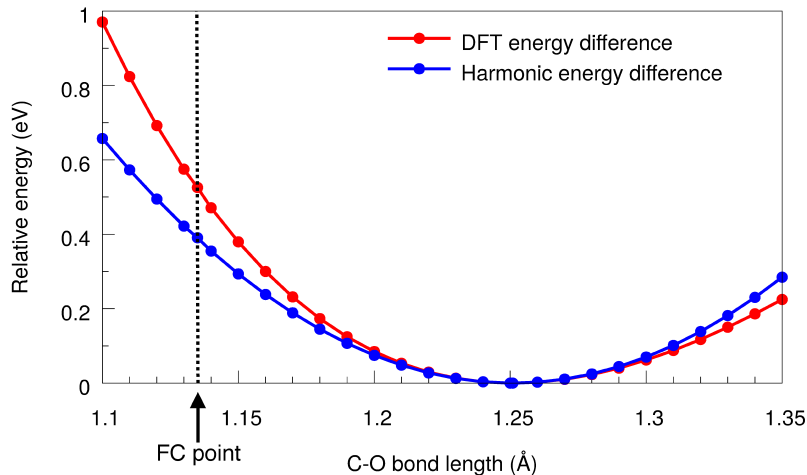
FIGURE 3.9: Scan of the carbon-oxygen bond length in carbon monoxide in the S_1 state. The DFT energy difference is the difference in energy at each point of the stretching coordinate relative to the minimum in the S_1 potential, calculated at the TDDFT/B3LYP/cc-pVDZ level of theory. The harmonic energy difference, ΔE_{harm}, is the sum of harmonic energies in every internal mode, calculated with the excited state JEDI analysis.

surrounding chemical structures, thus ultimately leading to the generation of mechanical work. Since there is only one internal mode in carbon monoxide and 100% of the released energy originates from the carbon-oxygen bond stretching, the "mechanical efficiency" of the carbon monoxide molecule is 100%.

An alternative method to derive the energy a photoswitch can release into its environment is to calculate the gradient of the energy at the Franck-Condon point and multiply it with the displacement vector between the Franck-Condon point and the minimum of the excited state potential. This approach has the advantage that the expensive calculation of the Hessian in the excited state is avoided. However, in the case of a potential that can be approximated as harmonic, this approach yields an energy that is much too high, especially if the displacement $\overrightarrow{\Delta q}$ is large. This is analogous to approximating a second order polynomial by a first order instead of a second order Taylor series. In the case of carbon monoxide, this approach overestimates the *ab initio* energy difference by a factor of 2.3. Hence, this gradient based analysis is refrained from and the use of the excited state JEDI analysis is recommended for the cases in which the harmonic approximation is applicable. Nonetheless, the linear approach described here can be considered an ansatz for treating systems in which the excited state PES can be approximated as linear rather than as harmonic.

3.3.3   The mechanical efficiency of *p*-coumaric acid

The photochemical properties of *p*-coumaric acid have been investigated extensively due to its role as chromophore in the photoactive yellow protein (PYP).[213–220] In PYP, the photochemical *trans*→*cis*-isomerization of *p*-coumaric acid triggers structural changes in the protein. The *cis*→*trans*-isomerization, in contrast, has primarily been studied in solution.[218] Irradiating *cis*-*p*-coumaric acid for a sufficiently long time triggers the isomerization to the *trans*-isomer, thus falling within the definition of photoswitches as used in organic chemistry (Figure 3.10A).[61,213,221,222] Moreover, the harmonic approximation as required for the JEDI analysis is only applicable in the excited state for the *cis*→*trans*-isomerization pathway, because in the DFT calculations the central dihedral angle does not change upon relaxation of the *trans*-isomer in the excited state. The S_1 state has $\pi\pi^*$ character, so that the torsion around the central dihedral angle is facilitated. Ground and excited state optimizations were performed at different values of the central dihedral angle (Figure 3.10B) and a shallow S_1-minimum with a dihedral angle of 28° was found. For comparison, the dihedral angle in the ground state is only 4°. This relatively large deformation upon relaxation in the excited state can be well described by the excited state JEDI analysis, since curvilinear internal modes are used as the coordinate system. Moreover, the displacement of the other internal modes is small, so that the harmonic approximation is applicable. Due to these effects, the harmonic energy difference overestimates the DFT energy difference by only 6%, which demonstrates that the excited state JEDI analysis can indeed be applied.

During the first step of the relaxation of *cis*-*p*-coumaric acid in the excited state, only 9% of the released energy originates from the torsional motion around the dihedral angle (Figure 3.10C). This number, which corresponds to only 0.068 eV, has been generated by adding up the contributions of all four dihedral angles (C−C−C−C, H−C−C−H, H−C−C−C and C−C−C−H) around the central carbon-carbon double bond. Hence, the purely photomechanical efficiency of *cis*-*p*-coumaric acid during the first step of the photoisomerization in the gas phase amounts to 9%. The rest of the energy released in the excited state is wasted on other modes that do not contribute to the torsional motion. In particular, 61% of the total energy released in the S_1 state is contributed by the covalent bonds, e.g. the carbon-oxygen double bond or the bond connecting
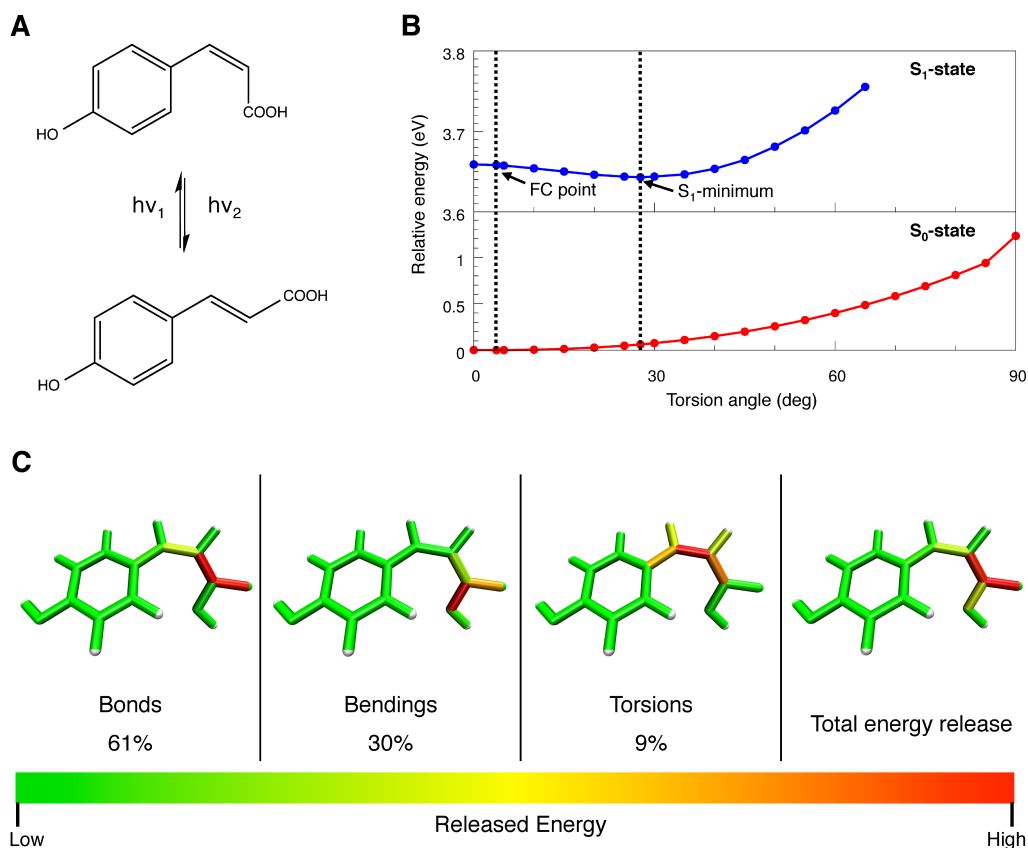
FIGURE 3.10: A) Photochemical and thermal *cis-trans*-isomerization of the *p*-coumaric acid photoswitch. B) Ground (S_0) and first excited singlet (S_1) state relaxed surface scans of the torsion around the carbon-carbon double bond in *p*-coumaric acid. The Franck-Condon (FC) point and the minimum in the S_1 state are indicated. Convergence problems prevented calculations in the S_1 state at dihedral angles larger than 65°. C) Distribution of the energy released upon relaxation in the S_1 state among different kinds of internal modes. Regions in which a large amount of energy is released are colored red, whereas regions that hardly release energy are green.

the carboxyl group to the rest of the molecule and 30% is contributed by the bond angles. These kinds of modes are not of primary interest if *cis-p*-coumaric acid shall fulfill a certain switching function, since their contribution to the change in volume of the photoswitch and therefore to the mechanical work it can perform is very small. It should be stressed that here only the first step of the excited state relaxation (the motion until the S_1 minimum is reached) is described. Despite the low mechanical efficiency of the *cis-p*-coumaric acid photoswitch, irradiating the molecule long enough still leads to isomerization to the *trans*-isomer.

Due to the limitation of the excited state JEDI analysis to a certain kind of excited state potential energy surface and the neglect of important factors like thermal vibrations,

the method yields qualitative results. A potential application of the excited state JEDI analysis is the comparison of similar photoswitches. The motion along the excited state PES proceeds in a similar manner for all of them and errors can be expected to be comparable. Hence, optimizations of the mechanical efficiency of photoswitches can be conducted *in silico*. An interesting perspective is also provided by the treatment of solvated photoswitches by including explicit solvent molecules. It can be assumed that the results reported here can hardly be validated experimentally in detail, because measurements of the energy generated by the motion of every single internal mode of a molecule in its excited state are intricate. However, the overall quantum yield of a photoswitch reveals its overall efficiency.

In the future, the excited state JEDI analysis should be extended to allow the calculation of the mechanical efficiency of a photoswitch if the excited state PES cannot be approximated as harmonic. Once an approach is available that can describe excited states that are, e.g., dissociative or decay through a conical intersection rapidly, the mechanical efficiency of a wider range of photoswitches can possibly be calculated. This would allow the investigation of the *trans*→*cis*-isomerization of p-coumaric acid, for example, which can be assumed to be significantly more efficient than its photochemical *cis*→*trans*-isomerization. However, due to the plethora of shapes of excited state potential energy surfaces, deriving a single approach that treats all of them equally well and that includes all potentially relevant internal modes constitutes a significant challenge.

3.4   Implementation and visualization

The matrix transformations and multiplications involved in the JEDI analysis (Chapter 3.1.3) are implemented in a Python script, which is interfaced with the Q-Chem program package.[94] Although an implementation of the JEDI analysis in a quantum chemical program package is in principle possible, such an implementation would severely reduce the flexibility of the method. A typical use of the JEDI analysis is the calculation of the distribution of stress energy in every point of a COGEF or EFEI deformation coordinate. While the mechanically deformed geometry needs to be calculated at every point of the coordinate, the relaxed geometry and the Hessian need to be calculated only once for

the entire coordinate. Calculating a JEDI coordinate with a quantum chemical program package and possibly refining this coordinate later would inevitably lead to unnecessary multiple calculations of the relaxed geometry and the Hessian.

At present, the following variants of the JEDI analysis are implemented in the JEDI Python script:

- **Ground state JEDI analysis (Chapter 3.1).** The reference geometry is generated by a relaxed ground state geometry optimization. The Hessian is computed in a frequency calculation at this reference geometry. The mechanically deformed geometry can be generated by COGEF, EFEI or RBS (single point) calculations (cf. Chapter 2).

- **Dynamic JEDI analysis (Chapter 3.2).** The reference geometry is generated by a ground or excited state geometry optimization. The Hessian is calculated at this reference geometry in the corresponding electronic state. The deformed geometries are generated during a regular BOMD simulation in the electronic state of interest.

- **Excited state JEDI analysis (Chapter 3.3).** An excited state geometry optimization generates the reference structure. At this geometry, an excited state frequency calculation generates the Hessian on the excited state PES. The deformed geometry can be generated via an ordinary ground state optimization or via COGEF, EFEI or RBS calculations in the excited state.

Due to the typically very large amount of internal coordinates in a molecule, the interpretation of the energy values resulting from the ground state JEDI analysis (Chapter 3.1), becomes tedious. Hence, using VMD,[223] a visualization tool was developed, which colors bonds according to the stress energy stored in them (green: low strain, yellow: medium strain, red: high strain; transitions are fluent). In the case of the bond lengths, this procedure is straightforward. The energy stored in the bond angles and dihedral angles, on the other hand, is split between the bonds involved in the given coordinate and finally the different contributions for each bond are added up. Moreover, the region that stores the highest amount of stress energy in a given type of coordinate is always colored red,

regardless whether this is a high or low percentage of the overall molecular strain. If the most strained bond length stores much more energy than the most strained bond angle, for example, both modes are colored red. Therefore, red in one type of coordinate is not the same red as in another type of coordinate. This procedure ensures a meaningful dissection of the stress energy in its various components at one glance. Additionally, a color-coded structure is created that indicates the total molecular strain. Here, the contributions in all bonds, bendings and torsions are mapped onto the bonds and added up. This procedure allows an estimation of the molecular strain in a specific region of a molecule without dissecting the energy into the different kinds of modes.

The same procedure is carried out in the dynamic JEDI analysis (Chapter 3.2). Since the geometry of the molecule in every time step is considered a mechanically deformed geometry, color-coded structures can be generated at every point of the trajectory, which can subsequently be merged into a movie. This kind of color-coded visualization of a BOMD trajectory allows a quick and efficient time-resolved analysis of the propagation of mechanical stress.

Analogous approaches are conducted in the case of the excited state JEDI analysis (Chapter 3.3). The only difference to the ground state variant is that the regions in which a lot of energy is released are colored red, while mechanically uninvolved regions are colored green.

Chapter 4

Applications of the JEDI analysis

In this Chapter, various applications of the JEDI analysis (cf. Chapter 3) are discussed. In Chapter 4.1, the mechanochemical properties of knotted polymer strands are investigated using the JEDI analysis. In Chapter 4.2, the mechanical efficiency of the stiff-stilbene photoswitch and its capability to induce bond rupture in cyclobutene is studied. Mechanochemical methods for the stabilization of strained hydrocarbons are discussed in Chapter 4.3.

4.1   Mechanical properties of knotted polymer strands

"My dear sir, in this world it is not so easy to settle these plain things. I have ever found your plain things the knottiest of all."

Herman Melville: Moby Dick

Please note that the following introductory remarks on the occurrence of knots in polymers are based on an invited review by Prof. Dr. Andreas Dreuw and myself, which has been submitted for publication in *Chemical Reviews*.

The concept of topological isomerism, which includes the isomerism between a knotted and an unknotted molecule, was introduced more than half a century ago.[224]

Throughout the following decades, a remarkable amount of research interest has been devoted to knotted molecules. For example, it was found that polymers of a certain length are inevitably tangled into knots.[225–227] While swollen coils in a good solvent are relatively unknotted, the compact globules that form upon abrupt quench to poor solvent conditions are extensively knotted.[226,228] The entanglement of polymers has been understood as a two-stage process: The initial rapid folding of the polymer to a compact globule does not change the knottedness of the coil. Rather, slow knotting or entangling of the coil proceeds via subsequent self-reptation.[226] The dynamics of molecular knots, including the diffusion of knots along a polymer chain, have also been investigated theoretically.[229,230]

It could be shown mathematically that polymers of a certain length are extensively knotted.[226] For short polymers with a chain length $N < 100$ the "unknot" is dominant, meaning that short polymers are usually not tangled into knots. The probability of knot occurrence increases exponentially with increasing chain length. At $N = 1000$, for example, the probability that the chain is unknotted is only 6%. At larger N, the probability of the unknot is approximately $\exp(-N/270)$. The occurrence probability of most simple knots such as the 3_1 or the 4_1 knot, which are commonly referred to as the overhand knot and the figure-of-eight knot, reaches a maximum near $N = 500$. The occurrence of unknown knots that could not be identified mathematically, however, increases dramatically beyond $N = 500$.

Turning to biological macromolecules, it was found that knots occur frequently in proteins[231–242] and certain kinds of DNA.[243–246] In an early Monte-Carlo study, Frank-Kamenetskii and co-workers predicted that 40% of the DNA molecules in bacteriophage λ that contain approximately 150 segments are knotted after closing *in vitro*.[243] The authors point out that knotted DNA molecules cannot finish the replication cycle, because the two daughter molecules are linked with each other. Hence, it is speculated that a special mechanism in the cell prevents knotting of DNA molecules. Experimentally, actin filaments and DNA molecules were knotted using optical tweezers.[247] In this experiment, it was found that the rupture force of knotted actin is two orders of magnitude lower than of unknotted actin. Knotted or unknotted DNA, however, could not be ruptured with optical tweezers.

The most common knot that occurs in polymers is the overhand knot, which is well-known from macroscopic ropes commonly used in sailing and rigging. Strictly speaking, a knot is a closed loop. Here, however, a knotted chain is considered in which the ends are not connected. Although the overhand knot is the easiest and smallest knot and consumes the least material, it is known to reduce the strength of the rope by approximately 50 percent.[248] Typically, an overstretched rope ruptures at the "entry" or "exit" of the knot. Both effects (the weakening of the rope and the rupture in the vicinity of the knot) can also be observed at the molecular level.[179,249] In polymers, the rupture results in the formation of two radicals, which was attributed to mechanical stress mostly localized in the carbon-carbon bonds at the entry or exit of the knot.[179,249,250] However, most previous work was based on constrained Molecular Dynamics (MD) simulations and the united atom scheme,[251,252] in which methylene bridges, e.g., are described as pseudo-atoms. These methods have a number of drawbacks when investigating mechanical bond rupture in a polymer knot, since electronic degrees of freedom are not included explicitly and not all internal modes of the molecule that potentially play a role in the mechanochemical processes (e.g. torsions involving hydrogen atoms) are included in the united atom scheme. Due to the neglect of these important factors, the questions why polymers are weakened by a knot and why they break in its immediate vicinity have not been answered in previous literature.

In this Chapter, the results of a first-principles study are reported, in which both static EFEI calculations and dynamic BOMD simulations under constant tensile stress were applied to investigate the mechanical properties of an overhand knot in a polyethylene chain under tensile stress.[208,209] The ground state JEDI analysis (Chapter 3.1) is used to quantify the various energy contributions that play a role in the rupture of the overhand knot. In contrast to previous work, this procedure ensures that electronic effects are treated explicitly and that all relevant degrees of freedom are included in the analysis of the distribution of stress energy in a polymer knot. Please note that parts of this Chapter have already been published by Prof. Dr. Andreas Dreuw and myself in *Angewandte Chemie International Edition* **2016**, *55*, 811-814.

All calculations reported in this Chapter were performed with the Q-Chem 4.0.1 program package,[253] in which the EFEI method was implemented. All EFEI calculations

were carried out at the BLYP/6-31G(d) level of theory, because DFT was found to deliver reliable results in the treatment of hydrocarbons and the BLYP functional in particular was used in Car-Parrinello Molecular Dynamics (CPMD) simulations in earlier work.[179,249,250,254–259]

The starting structure for the polyethylene chain with 40 carbon atoms that involves an overhand knot was generated manually. Subsequently, it was tightened by an external force of 2 nN in opposite directions using the EFEI approach. Afterwards, it was relaxed slowly, while lower forces were still acting (Chapter 4.1.2). Here, the step size of the geometry optimization was set to 10^{-3} a.u. The starting structures for the model systems with a chain length of 14 carbon atoms were also generated manually. In this case, however, the chain was stretched directly by different forces.

In the BOMD simulations, the forces were applied directly by an approach that is equivalent to the EFEI method in the static calculations: In every step of the gradient calculation, the constant external force is added to the gradient along the vector connecting the two atoms. In all simulations, the time step was set to 20 a.u. (0.0484 fs). A total of 2000 time steps were calculated, so that the total simulation time amounts to 968 fs. The same level of theory that was used in the EFEI calculations was applied as the electronic structure method in the BOMD simulations. In addition to BOMD trajectories at 0 K, simulations of the knotted polyethylene chain were carried out at 100 K, 200 K and 300 K, in which different forces, ranging between 1.25 nN and 2.1 nN, were applied. It is important to note that bond rupture events in BOMD simulations that involve temperatures higher than 0 K are statistical processes. Due to the large system size, however, it was not possible to simulate ensembles.

4.1.1   Linear, unknotted polymer chains

When a linear polyethylene chain with a length of 28 carbon atoms is stretched, most stress energy is stored in the covalent bonds (Figure 4.1A). At low forces, the bond angles store almost as much strain energy, but their share becomes smaller with increasing force. Not surprisingly, the energy apportioned to the dihedral angles can be neglected. In the EFEI calculations, the terminal bonds rupture simultaneously at 5.6 nN due to
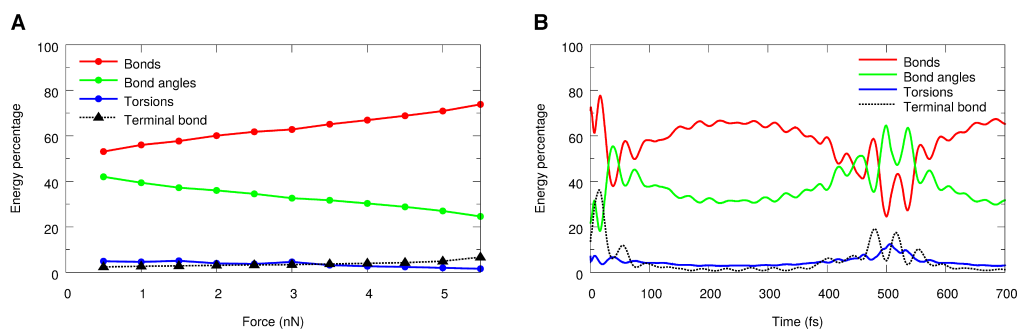
FIGURE 4.1: Distribution of stress energy among the internal modes of a stretched linear polyethylene chain. A) Static EFEI calculations. B) BOMD trajectory under a constant external force of 2 nN.
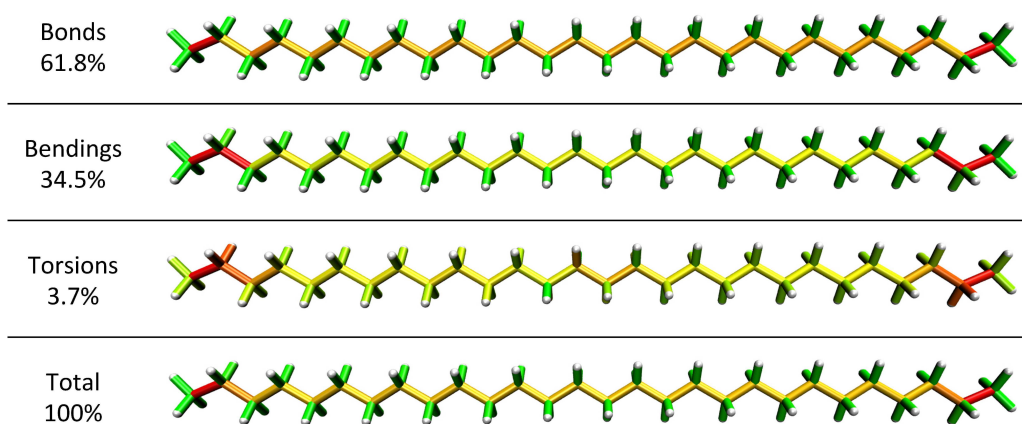
FIGURE 4.2: Color-coded representation of the distribution of stress energy among the internal modes of a linear polyethylene chain that is stretched by an external force of 2.5 nN. Regions that store a high amount of stress energy are colored red.

the symmetry of the molecule and its alignment with the stretching coordinate. The percentage of the stress energy stored in the terminal bonds remains relatively low during the stretching coordinate, although their share increases slightly in the end. The energy distribution is examined in more detail in Figure 4.2, in which the energy distribution is shown for a polyethylene chain that is stretched by 2.5 nN: The terminal bonds, angles and even torsions store higher amounts of stress energy than those modes in the middle of the chain. This discrepancy between the two regions of the chain is most pronounced in the case of the bond angles. Taking all degrees of freedom into account, this results in the localization of most strain in the terminal regions of the polyethylene chain (lowest panel of Figure 4.2).

The effect that stress is not distributed uniformly over a hydrocarbon, but rather

accumulated at the end, has been documented in literature.[180,249,260,261] However, the uncoupled force constant d^2E/dq_i^2 calculated in the JEDI analysis amounts to 0.263 a.u. for the terminal bond and to 0.256 a.u. for a bond in the middle, signifying a slightly stiffer terminal bond. Moreover, it is more intuitive that a molecule dissociates into two alkyl radicals than into one alkyl and one methyl radical. In literature, similar effects have been attributed to the existence of several minima of the Potential Energy Surface (PES) and the computational method used to calculate the stretching coordinate failed to find the energetically more favorable dissociation pathway, in which the hydrocarbon ruptures in the middle.[260,261] This effect, however, was observed only above a certain force threshold. In the present study, on the other hand, the remarkably high amount of strain in the terminal bond lengths was observed even at low forces. Furthermore, an odd-even-effect can be observed: The second, fourth, sixth, ..., bond stores less energy than the first, third, fifth, ..., bond. The same applies for the bond angles. This effect is not an artifact of the JEDI analysis, since the differences in the energy are mirrored by the variations in the bond lengths. The existence of several minima of the PES is not a satisfactory explanation for the odd-even-effect, since symmetrizing the bond lengths in the molecule prior to the EFEI calculations still yields the same, asymmetric result. Smalø and Uggerud have attributed bond rupture at the end of an alkyl chain to the soft angle bending modes in the terminal region, which leads to a better alignment of the terminal carbon-carbon bonds with the external force.[180] Certainly, this observation plays an important role for the odd-even effect reported here.

BOMD simulations were carried out to investigate the propagation of mechanical stress through the polyethylene chain. In the BOMD trajectories, the chain ruptures at 3.6 nN and, in contrast to the static EFEI calculations, bond rupture occurs in the middle of the chain. The reason is the nature of the pulling: At t = 0, the molecule is in its equilibrium position. Applying a force to the terminal carbon atoms causes the strain to propagate rapidly from the end of the chain into the middle. In analogy to constructive interference in waves, these two strain packets add up in the middle of the chain, leading to bond rupture. At lower forces, e.g. 2 nN, the strain oscillates between the end and the middle of the chain. The potential energy oscillates between the bonds and angles, while only minor energy contributions are stored in the dihedral angles (Figure 4.1B).
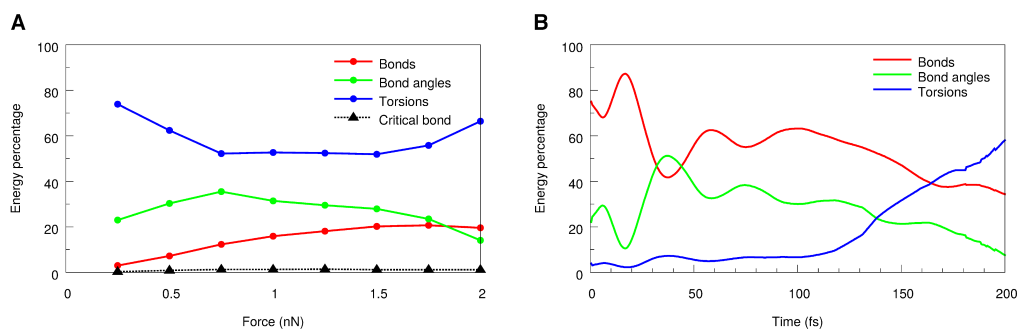
FIGURE 4.3: Distribution of stress energy among the internal modes of a knotted polyethylene chain. A) Static EFEI calculations. B) BOMD trajectory under an external force of 2 nN.

These results agree well with the observations of Smalø and co-workers, who found that bond rupture is preferred in the center of the chain if the force is applied suddenly.[181]

4.1.2   Knotted polymer chains

When a knotted polyethylene chain is stretched, most stress energy is stored in the torsions (Figure 4.3A). The bond angles also store crucial parts of the energy and the significance of the bonds as reservoirs of stress increases with increasing force. However, the percentage of stress energy in the carbon-carbon bond that ultimately breaks remains very low throughout the entire coordinate. In the EFEI calculations, bond rupture occurs at a pulling force of 2.6 nN in opposite directions in the immediate vicinity of the knot (in comparison to 5.6 nN in a linear, unknotted chain), demonstrating that an overhand knot indeed substantially weakens a polyethylene chain.

To investigate the reason for this remarkable decrease in resistance to tensile stress, a more detailed analysis of the distribution of mechanical stress in the overhand knot that is stretched by 2 nN in opposite directions is helpful (Figure 4.4). Most of the stress energy in the bond lengths is stored by those bonds at the entry or exit of the knot. This proportion, however, is much smaller than the energy stored by the torsions around the curved part of the knot. This effect can also be observed when the total strain is considered (panel "Total" in Figure 4.4): While mechanical stress is visible in the bonds in the vicinity of the knot, much more strain is distributed around the curved part of the knot. This observation leads to the physical picture that the curved part of
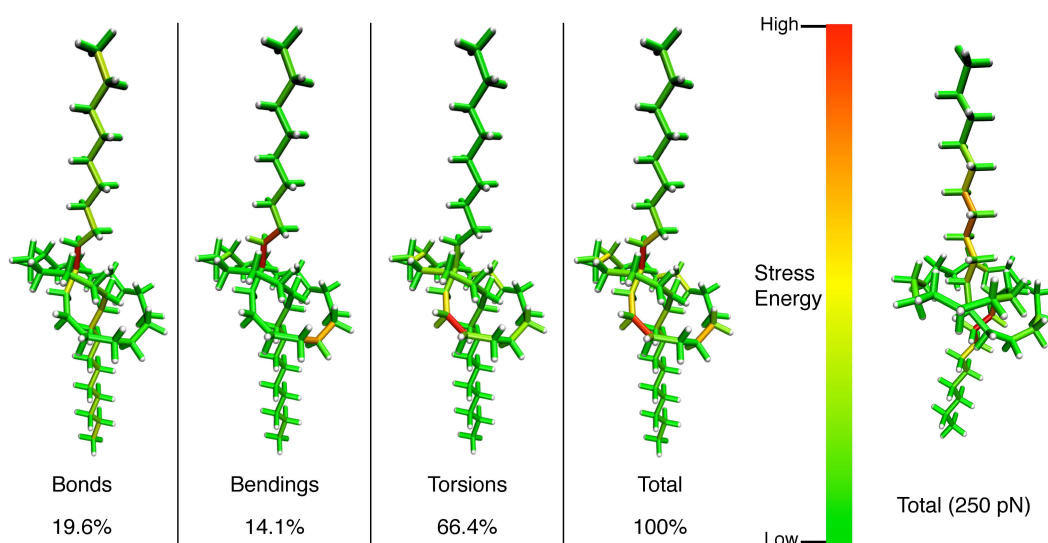
FIGURE 4.4: Color-coded representation of the distribution of stress energy among the internal modes of a knotted polyethylene chain that is stretched by an external force of 2 nN. On the right, the total stress distribution for a pulling force of 250 pN is shown.

the structure essentially chokes the chain and cuts it at the entry or exit of the knot. The mechanism of the choking becomes clear upon comparison to a linear, unknotted polymer (Chapter 4.1.1), where all bonds are stretched and all angles are displaced, so that mechanical stress is distributed more evenly over the entire chain. Hence, it takes strong forces to accumulate enough energy to break a bond in the chain, because all other bonds are also stretched significantly. If, on the other hand, a knotted chain is stretched, the torsions in the curved part of the knot act as "work funnels" that efficiently pass on the stress energy to the bonds that ultimately break, thus localizing the mechanical stress at the entry or exit of the knot and preconditioning the bonds in this region for bond rupture. As a result, the rupture of the chain occurs at much lower forces than in the case of the unknotted chain, since the other bonds remain relatively relaxed and mechanical stress is not "wasted" on them. It should be noted that this effect is clearly a result of the tightening of the knot: If the stretching force is too weak (see the right panel in Figure 4.4), mechanical stress is mostly localized in the linear part of the chain and the torsions are not strained enough to act as work funnels.

The conclusions drawn from the static EFEI calculations are supported by dynamic BOMD simulations of the overhand knot under a constant external force. At 0 K, a force of 2.05 nN ruptures the chain in the immediate vicinity of the knot after 932 fs. During
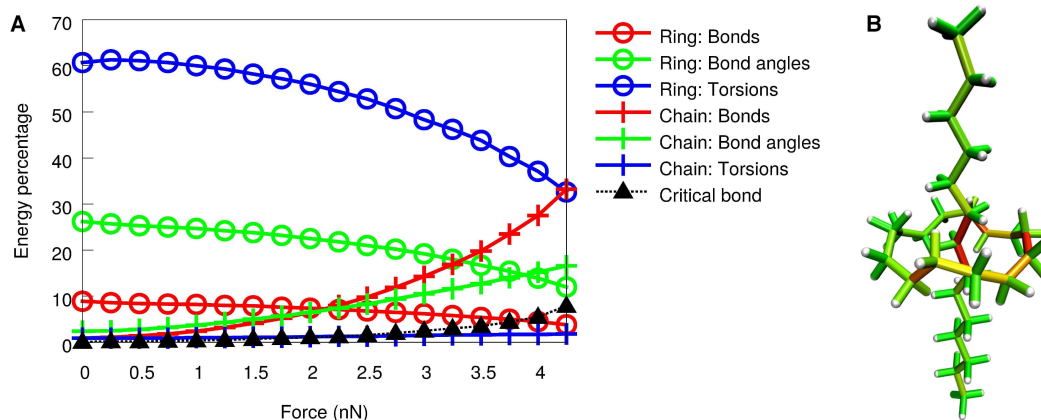
FIGURE 4.5: Distribution of stress energy in a model system with a 14-membered ring placed around a linear polyethylene chain A) as a function of the external force and B) at an external force of 3.5 nN.

the first 200 fs of the trajectory in which the knot is tightened by a force of 2 nN in opposite directions, the build-up of strain in the torsions is observable (Figure 4.3B): The stress energy propagates rapidly from the terminal bonds, where the force is applied, to the center of the knot and then accumulates in the dihedral angles around its curved part. The dissection of stress energy among the degrees of freedom in the overhand knot is only shown until 200 fs in Figure 4.3B, since several dihedral angles flip after this point and the harmonic behavior, which is a prerequisite for the JEDI analysis, can no longer be ensured in the further course of the simulation. BOMD trajectories carried out at 100 K, 200 K and 300 K with different stretching forces show that thermal oscillations resulting from a higher temperature have a destabilizing effect on the knot. At 300 K, for example, the time until bond rupture decreases from 795 fs upon application of 2 nN to 679 fs (2.05 nN) and 550 fs (2.1 nN), a result that is consistent with previous observations (cf. Chapter 2.4).

4.1.3   Calculations on a knot model system

To further investigate why an overhand knot weakens a polymer, a model system was developed, in which a closed hydrocarbon ring was placed around a polyethylene chain with a length of 14 carbon atoms. The tightness of the knot is then simply replaced by the size of the ring, with smaller rings signifying a tighter knot. As an example, the distribution of stress energy in the model system with a 14-membered ring, in which the
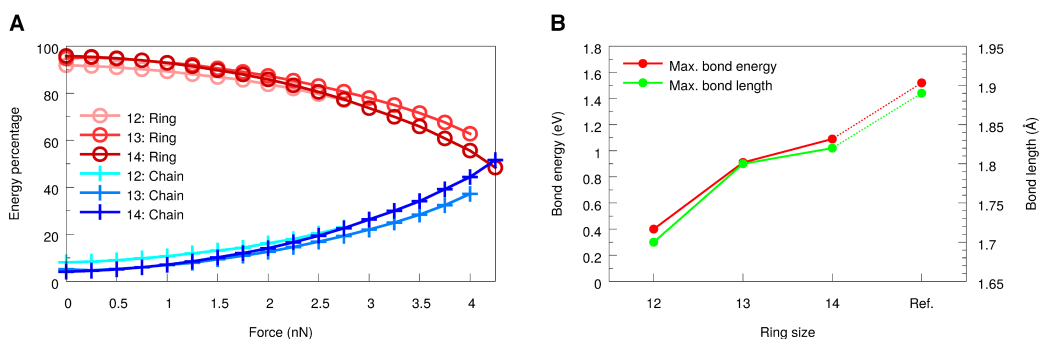
FIGURE 4.6: Comparison of model systems with rings of different sizes placed around a linear polyethylene chain. A) Force dependence of the percentages of stress energy stored in the ring and in the chain. B) Dependence of maximum bond energy and maximum bond length of the scissile bond in the chain on the ring size. A 14-membered chain without a ring, in which two bonds in the middle of the chain are exposed to a force, is taken as a reference (Ref.). The lines are included to guide the eye.

chain is stretched by different forces, is considered (Figure 4.5A). In the beginning of the stretching coordinate, by far the highest amount of energy is located in the torsions of the ring. Stretching the chain further leads to a transfer of stress energy from the ring to the chain. The bonds of the chain are particularly susceptible to this energy transfer and bond rupture ultimately occurs in the middle of the chain. This effect can also be observed in Figure 4.5B, in which the model system with a 14-membered ring and an external stretching force of 3.5 nN is shown. The region closest to the ring stores by far most stress energy that is attributed to the chain. On the other hand, the amount of stress energy stored in the chain amounts to only one third of the total strain of the system, while the rest is mostly localized in torsions of the ring.

The transfer of stress energy from the ring to the chain proceeds in a very similar fashion for all ring sizes (Figure 4.6A). Only the rupture forces are different: The smaller the ring (signifying a tighter knot), the less force is needed to break the chain. Accordingly, the stress energies in the bond lengths, obtained via the JEDI analysis, as well as the maximum bond lengths before bond breaking decrease with decreasing ring size (Figure 4.6B). A 14-membered chain without a ring, in which two bonds in the middle of the chain are stretched, is used as a reference and it is observed that, with increasing ring size, the maximum bond energies and bond lengths approach the values for the reference system. It is important to note that the energies shown in Figure 4.6B are used exclusively for the stretching of the bonds that ultimately break. Despite the decrease of these energies with decreasing ring size, the total energy needed to break a

carbon-carbon bond (typically between 1.5 and 2 eV) of course does not change when rings of different sizes are placed around a hydrocarbon chain. The torsions of the ring contribute the rest of the energy needed to break the bonds in the chain. As can be seen in Figures 4.5A and 4.6A, these two kinds of modes are coupled and transfers of energy from the torsions of the ring to the bonds in the chain are possible. In other words, the deformation of the ring preconditions the critical bonds in the chain for facilitated rupture. Mechanistically, the transfer of energy from the ring to the chain is a result of the angle bendings in the chain, since, as the angles gradually approach linearity upon stretching, the torsions of the ring can relax and the ring gets "smaller" and less strained. Hence, the bond rupture is a combined effect of bond stretching, angle bending and torsional motions and it is not enough to consider only the mechanochemistry of the scissile bonds in pulling experiments. These observations support the notion that the curved part of the overhand knot, for which the ring is a model, chokes off the chain in its immediate vicinity due to the capability of the torsions to act as work funnels that localize mechanical stress.

In summary, using the JEDI analysis it was found that most mechanical stress is localized in the torsions around the curved part of a knotted polyethylene chain under tensile stress. The bonds at the entry or exit of the knot, one of which ultimately breaks, somewhat surprisingly do not store particularly large amounts of stress energy. Pulling at the ends of the chain rather tightens the knot, which in turn causes the curved structure to choke off the chain in the immediate vicinity of the knot. This effect can be explained by the capability of the torsions in the knot to act as work funnels by effectively localizing the mechanical stress at the entry or exit of the knot and predissociating the bonds in this region. This is the reason why an overhand knot leads to a substantial weakening of a polymer chain. To what extent this observation can be transferred to macroscopic ropes remains unclear. Nevertheless, it is surprising that both kinds of ropes - macroscopic and microscopic - are weakened by an overhand knot by around 50% and rupture occurs at the same position. Moreover, this investigation demonstrates that bonds do not have to be excessively stretched to be broken in mechanochemical reactions. Investigating this effect further could lead to new perspectives in mechanochemical synthesis.

4.2   Calculating the mechanical efficiency of the stiff-stilbene photoswitch

As shown in Chapter 3.3, mechanical energy can be generated by the isomerization of a photoswitch and the efficiency of this conversion can be calculated with the excited state JEDI analysis. In this Chapter, the excited state JEDI analysis is used to compute the mechanical efficiency of the 1-(1-indanyliden)indan photoswitch, hereafter referred to as stiff-stilbene, and to investigate the capability of this photoswitch to rupture covalent bonds. Please note that parts of this Chapter have already been published by Prof. Dr. Andreas Dreuw and myself in *Physical Chemistry Chemical Physics* **2016**, *18*, 15848-15853.

Typically, a plethora of internal modes of a photoswitch changes during isomerization. As a result, the mechanical efficiency of the photoswitch, i.e. its capability to apply forces to its environment and to generate mechanical work during photoisomerization, is generally limited.[262] A method to maximize the mechanical output of a photoswitch is to increase its spatial extension, which in turn maximizes the displacement during isomerization.[205] A further possibility is to modify the size and stiffness of the linkers connecting the photoswitch to its chemical environment. Intuitively, a short and stiff linker is well-suited for an efficient transmission of the mechanical energy from the photoswitch to the mechanophore. Following this approach, it has been possible to facilitate the rupture of a carbon-carbon bond.[139,144,145,206] In particular, the ring opening of cyclobutene was triggered by a combination of heating and the photochemical *cis→trans*-isomerization of stiff-stilbene. For this, stiff-stilbene and cyclobutene were connected via different linkers, the shortest one of which was CH_2-O-CH_2 (Figure 4.7). Formally, the ring-opening of isolated cyclobutene is a retro [2+2] cycloaddition, which in the case of the macrocycle shown in Figure 4.7 is thermally allowed according to the Woodward-Hoffmann rules. The forces stiff-stilbene generates during *cis→trans*-photoisomerization were previously calculated with an approach based on fragments of the macrocycle by arguing that the distance between the carbon atoms of stiff-stilbene to which the linkers are attached is the only relevant coordinate.[139] In Chapters 2.5 and 2.6.1, however, it was shown that single-coordinate descriptions of mechanochemical
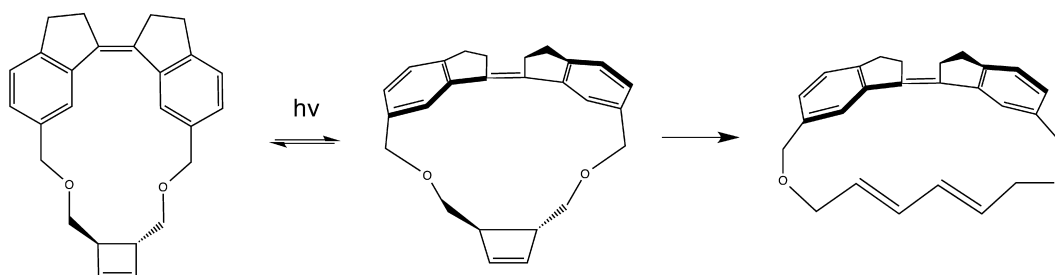
FIGURE 4.7: Photoisomerization of stiff-stilbene was found to facilitate bond rupture in *trans*-3,4-dimethylcyclobutene, thus leading to *trans*,*trans*-2,4-hexadiene. [139,144,145,206]

transformations are highly problematic. Moreover, the calculated forces are limited to approximately 700 pN and little evidence exists that the photoswitch pulls "strong enough" to break the covalent bond in cyclobutene. Indeed, as pointed out by Beyer and Clausen-Schaumann,[2] forces between 2.6 and 13.4 nN are needed to rupture carbon-carbon bonds at room temperature. An alternative explanation is that the energy absorbed by stiff-stilbene during photoexcitation is efficiently converted into heat, which, in combination with conventional heating, of course facilitates the rupture of a bond that is thermally labile by nature.[100,263–269] The significant influence of thermal effects in this reaction has been acknowledged.[206]

In this Chapter, the mechanochemical and thermal effects playing a role in the ring opening of cyclobutene are juxtaposed. Isolated stiff-stilbene, the macrocycle in which stiff-stilbene is connected to cyclobutene as well as fragments of the macrocycle are investigated using the JEDI analysis. It is shown that the mechanical energy transmitted from stiff-stilbene to cyclobutene is far too low to account for the bond breaking and that local heating is the key element in this reaction. Stiff-stilbene does not pull strong enough to break the bond by force alone.

All quantum chemical calculations reported in this Chapter were carried out with the Q-Chem 4.3 program package.[94] Ground state single point calculations, geometry optimizations and frequency calculations were performed at the B3LYP[66,67]/cc-pVDZ[68] level of theory. Geometry optimizations in the electronically excited state were carried out with TDDFT[210] at the same level of theory. Forces were applied with the EFEI method.[89] In the case of *trans*-3,4-dimethylcyclobutene, forces were applied to the carbon atoms of the methyl groups, driving them apart. The same atoms were used in

the case of the macrocycle in which stiff-stilbene is connected to cyclobutene. Forces
needed for bond breaking were determined iteratively.

BOMD simulations under external forces were conducted by adding a constant equal
to the external force to the nuclear gradient in every time step of the BOMD simulation in
the desired direction. In *trans*-3,4-dimethylcyclobutene, the same atoms as in the EFEI
calculations were used as attachment points of the force. The step size in the trajectory
was set to 20 a.u., which corresponds to 0.484 fs. The trajectories were run for a total
of 2500 time steps, so that the total simulation time amounted to 1.2 ps. The initial
velocities for the different temperatures were sampled from a Boltzmann distribution. Of
course, for an accurate description of the processes discussed here, longer simulation times
would be beneficial. However, due to the large amount of temperature/force pairs and the
plethora of trajectories needed for a thorough sampling, this is prohibitively expensive.
The same is true for BOMD trajectories in the electronically excited state (S_1): Further
insights into the connection of photo-mechanical and thermal effects would be gained if
BOMD trajectories of the *cis→trans*-photoisomerization of isolated stiff-stilbene or the
macrocycle in the S_1 state were available, but these calculations are computationally not
feasible.

4.2.1   Isolated stiff-stilbene

To answer the question how strong isolated stiff-stilbene can pull or in other words how
much mechanical work stiff-stilbene can exert in the direction of pulling, the *cis→trans*-
photoisomerization of isolated stiff-stilbene was investigated (Figure 4.8A). The electronic
structure of the excited states of stiff-stilbene has been investigated thoroughly.[270–275]
In the ground state (S_0) minimum, the central dihedral angle θ is 9°, calculated at
the B3LYP/cc-pVDZ level of theory. This value compares favorably with the CASSCF
result (7°) reported in literature.[274] The first excited singlet state (S_1), calculated with
TDDFT, has π-π* character with an anti-bonding interaction along the central double
bond, which facilitates the torsion around the central dihedral angle θ. Indeed, the S_1
state is the relevant state for the *cis→trans*-photoisomerization of stiff-stilbene.[273,274]
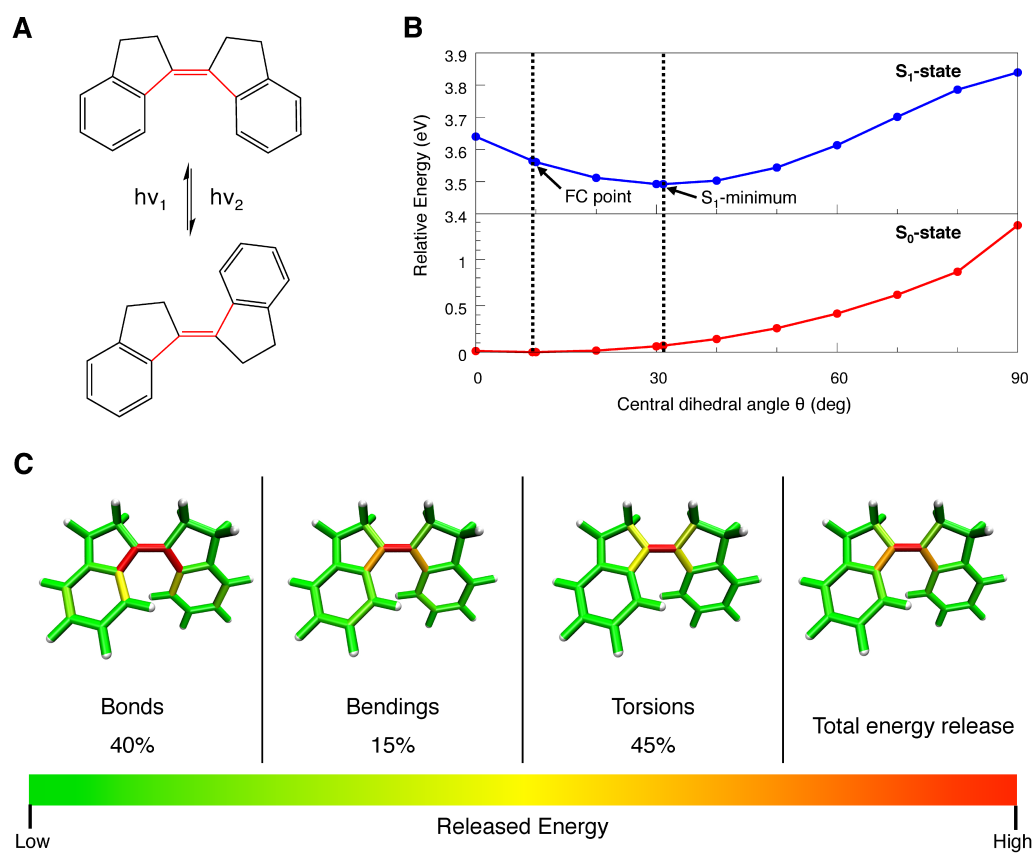
FIGURE 4.8: A) Photoisomerization of stiff-stilbene. The central dihedral angle θ is colored red. B) Relaxed surface scans of θ in the ground (S_0) and first excited singlet (S_1) state. The Franck-Condon (FC) point and the minimum in the S_1 state are indicated. C) Distribution of the energy released during relaxation in the excited state among different kinds of internal modes of stiff-stilbene. Regions in which a high amount of stress energy is released are colored red.

A relaxed surface scan of θ reveals a minimum in the S_1 state with a dihedral angle of 31° (Figure 4.8B), which is somewhat lower than the CASSCF value of 43°.[274]

To judge its switching capability, the JEDI analysis was used to analyze the distribution of the energy released during relaxation of stiff-stilbene in the S_1 state prior to relaxation to the S_1 minimum. Since the harmonic energy difference between the Franck-Condon point and the S_1 minimum overestimates the TDDFT energy difference by only 8%, the harmonic approximation is sufficiently accurate and the JEDI analysis can be applied.

The energy released by stiff-stilbene during relaxation on the S_1 PES can be split among the various kinds of internal modes of the molecule (Figure 4.8C). 40% of the

available energy is assigned to bond length relaxation, 15% becomes available due to changes in the bond angles and 45% is released by the relaxation of the dihedral angles. For stiff-stilbene to rupture the scissile bond in cyclobutene by pulling, only the energy released by the central dihedral angle is relevant, since only this torsional motion leads to a pronounced change in spatial extension of stiff-stilbene. As can be seen in Figure 4.8C, only the central dihedral angles change in the S_1 state, so that 45% of the total mechanical energy available in the excited state, which corresponds to 0.18 eV, is available for this motion, resulting in pulling. Hence, the photochemical efficiency of stiff-stilbene is 45% and the rest of the energy (0.22 eV) is "wasted" on other internal coordinates that change as a side effect of the excited state relaxation but do not contribute to the desired switching function. Also, not the entire energy of 0.18 eV can be transmitted to cyclobutene, as some energy is used to deform the linkers. Hence, this number corresponds to an upper limit of the available mechanical pulling energy. It is important to note that the results discussed here only apply to the first step in the photoisomerization of stiff-stilbene.

4.2.2   Calculations on the macrocycle involving cyclobutene

To estimate the energy used to deform the linkers, the macrocycle in which stiff-stilbene is coupled to cyclobutene (Figure 4.7) was investigated. In the *cis*-isomer of the macrocycle, the central dihedral angle is 7°, which is close to the value of isolated stiff-stilbene (9°, cf. Chapter 4.2.1). In the *trans*-isomer, however, the dihedral angle is 136°, thus differing tremendously from planarity. The consequences of this discrepancy are discussed in Chapter 4.2.3, where an analysis based on fragments of the macrocycle is carried out. The *cis*- and *trans*-conformers of the macrocycle were stretched using the EFEI method. The force was applied to the carbon atoms of the linkers next to the cyclobutene moiety, driving them apart (Figure 4.9). This stretching allows to estimate the strain in the *cis*- and *trans*-macrocycle. At all applied forces the energy of the *trans*-isomer is much higher than the energy of the *cis*-isomer, demonstrating that the *cis*-isomer is most stable. Moreover, 3.3 nN are needed to open the cyclobutene ring in the *trans*-isomer, while 4.15 nN are needed in the *cis*-isomer. The observation that immediately before bond rupture the energy in the *trans*-macrocycle is much higher than in any point of the
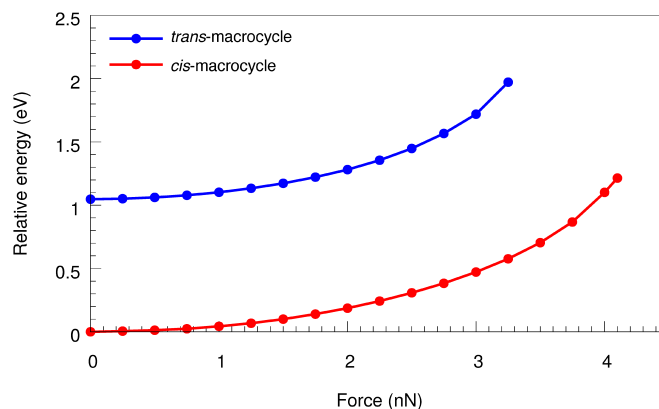
FIGURE 4.9: Stretching coordinates of the *cis*- and *trans*-isomers of the macrocycle in which stiff-stilbene is coupled to cyclobutene. Forces were applied to the carbon atoms in the linker next to the cyclobutene moiety via the EFEI method. The energy of the relaxed *cis*-isomer was defined as zero. The curves are shown until the bond breaking point.

EFEI coordinate of the *cis*-macrocycle shows that a large amount of energy is wasted on the displacement of other modes in the macrocycle that are not involved in the ring opening of the cyclobutene moiety.

If the same EFEI coordinate is scanned in the S_1 state, the situation hardly changes. The bond rupture force in the *cis*-isomer, for example, still amounts to 4.15 nN, demonstrating that the electronic state has only little mechanical influence on the investigated reaction. However, the JEDI analysis cannot be applied in the S_1 state of the macrocycle, since the harmonic approximation is not applicable and leads to an overestimation of the energy by more than a factor of 2. However, it can be observed that the bond in cyclobutene that ultimately breaks is hardly displaced during the initial phase of the *cis*→*trans*-photoisomerization. Instead, several internal coordinates of the linkers are displaced. This strongly suggests that the mechanical pulling energy provided by stiff-stilbene is used to deform the linkers and not to stretch the scissile bond in cyclobutene, at least in the initial part of the photoisomerization.

An interesting question is which part of the macrocycle is initially excited. Exciton analysis[276–278] at the RI-ADC(2)-s level of theory[279–282] reveals that the S_1 state of the macrocycle has 85.1% single excitation character and that the exciton is completely localized on the stiff-stilbene moiety (Figure 4.10). In general, although stiff-stilbene is excited initially, motion along the excited state PES could lead to a situation where the
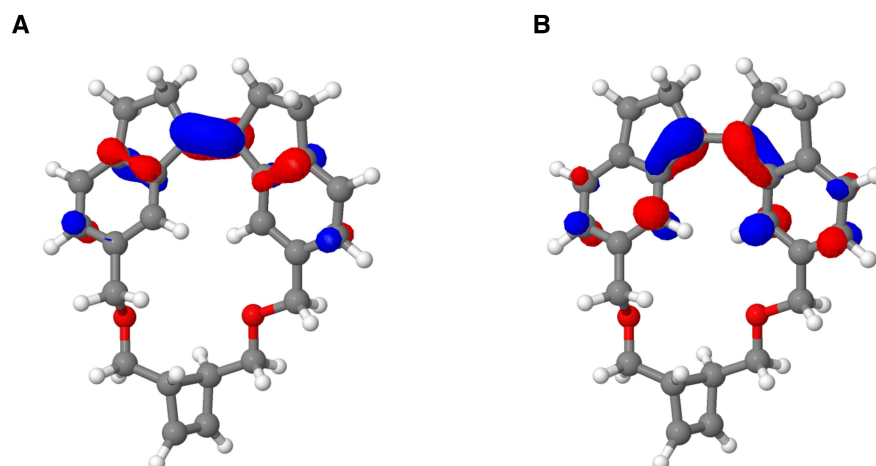
FIGURE 4.10: Natural transition orbitals (NTOs) of the macrocycle in which stiff-stilbene is coupled to cyclobutene, accounting for 78.5% of the excitation into the first electronically excited singlet state (from A to B). The exciton is located on the stiff-stilbene moiety. The pictures were generated using JMol (version 13.0.8). [283]

exciton is located on the cyclobutene moiety, thus potentially weakening the scissile bond. However, this is highly unlikely, since the excitation energy of the isolated cyclobutene moiety is much higher than the one of stiff-stilbene. Hence, a large amount of energy would be needed to transfer the exciton to cyclobutene, which thermodynamically is connected with a very long timescale, much longer than the non-radiative decay of stiff-stilbene. Therefore, this scenario can be discarded.

4.2.3   Fragments of the macrocycle involving cyclobutene

To further corroborate the hypothesis that stiff-stilbene is not strong enough to rupture the bond in cyclobutene by force alone, stiff-stilbene and *trans*-3,4-dimethylcyclobutene fragments were cut out of the different conformers of the macrocycle. This enables the calculation of the strain energies of these fragments as the differences between the single point energies of the fragments and the energies of the optimized molecules (Table 4.1). Remarkably, the computed strain energy of *trans*-3,4-dimethylcyclobutene in the *cis*-isomer of the macrocycle (0.20 eV) is slightly higher than in its *trans*-isomer (0.17 eV). This demonstrates that the conformation of stiff-stilbene is relatively insignificant for the strain of the cyclobutene moiety of the macrocycle, although the linkers are short. In contrast, the strain energy in the stiff-stilbene fragment is significantly higher in
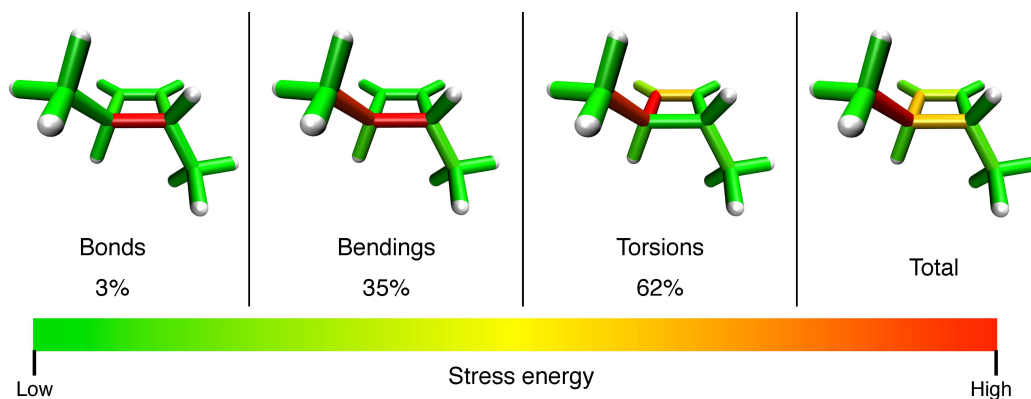
FIGURE 4.11: Ground state JEDI analysis of the *trans*-3,4-dimethylcyclobutene fragment cut out of the *trans*-macrocycle containing stiff-stilbene. All internal modes except for the most relevant coordinates (those modes connecting the methyl groups, i.e. three bonds, two bond angles and a torsion) were relaxed.

the *trans*-isomer of the macrocycle (1.08 eV) than in its *cis*-isomer (0.16 eV), which can be traced back to the significant deviation from planarity of stiff-stilbene in the *trans*-macrocycle. As a result, the total strain of the two fragments in the *cis*-macrocycle is only 0.36 eV in comparison to 1.25 eV in the *trans*-isomer. Hence, any mechanical strain caused by the *cis*→*trans*-isomerization of stiff-stilbene is wasted on the photoswitch itself (and possibly on the linkers) and has no significant effect on the cyclobutene moiety.

The distribution of stress energy in *trans*-3,4-dimethylcyclobutene cut out of the *trans*-macrocycle was calculated with the ground state JEDI analysis (Figure 4.11). For this, all internal modes except for those connecting the methyl carbon atoms (three bonds, two bendings and a torsion) were relaxed. As a result, the deformation of *trans*-3,4-dimethylcyclobutene can be considered a result of an external force, leading to an overestimation of the stress energy by only 2.8%. Remarkably, only 3% of the stress energy, which corresponds to $6 \cdot 10^{-4}$ eV, is stored in the bond that needs to be ruptured

Molecule	Strain (*cis*, eV)	Strain (*trans*, eV)	Strain (ruptured, eV)
cyclobutene	0.20	0.17	-
stiff-stilbene	0.16 (7°)	1.08 (136°)	0.55 (153°)
total	**0.36**	**1.25**	**0.55**

TABLE 4.1: Strain energies in eV for the *trans*-3,4-dimethylcyclobutene and stiff-stilbene molecular fragments of the *cis*- and *trans*-isomers of the macrocycle as well as its isomer in which *trans*-3,4-dimethylcyclobutene is ruptured. For stiff-stilbene, the values of the central dihedral angle θ are given in parentheses. In isolated stiff-stilbene, θ amounts to 9° and 180° for the *cis*- and *trans*-isomer, respectively.

for ring opening of cyclobutene. Although the dependence of the reaction rate on the force is often exponential (cf. Chapter 2.5), this energy is much too low to account for the experimentally observed enhancement of the bond breaking. The observation that hardly any energy is stored in the scissile bond is chemically intuitive, since the "soft" modes (bond angles and torsions) are displaced before the bonds are stretched, which can easily be shown mathematically. Within the harmonic approximation, the energy E is connected to the displacement Δx via

$$E = \frac{1}{2}k(\Delta x)^2 \; . \tag{4.1}$$

The stretching force F is connected to the displacement via

$$F = k\Delta x \; . \tag{4.2}$$

Hence, for a constant stretching force, one can write

$$\Delta x \sim \frac{1}{k} \; . \tag{4.3}$$

Inserting Equation 4.3 in Equation 4.1 establishes a link between the energy stored in a mechanically stretched mode and its displacement:

$$E \sim \frac{1}{k} \tag{4.4}$$

Hence, the higher the force constant, the less energy is stored in it. Although it is not possible to rigorously define force constants for every redundant internal mode in a molecule, the concept shown here illustrates the observation that "soft" modes (dihedral angles, bond angles) are displaced more easily than "hard" modes (single, double, triple bonds) by the same stretching force.
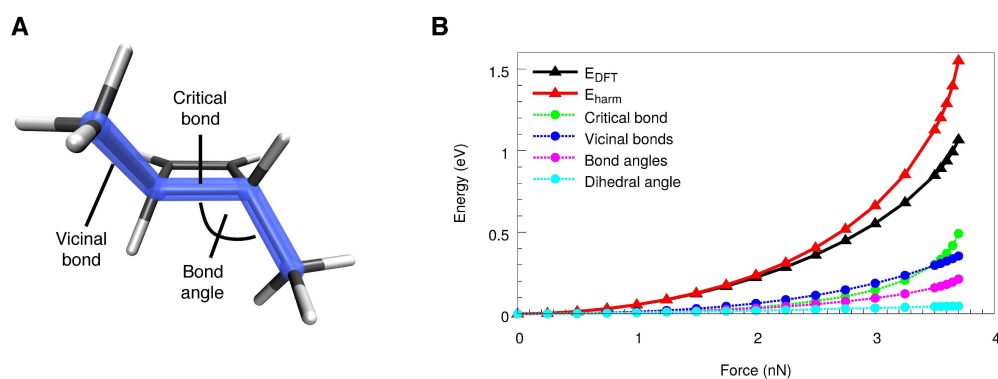
FIGURE 4.12: Ground state JEDI analysis of *trans*-3,4-dimethylcyclobutene. A) "Critical bond" refers to the bond that ultimately breaks, the "vicinal bonds" are those bonds connecting the methyl groups to the cyclobutene ring, the "bond angle" is the angle between these two kinds of bonds and the "dihedral angle" is shown in blue. B) The distribution of stress energy among the internal modes shown in A) throughout the EFEI stretching coordinate. E_{DFT} is the energy difference between the relaxed and the stretched molecule, calculated at the B3LYP/cc-pVDZ level of theory. E_{harm} is the sum of the harmonic energies in every internal mode, calculated with the JEDI analysis.

Furthermore, it is insightful to calculate the loss of strain energy in the macrocycle after bond rupture in *trans*-3,4-dimethylcyclobutene (Figure 4.7). When the cyclobutene ring is opened and *trans,trans*-2,4-hexadiene is generated, the central dihedral angle in stiff-stilbene increases from 136° to 153°, leading to a decrease in strain energy from 1.08 eV to 0.55 eV (Table 4.1). The loss of 0.53 eV, however, is not sufficient to account for the ring opening of cyclobutene, since, according to EFEI calculations, 1.07 eV are needed at the DFT level to open the cyclobutene ring. To analyze the distribution of stress energy in *trans*-3,4-dimethylcyclobutene, an EFEI coordinate was calculated in which the force was applied to the carbon atoms of the methyl groups, driving them apart. In this setup the force vector is not parallel to the bond that ultimately breaks, which decreases the effective force that stretches this bond. This, however, closely mimics the situation in the macrocycle in which stiff-stilbene is linked to cyclobutene. In each point of the EFEI coordinate, the distribution of stress energy among all internal coordinates of *trans*-3,4-dimethylcyclobutene was calculated using the ground state JEDI analysis. Here, the modes shown in Figure 4.12A are of particular interest. The harmonic stress energies of these modes are shown in Figure 4.12B. In the beginning of the stretching coordinate, most energy is stored in the "vicinal bonds", which are those bonds adjacent to the bond that ultimately breaks. The bond angles between these two kinds of bonds and the dihedral angle involving both carbon atoms of the methyl groups also store significant
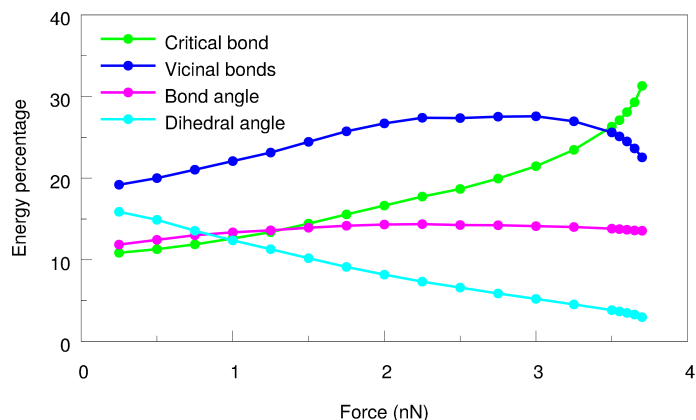
FIGURE 4.13: Distribution of stress energy among the most relevant internal modes of *trans*-3,4-dimethylcyclobutene (cf. Figure 4.12) throughout the EFEI stretching coordinate.

amounts of stress energy. Only at large stretching forces the "critical bond", which is the one that ultimately breaks, stores most stress energy. However, it should be noted that at large forces the harmonic approximation becomes less and less reliable (Figure 4.12B), so that this effect might also be an artifact of the harmonic approximation.

Immediately before bond breaking, the "critical" bond stores only 31% of the total harmonic stress energy (Figure 4.13), which can be considered an upper bound to the real value due to the unreliable harmonic approximation in this part of the stretching coordinate. As such, it is also an upper bound to the mechanochemical susceptibility of cyclobutene itself, since the mechanical energy it receives from stiff-stilbene is not fully passed on to the scissile bond. The limited mechanochemical susceptibility of cyclobutene is mainly due to the poor alignment of the scissile bond and the external force vector in *trans*-3,4-dimethylcyclobutene. This demonstrates that the efficiency of the ring opening reaction is not only limited by the photochemical efficiency of stiff-stilbene but also by the mechanochemical susceptibility of *trans*-3,4-dimethylcyclobutene. The rest of the stress energy is wasted on the displacement of other internal modes in *trans*-3,4-dimethylcyclobutene. This suggests that the photo-mechanical influence of stiff-stilbene is by far not sufficient to account for the observed enhancement of the ring-opening in cyclobutene.

Considering these results, a more reasonable picture is that the energy gained by stiff-stilbene through absorption of a photon is converted into heat by ultrafast non-adiabatic

decay to the ground state, which of course accelerates the dissociation of the thermally labile bond in *trans*-3,4-dimethylcyclobutene. Indeed, depending on the substitution of the cyclobutene ring, only moderate heating is required for bond rupture.[100,263–269] A crude estimate of the local temperature in the system after absorption of a photon can be calculated via $h\nu = n \cdot \frac{3}{2}kT$. The relevant degrees of freedom n can be estimated from the excited state JEDI analysis of isolated stiff-stilbene, in which five bond lengths, two bond angles and four dihedral angles were identified as energetically relevant (Figure 4.8C). The result, $n = 11$, can be considered an upper bound, since the JEDI analysis is based on redundant internal coordinates. Assuming a wavelength of 375 nm for the incident photon[144] and neglecting the fact that the reactant is heated in the experiment, a temperature of 2325 K is calculated in the central part of the stiff-stilbene moiety. Rapid dissipation of the thermal energy in the macrocycle leads to heating of the cyclobutene moiety, thus accelerating bond rupture.

BOMD simulations of *trans*-3,4-dimethylcyclobutene under an external force at different temperatures support this hypothesis. In these simulations, it is found that the force needed to rupture the labile bond decreases with increasing temperature, or, equivalently, the time until bond rupture at a given force decreases with increasing temperature. In the case of 0 K and a force of 2.5 nN that drives the methyl groups apart, for example, bond rupture is not observed at all on the time scale of the simulation (1.2 ps). At 500 K, rupture occurs after 505 fs, while at 900 K this time decreases to 41 fs. The observation that higher temperatures lead to lower rupture forces is consistent with the existing literature.[181,208,209,284]

In summary, the reported calculations suggest that the mechanical efficiency of stiff-stilbene and the mechanochemical susceptibility of cyclobutene are much too low to explain the experimentally observed acceleration of bond rupture upon photoisomerization of stiff-stilbene. Instead, stiff-stilbene acts as a local heater by converting the energy gained by photo-excitation into heat and this energy is dissipated in the macrocycle, which explains the observed acceleration of the cyclobutene ring opening.

It can be speculated that the conversion of light into thermal energy and the capability of the latter to initiate various chemical processes is a general working principle of photoswitches. Azobenzene, for example, can be used to trigger structural changes

in proteins[46–53] and DNA.[54–56] It is reasonable to assume that in these systems, too, the dissipation of thermal energy leads to the observed transitions rather than the increased spatial extension of the photoswitch. Further examples include photoswitches from the spiropyran family, which can also be used to trigger structural transitions in biomolecules.[61] Moreover, in nature the photoisomerization of *p*-coumaric acid and retinal initiate structural changes in proteins, thus constituting the first steps of signal transduction.[213–220,285–287] A possible experimental proof of the presented findings is provided by substituting stiff-stilbene in the macrocycle that includes cyclobutene by a compound that exhibits a high quantum yield of photon absorption and decays non-radiatively while retaining its spatial extension during the entire photocycle. 10-hydroxybenzo[h]quinoline (10-HBQ), for example, or a derivate thereof could be used as a substitute for stiff-stilbene in the macrocycle, since a barrierless intramolecular proton transfer proceeds in the excited state of this molecule.[288,289] If the bond rupture of cyclobutene was still accelerated in this modified macrocycle, further evidence would be found that the dissipation of the thermal energy gained by the absorption of a photon is the key element in the working principle of many photoswitches.

4.3   Forcing strained hydrocarbons to be stable

Strained hydrocarbons have aroused considerable interest since the formulation of Bredt's rule almost a hundred years ago.[290–296] Due to the efforts of chemists to bend and break Bredt's rule, a large number of anti-Bredt compounds have been synthesized. Bridgehead alkenes, for which Bredt's rule was originally formulated, are only one class of well-investigated strained hydrocarbons.[291,293,296] Angle-strained cycloalkynes constitute another class of strained hydrocarbons that has aroused profound experimental interest.[297–300] The $C\equiv C-C$ bond angles in cycloalkynes with small to medium-sized rings deviate significantly from linearity, which leads to a substantial destabilization of the compounds. Cycloheptyne, for example, is prone to dimerization under normal laboratory conditions at room temperature.[296] In dichloromethane, it has a half-life of less than a minute at -25 °C and of an hour at -78 °C.[301–307] Usually, smaller cycloalkynes can only be observed indirectly via trapping reactions, as the compounds isomerize or trimerize

quickly. However, the synthesis of angle-strained cycloalkynes is highly desirable due to their potential use as intermediates in organic synthesis.

In this Chapter, the possibility of stabilizing angle-strained cycloalkynes by using mechanical force is investigated. The aim is to make cycloakynes less prone to isomerization, dimerization or trimerization under normal laboratory conditions. Presumably, a sufficiently large force pulling the carbon atoms adjacent to the triple bond apart leads to a partial linearization of the $C \equiv C - C$ bond angles in strained cycloalkynes. It is shown that an appropriately applied external force can sufficiently linearize the $C \equiv C - C$ bond angles of cycloheptyne to stabilize the molecule significantly (Chapter 4.3.1). Subsequently, various methods to apply such a stretching force permanently are discussed, including Atomic Force Microscopy, ultrasound baths and ball milling techniques (Chapter 4.3.2) as well as the use of the stiff-stilbene photoswitch (Chapter 4.3.3) and the incorporation of cycloheptyne into another strained hydrocarbon (Chapter 4.3.4). Please note that the content of this Chapter is based on a paper by Benjamin Günther, Prof. Dr. Andreas Dreuw and myself, which has been submitted for publication in *The Journal of Physical Chemistry A* and is currently in revision.

All calculations were carried out with the Q-Chem 4.3 progam package[94] using DFT[71,72] and TDDFT[210] at the B3LYP[66,67]/cc-pVDZ[68] level of theory. Geometry optimizations under an external force were conducted with the EFEI method.[89] To analyze the distribution of stress energy in mechanically deformed cycloheptyne, the ground state (cf. Chapter 3.1) and excited state (cf. Chapter 3.3) JEDI analysis was applied.

4.3.1   Isolated cycloheptyne

To assess the possibility of stabilizing cycloheptyne mechanically, the influence of force on the isolated molecule was investigated by pulling the carbon atoms adjacent to the triple bond apart using the EFEI approach (Figure 4.14A). The connection between these carbon atoms is colinear with the triple bond and pulling them apart is expected to decrease the $C \equiv C - C$ bond angles. In relaxed cycloheptyne, the $C \equiv C - C$ bond angles amount to 145.7° at the B3LYP/cc-pVDZ level of theory, which compares favorably
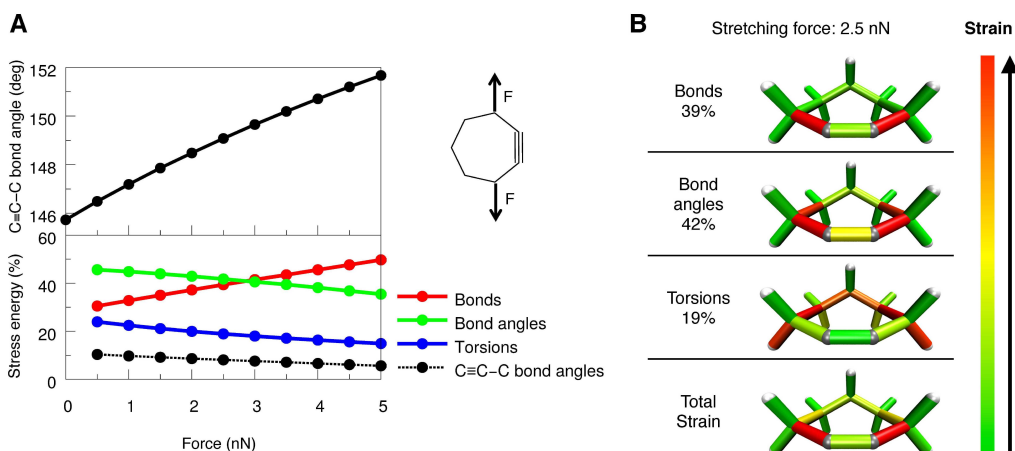
FIGURE 4.14: A) C≡C−C bond angles (top) and distribution of stress energy among different kinds of internal modes (bottom) as a function of external force pulling the carbon atoms adjacent to the triple bond apart in cycloheptyne. B) Color-coded representation of the stress energy stored in each kind of internal mode of cycloheptyne that is stretched by a force of 2.5 nN.

with the experimental value of 145.8° for a derivate of cycloheptyne.[308] Pulling the carbon atoms apart with the EFEI method leads to an increase in the C≡C−C bond angles (Figure 4.14A, upper panel). Within the calculated force range, the changes in bond angles are moderate and do not approach the value for cyclooctyne (154.5°). The latter molecule is stable towards isomerization and dimerization under normal laboratory conditions and enjoys widespread use in organic synthesis.[296,309] While the application of a force indeed leads to a profitable relaxation of the C≡C−C bond angles in cycloheptyne, the other internal modes of the molecule are of course also displaced and therefore exert a restoring force. As a result, the stress energy, calculated with the JEDI analysis, is distributed among numerous internal modes in cycloheptyne (Figure 4.14A, lower panel). The bonds and bond angles in the molecule store most of the stress energy throughout the entire coordinate, while only between 5% and 10% of stress energy is stored in the C≡C−C bond angles. This value can be considered the "mechanochemical susceptibility" of the molecule, since the deformation of the C≡C−C bond angles is of primary interest for the purpose of stabilizing cycloheptyne.

For a stretching force of 2.5 nN, the distribution of stress energy in cycloheptyne is visualized in Figure 4.14B. The bonds and bond angles store almost the same percentage of stress energy (39% and 42%, respectively), and a smaller proportion is attributed to the torsions (19%). Only 8% of the stress energy is stored in the C≡C−C bond

angles. For the stabilization of cycloheptyne it would be beneficial if most stress energy was stored in the C≡C−C bond angles, because then the displacement of these modes would be maximized. This, however, can hardly be achieved, since the internal modes in cyclic molecules are heavily coupled. Therefore, 92% of the stress energy is wasted on the displacement of internal modes that do not contribute to the stabilization of cycloheptyne.

An interesting question is in how far the changes in the C≡C−C bond angles influence the stability and the mechanical strain of cycloheptyne. A well-known method to quantify strain in a molecule is the calculation of reaction enthalpies ΔG in isodesmic and homodesmotic reactions. Isodesmic reactions are hypothetical reactions in which the number of each type of bond is the same on each side of the equation. Isodesmic reactions are typically used to quantify functional group strain.[310] Homodesmotic reactions are a subset of isodesmic reactions, in which, additionally, the number of hydrogen atoms attached to each carbon atom and the number of carbon atoms in each hybridization state are the same on each side of the equation. Homodesmotic reactions can be used to quantify total molecular strain. Here, the contribution ΔG_i of each educt and product i to ΔG in the isodesmic and homodesmotic reactions was calculated via

$$\Delta G_i = \Delta E_{\mathrm{DFT},i} + \Delta E_{\mathrm{ZPV},i} + \Delta H_i - T\Delta S_i \ , \tag{4.5}$$

where $\Delta E_{\mathrm{DFT}_i}$ is the total energy of the optimized molecule i at the B3LYP/cc-pVDZ level of theory, $\Delta E_{\mathrm{ZPV},i}$ is its zero point vibrational energy, ΔH_i is its enthalpy, ΔS_i is its entropy and T is the temperature (298.15K). To calculate the ΔG value of the entire reaction, the ΔG values of the educts were subtracted from the sum of the ΔG values of the products.

The isodesmic and homodesmotic reactions considered here (Figure 4.15A/B) have been used before.[299] However, changes in reaction enthalpies ΔG upon application of an external force for isodesmic and homodesmotic reactions (Figure 4.15C) have not been calculated previously. ΔG calculated in the isodesmic reaction increases with increasing external force. This demonstrates that the functional group strain decreases, since the
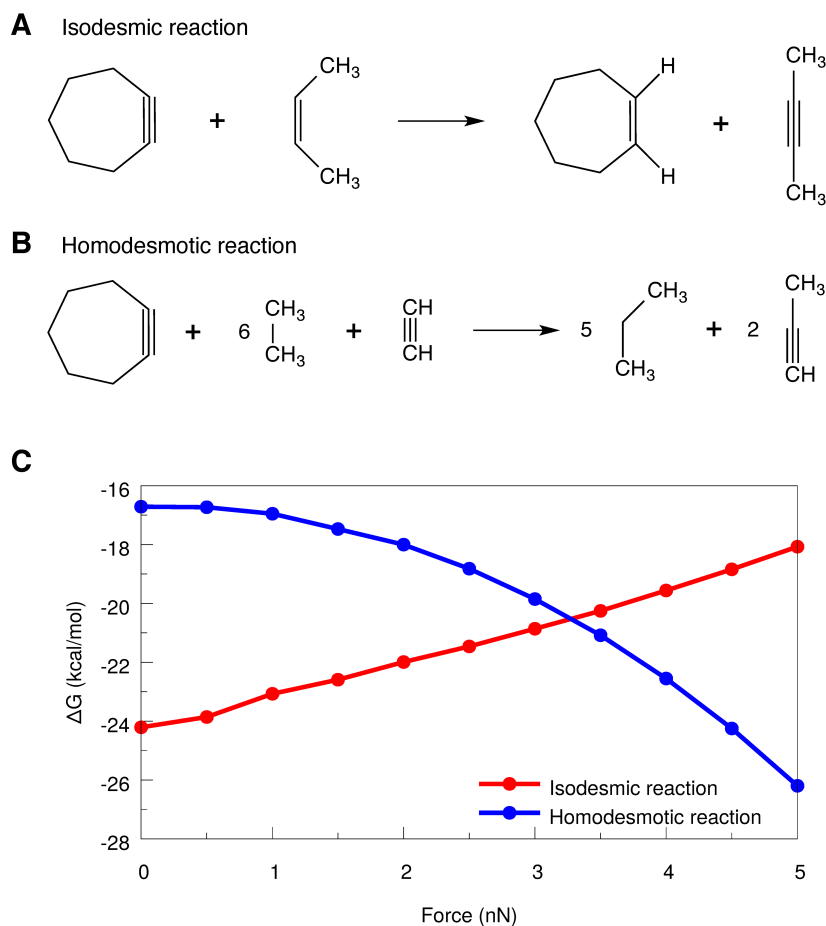
FIGURE 4.15: A) Isodesmic reaction quantifying the functional group strain in cycloheptyne. B) Homodesmotic reaction quantifying the total molecular strain in cycloheptyne. C) Reaction enthalpies ΔG calculated via the isodesmic and homodesmotic reactions of cycloheptyne as a function of the force pulling the carbon atoms adjacent to the triple bond apart.

C≡C−C bond angles relax. Hence, the external force pulling the carbon atoms adjacent to the triple bond apart indeed has a stabilizing effect. The total strain, in contrast, calculated via the homodesmotic reaction, increases with external force. This finding rationalizes the observed low mechanical susceptibility of the C≡C−C bond angles. A large number of other internal modes are deformed upon application of an external force, which counteracts the loss of strain caused by the partial linearization of the C≡C−C bond angles.

4.3.2 Experimental methods for the stabilization of cycloheptyne

Methods that are commonly used to apply mechanical forces to molecules include Single-Molecule Force Spectroscopy (SMFS) experiments using, e.g., an Atomic Force Microscope (AFM), as well as sonochemistry and ball milling or grinding techniques (cf. Chapter 1). For the purpose of stabilizing angle-strained hydrocarbons by stretching, AFM[2] and related techniques[13] are inappropriate, since typically only single molecules are stretched in these experiments. Therefore, it is not possible to generate large amounts of stabilized cycloheptyne molecules that can be used in organic synthesis. Cycloheptyne could, in analogy to mechanophores,[26,60,311–313] be incorporated into a polymer that can be subjected to mechanical forces more easily. However, it is unlikely that the forces needed to stabilize cycloheptyne significantly (in the order of a few nN) can be exerted for a sufficiently long time in an AFM experiment without bond rupture occurring somewhere in the chain.

Sonochemical experiments, which are conducted in ultrasound baths, have also been shown to involve a mechanical component.[20] During the collapse of cavitational bubbles, mechanical forces are generated that can be efficiently transmitted to a mechanophore via polymer linkers and can reach a magnitude of approximately 5 nN in the center of the chain.[314] Although these forces can be used to trigger various chemical processes like bond rupture,[26,311,312,315,316] they are not permanent in that they depend on the amplitude of the ultrasonic wave at a given time and on the growth and collapse of the cavitational bubble. For the stabilization of cycloheptyne, however, permanent forces are needed.

Unfortunately, ball milling or grinding techniques are far too unselective for the desired application. While it is clear that the impact of balls generates local forces at the molecular level,[5,38] until today it is not possible to direct these forces to a specific pair of atoms in a molecule and to sustain them for a sufficiently long time.
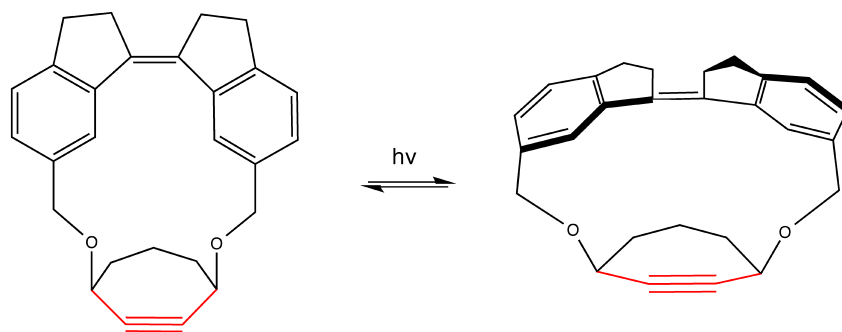
FIGURE 4.16: The *cis-trans*-photoisomerization of stiff-stilbene leads to an increase in spatial extension of the photoswitch. As a result, a constant pulling force is exerted to the carbon atoms adjacent to the triple bond in the cyclobutene moiety. The $C\equiv C-C$ bond angles (red) are expected to be partially linearized.

4.3.3   Coupling cycloheptyne to stiff-stilbene

An alternative method to apply forces is based on the capability of stiff-stilbene to exert forces on its chemical environment (cf. Chapter 4.2). For the purpose of stabilizing cycloheptyne, the idea is to synthesize the macrocycle shown in Figure 4.16, in which cycloheptyne is stabilized by the "mechanochemical protecting group" stiff-stilbene, and subsequently to use the cycloheptyne moiety in the desired chemical reaction. Finally, stiff stilbene can be removed.

The aforementioned change in the $C\equiv C-C$ bond angles with external force (Chapter 4.3.1) suggests an opposite mapping in that an observed angle should warrant conclusions concerning the stretching force, e.g. during $cis\rightarrow trans$-photoisomerization of the stiff-stilbene moiety that is coupled to cycloheptyne. However, this opposite mapping is not straightforward in the case of this macrocycle, since the $C\equiv C-C$ bond angles are not symmetric. To quantify the mechanical work that is transmitted from the stiff-stilbene moiety to cycloheptyne in the macrocycle, it is useful to investigate the first step of the $cis\rightarrow trans$-photoisomerization of the stiff-stilbene moiety in this system. The excited state JEDI analysis underestimates the energy difference between the Franck-Condon point and the minimum in the first electronically excited singlet state (S_1) minimum by only 0.6%, demonstrating that the potential around this minimum can be approximated as harmonic. The S_1 state has $\pi\pi^*$ character with an antibonding interaction along the central double bond of stiff-stilbene, so that the torsion along the central dihedral angle is facilitated. This dihedral angle is -6° at the Franck-Condon point and -29° in
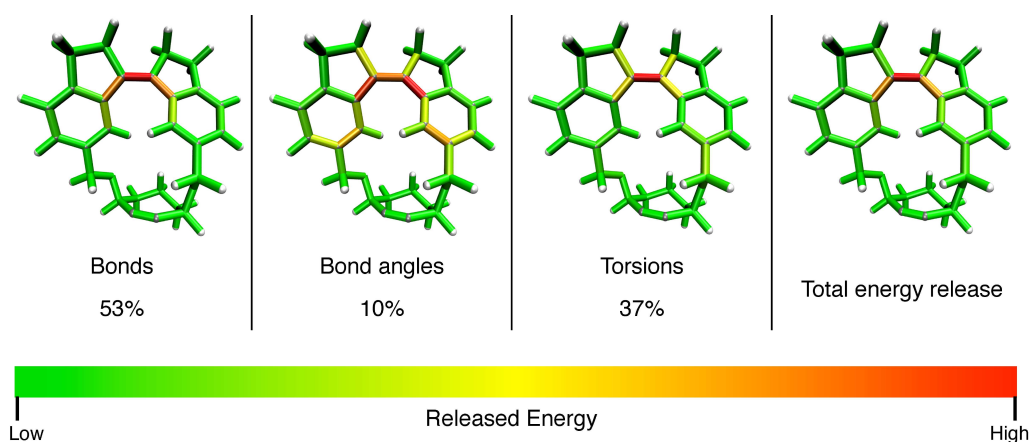
FIGURE 4.17: Distribution of the energy released during the first step of the excited state relaxation of the macrocycle containing stiff-stilbene and cycloheptyne among the different kinds of internal modes.

the S_1 minimum. The energy released upon relaxation from the Franck-Condon point to the minimum in the S_1 state was quantified for each internal mode with the excited state JEDI analysis (Figure 4.17). 37% of the energy released in the excited state is contributed by the torsions, the largest part of which (25.5%) stems from those torsions around the central dihedral angle. Most of the remaining energy is contributed by bond length relaxations in the excited state. These modes, however, are insignificant for the desired switching function, since they do not lead to a substantial increase in spatial extension of the stiff-stilbene moiety or to a linearization of the $C \equiv C - C$ bond angles in cycloheptyne. Hence, the mechanical efficiency of the stiff-stilbene moiety during the first part of the excited state relaxation is only 25.5%.

To gain further insights into the influence of the *cis→trans*-photoisomerization of the stiff-stilbene moiety on cycloheptyne, it is useful to quantify the strain in fragments of the *cis*- and *trans*-conformers of the macrocycle. For this, the strain energies were calculated as the differences between the single point energies of the stiff-stilbene and cycloheptyne fragments cut out of the macrocycle and the energies of the optimized fragments. The results are summarized in Table 4.2. Surprisingly, cycloheptyne has approximately the same strain energy in the *cis*-macrocycle (0.14 eV) and in the *trans*-macrocycle (0.13 eV). Although the difference between these values is beyond numerical accuracy, it can be concluded that the conformation of the stiff-stilbene moiety in the macrocycle has no significant influence on the strain in the cycloheptyne moiety. On the contrary, the discrepancy in strain energies of the different conformers of the stiff-stilbene moiety is

immense: In the *cis*-isomer, the strain energy of stiff-stilbene is only 0.18 eV, since in the macrocycle the central dihedral angle (-6°) is almost the same as in the isolated molecule (-9°). In the *trans*-isomer, on the other hand, the strain energy amounts to 1.07 eV, as the central dihedral angle is -138°. This substantial deviation from planarity is responsible for the enormous strain in the stiff-stilbene moiety in the *trans*-macrocycle. As a result, the total strain, calculated by adding up the strain contributions of the two fragments, amounts to 1.20 eV in the *trans*-macrocycle and to 0.32 eV in the *cis*-macrocycle. This demonstrates that the strain in the *trans*-isomer of the macrocycle is mainly localized on the stiff-stilbene moiety and that the cycloheptyne fragment remains essentially relaxed during photoisomerization.

These results are in agreement with previous observations that the forces generated by stiff-stilbene upon photoisomerization are limited to approximately 700 pN, which is too low to lead to a significant stabilization of cycloheptyne (Chapter 4.3.1).[139] Moreover, the local heating caused by the absorption of a photon and the efficient non-radiative decay, which has been identified as the determining factor in the bond rupture process of cyclobutene in a similar macrocycle (Chapter 4.2) cannot be exploited for the stabilization of strained hydrocarbons, since permanent stretching forces are needed. Finally, it should be pointed out that the stiff-stilbene moiety is excited and not the triple bond in cycloheptyne, so that photochemical rearrangement of the triple bond can be ruled out (Figure 4.18). This result was obtained by exciton analysis[276–278] at the RI-ADC(2)-s level of theory[279–282] with the VDZ basis set and the RI-MP2-VDZ auxiliary basis set.

Fragment	Strain (*cis*, eV) (eV)	Strain (*trans*, eV)
cycloheptyne	0.14	0.13
stiff-stilbene	0.18 (-6°)	1.07 (-138°)
total	**0.32**	**1.20**

TABLE 4.2: Strain energies in eV for the cycloheptyne and stiff-stilbene fragments of the the *cis*- and *trans*-isomers of the macrocycle in which stiff-stilbene is coupled to cyclohepytne. For stiff-stilbene, the values of the central dihedral angle θ are given in parentheses. In isolated stiff-stilbene, θ amounts to -9° and 180° for the *cis*- and *trans*-isomer, respectively.
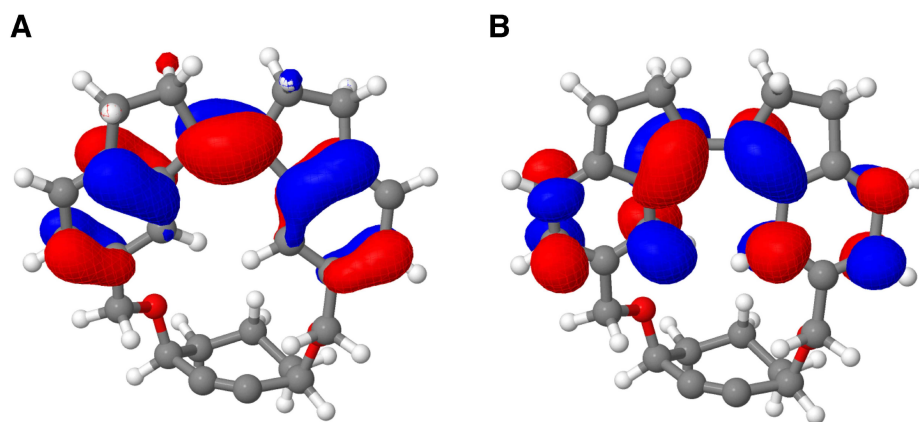
FIGURE 4.18: Natural Transition Orbitals (NTOs) of the macrocycle in which stiff-stilbene is coupled to cycloheptyne, accounting for 77.3% of the excitation into the first excited singlet state (from A to B). The exciton is localized solely on the stiff-stilbene moiety. The pictures were generated using JMol (version 13.0.8).[283]

4.3.4 Coupling cycloheptyne to other strained hydrocarbons

A further possibility of applying pulling forces is the incorporation of cycloheptyne into another macrocycle that exerts force not by photoisomerization but by its own inherent strain. As a first example, a macrocycle is proposed in which cycloheptyne is coupled to a [5]para-cyclophane (Figure 4.19). Depending on the size of the bridge, cyclophanes themselves belong to the class of strained hydrocarbons.[296] A short bridge of five atoms causes the carbon atoms of the benzene ring that are attached to the bridge to bend out of the ring plane. As a result, the heat of formation of [5]para-cyclophane amounts to 53.8 kcal/mol, calculated with semi-empirical methods, which indicates significant strain in the molecule. This strain can be used to partially linearize the C≡C−C bond angles of cycloheptyne. In the macrocycle in which cycloheptyne is coupled to [5]para-cyclophane, the C≡C−C bond angles amount to 149.5°, which lies almost halfway between the value of isolated cycloheptyne (145.7°) and the stable cyclooctyne (154.5°). This demonstrates that coupling [5]para-cyclophane and cycloheptyne leads to a significant stabilization of the cycloheptyne moiety in the macrocycle, since it is the deviation of the C≡C−C bond angles from linearity that leads to the high reactivity of cycloalkynes with small to medium-sized rings. Using the EFEI coordinate of isolated cycloheptyne as a calibration curve (Figure 4.14A), the observed angle of 149.5° suggests that a force of 3 nN is stretching the cycloheptyne moiety apart. Judging from the isodesmic reactions (Figure 4.15), this
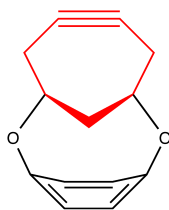
FIGURE 4.19: Macrocycle in which cycloheptyne (red) is attached to a strained cyclophane. The strain of the cyclophane exerts a stretching force on the cycloheptyne moiety, leading to a partial linearization of the C$\equiv$C$-$C bond angles.

corresponds to a significant stabilization of cycloheptyne by approximately 3.5 kcal/mol. In addition, the out-of-plane angles of the carbon atoms that are attached to the bridge in the cyclophane moiety slightly decrease from 26.3° in the isolated [5]para-cyclophane to 25.8° in the macrocycle, suggesting also a minor stabilization of the cyclophane moiety.

In summary it was shown that, while isolated cycloheptyne can indeed be stabilized by a stretching force, the force generated by stiff-stilbene upon *cis-trans*-photoisomerization is too low to lead to a significant stabilization of cycloheptyne. As stiff-stilbene is widely considered one of the "strongest" photoswitches, it can be concluded that the forces generated by photoswitches that are available today are too low to stabilize cycloheptyne significantly. It is possible that future photoswitches will be capable of performing this function, the mechanical efficiency of which can be assessed with the excited state JEDI analysis. A promising perspective is the extension of the spatial dimensions of a photoswitch, which maximizes the displacement during photoisomerization.[205]

In contrast to stiff-stilbene, the coupling of cycloheptyne to cyclophane, which is itself strained, stabilizes the angle-strained cycloalkyne tremendously. The macrocycle shown in Figure 4.19 is only one conceivable molecule in which the inherent strain of two subunits is coupled in such a way that the functional group strain decreases significantly, thus leading to a stabilization of the molecules. In the future, other macrocycles should be investigated, which potentially lead to even greater gains in stability of strained hydrocarbons.

Chapter 5

Molecular force probes

In this Chapter, molecular force probes are introduced, which allow the real time monitoring of mechanical forces in macromolecules. In Chapter 5.1 it is shown that the reduction of point group symmetry upon mechanical deformation enhances the sensitivity of molecular force probes. The incorporation of molecular force probes into proteins is discussed in Chapter 5.2. Prior to this, a brief account of the changes in spectroscopic properties of molecules under an external force is given. This discussion is based on an invited review by Prof. Dr. Andreas Dreuw and myself that has been submitted for publication in *Chemical Reviews.*

If a molecule is subject to an external force, its spectroscopic properties, i.e. absorption and emission wavelengths and intensities, are generally different to the corresponding properties in its relaxed state. The influence of mechanical stress on the vibrational modes of polymers, for example, has been investigated thoroughly several decades ago. A remarkable amount of interest has been devoted to the change in frequency and shape of backbone vibrations of polymers under external load. It was found that the peak shift is generally proportional to external stress and that the low-frequency wing of a vibrational band is often distorted asymmetrically.[317] Using polarized infrared (IR) spectroscopy it was possible to track stress- and orientation-sensitive bands in the IR spectrum and it was found that, as suggested by intuition, those polymer chains that are maximally aligned with the external force are most likely to rupture quickly. In a

recent computational study, the red-shift of a large number of vibrational modes upon mechanical stretching was reported.[106] Conversely, compression was often found to lead to higher wavenumbers, indicating a stiffening of the modes. Although some modes show the opposite behavior, which makes the derivation of general rules difficult, the observed trends are consistent with experiments[318–320] and MD simulations.[321]

Pill and co-workers investigated the change in frequencies and intensities of isotactic 3,5-dimethylheptane under tensile load, which serves as a model system for stretched polypropylene.[90] The authors used the EFEI method to simulate the stretching force and subsequently calculated IR spectra at the deformed geometries. Although anharmonic and thermal effects as well as interactions with the environment were neglected, the study yielded valuable insights into the spectroscopic changes of polymers under a stretching force. In general, vibrational frequencies were found to increase or decrease monotonically with external force. The force dependence of the frequency is pronounced and negative when the vibrations involve large-amplitude motions of the carbon atoms along the polymer backbone, i.e. when they are aligned with the force vector. The authors explained this finding by arguing that stretching reduces the force constant by widening the potential well, which leads to a decrease in vibrational frequency. Conversely, bond stretching vibrations perpendicular to the force vector occasionally exhibit a positive force dependence. In the fingerprint region, however, the force-dependence of many modes was found to be weak. Throughout the entire spectrum, the intensities often change non-monotonically with external force, which the authors trace back to the mixing of modes. In general, it was found that at many points of the EFEI coordinate different modes become nearly degenerate. Lorentzian fits of the calculated stick spectra revealed that peaks may move, split, coalesce, emerge or disappear under external force. This effect complicates the interpretation of experimental spectra under external force. Peak splitting can even lead to the counterintuitive result that a peak can move to higher wavenumbers, even if all contributing modes have negative force dependence. To aid the interpretation of experimental IR spectra, the authors suggest incorporating strong IR chromophores like amides or ester groups into the polymer backbone, since these groups are expected to give strong signals with pronounced negative force dependence.

While the influence of force on vibrational spectra has been investigated in detail, the

mechanically induced changes in UV/Vis spectra have been studied to a somewhat lesser extent. A straightforward approach to explain the change in electronic excitation energies of a molecule is the particle in a box model. In this simplified approach, stretching a molecule is equivalent to an increase in box size. Since the box size appears in the denominator of the energy of a particle in a box, a decrease in energy for all orbitals is predicted upon stretching. A study by Röhrig and co-workers, however, found that this model is too simplistic to account for the intricacies of the changes in spectroscopic properties under mechanical stress.[322] In this study, semi-empirical methods were used to investigate the absorption spectra of organic dyes under tensile stress. A destabilization of the HOMO and a stabilization of the LUMO were observed, with effects decreasing in intensity with increasing size of the π system. In general, changes in the absorption wavelength are particularly pronounced if the binding interactions in the HOMO are distorted tremendously by deformation. The LUMO, however, was found to have a minor influence. Oscillator strengths change significantly if steric hindrance is diminished by stretching.

In addition to IR and UV/Vis spectra, fluorescence spectra also change if a molecule is deformed mechanically. This property is extremely useful and promising for the development of fluorescence force sensors, since the sensitivity of fluorescence spectroscopy makes this method ideal for the detection of forces in molecules. This concept was exploited by Marawske and co-workers, who used a derivative of oligoparaphenylenevinylene (OPV5) with a twisted backbone as a fluorophore and incorporated it into a PVC matrix.[323] Mechanical strain that is transmitted from the matrix to OPV5 induces geometrical changes in the fluorophore. Experiments and semi-empirical calculations demonstrate that fluorescence energies and oscillator strengths increase and fluorescence lifetimes decrease as a function of stretching force. Upon comparison with experiment, it was found that a decrease in fluorescence lifetime of 22 ps and a blue-shift of 1.2 nm in fluorescence wavelength can be unambiguously attributed to mechanical force. Based on these results, mean local forces on a single chromophore between 0.2 and 0.55 nN were calculated. These findings demonstrate the power of molecular force probes in providing insight into forces at the molecular level.
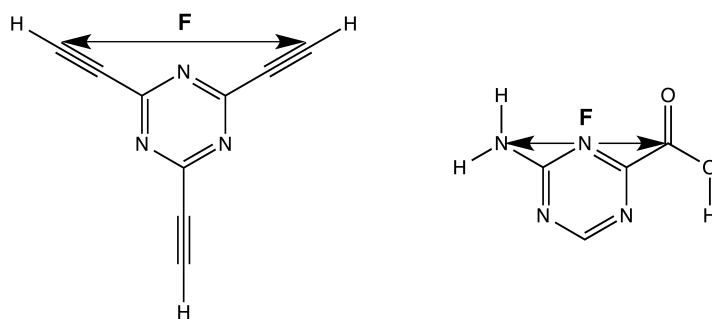
FIGURE 5.1: Structures and EFEI stretching coordinates of D$_{3h}$ symmetric 2,4,6-triethinyl-1,3,5-triazine (left) and C$_s$ symmetric 4-amino-1,3,5-triazine-2-carboxylic acid (right).

5.1   Symmetric force probes

In this Chapter, molecular force probes in which the point group symmetry is reduced as a result of mechanical deformation are introduced. The reduction of point group symmetry leads to significant and characteristic changes in the UV/VIS, IR and Raman spectra of the deformed molecules.[324,325] Beneficially, these spectroscopic changes are reversible and occur even if the applied forces are small. The discussion focuses on D$_{3h}$ symmetric 2,4,6-triethinyl-1,3,5-triazine and C$_s$ symmetric 4-amino-1,3,5-triazine-2-carboxylic acid (Figure 5.1). The mechanochemical behaviors of these force probes were investigated theoretically by applying forces to the molecules via the EFEI method along the coordinates shown in Figure 5.1. The substituents of the triazine scaffold in each of the force probes represent linkers to larger molecules. The ethinyl linkers preserve the scaffold's D$_{3h}$-symmetry, whereas the amino and carboxyl groups break this symmetry. Please note that parts of this Chapter have already been published by Prof. Dr. Andreas Dreuw and myself in *Angewandte Chemie International Edition* **2014**, *53*, 2759-2761.

All calculations reported in this Chapter were carried out using a developer's version of the Q-Chem 4.0.1 program package, in which the EFEI method was implemented.[253] The EFEI calculations and the calculations of the IR and Raman spectra were conducted with DFT at the B3LYP[66,67]/cc-pVDZ[68] level of theory. The IR and Raman spectra were obtained by performing a Lorentzian fit on each of the spectra and subsequently subtracting the spectrum in the equilibrium (F = 0 nN) from the spectrum at each force value. The calculations of the electronic excitations were conducted using TDDFT at

the B3LYP/cc-pVDZ level of theory. The BOMD calculations were carried out using B3LYP/cc-pVDZ as the electronic structure method. The optimized geometry was used as the starting structure. In total, 5000 time steps were calculated with a step size of 20 a.u. (0.484 fs) each, so that the total simulation time amounts to 2.42 ns. To avoid loss of symmetry due to random vibrations caused by asymmetric initial nuclear velocities, derived, e.g., from a Maxwell-Boltzmann distribution, the initial velocities of the nuclei were set to zero. The trajectories were simulated at room-temperature (298K). As in the case of the static EFEI calculations, forces were included by adding a constant to the nuclear gradient of the appropriate atoms in every time step. In every fifth time step of the BOMD simulation, the electronic excitation energies into the five lowest excited singlet states were calculated.

5.1.1   Absorption spectra

Mechanical deformation (stretching or compressing) causes a change of excitation energies of the four lowest excited singlet states of the D_{3h} symmetric force probe (Figure 5.2A). In the equilibrium (F = 0 nN), the second and the third excited singlet states (S_2 and S_3) are degenerate (4.14 eV), because all orbitals that play a role for the excitations into the S_2 and S_3 states in the equilibrium geometry belong to two-dimensional irreducible representations of D_{3h}. As soon as the molecule is stretched or compressed, however, the original D_{3h} symmetry is broken and the molecule assumes a C_{2v} symmetry. Consequently, the degeneracy of S_2 and S_3 is lifted, since the point group C_{2v} does not include any two-dimensional irreducible representations. In the course of the deformation coordinate, the energies of virtually all states decrease in energy. An exception is the S_4 state, which increases in energy if compressive forces are applied.

The excited singlet states of the C_s symmetric force probe, in contrast, are not degenerate in the equilibrium geometry (Figure 5.2B). The C_s symmetry of the molecule, which does not include any two-dimensional irreducible representations, is never broken during the entire deformation coordinate. The electronic excitation spectrum of the force probe is influenced only slightly by mechanical stress: The S_2 state increases minimally in energy when the molecule is compressed, while the energies of the S_3 and S_4 states
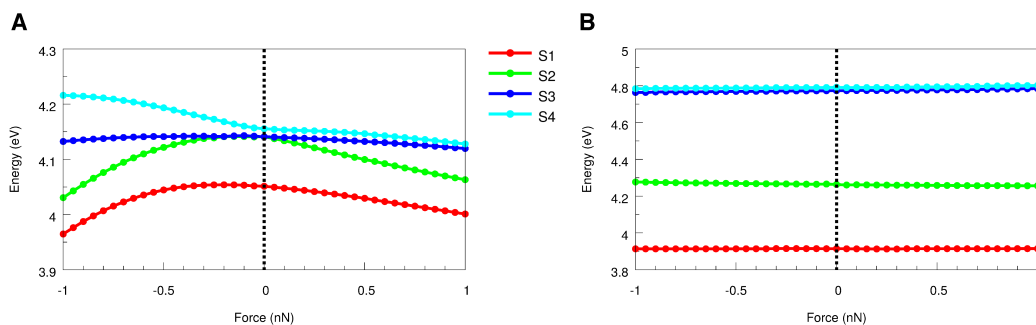
FIGURE 5.2: Excitation energies into the four lowest excited singlet states (S_1-S_4) of the D_{3h} symmetric (A) and the C_s symmetric (B) force probes as a function of external force. Stretching forces are denoted by a positive sign, compressive forces by a negative sign.

increase slightly as a result of tensile stress. The changes in spectroscopic properties are much more pronounced in the D_{3h} symmetric force probe, which demonstrates that the reduction of point group symmetry is a useful feature for molecular force probes.

Considerations concerning the symmetry of a molecule allow the prediction of the change of energetic degeneracies in the course of the deformation coordinate. However, no reliable assumptions can be made *a priori* whether the electronic excitation energies increase or decrease as a result of the mechanical deformation in either of the two force probes. The particle in a box model is, despite its oversimplification documented in literature,[322] often applied for the description of the spectroscopic changes of a molecule under tensile stress. In this model, the compression of a molecule is equivalent to a reduction of the size of the box. Hence, compressive stress is predicted to bring about an increase in the energies of the electronic eigenstates. Consequently, the energy differences between the states are predicted to increase, resulting in a blue-shift of the absorption spectrum. However, the opposite can be observed in the S_1, S_2 and S_3 states of the D_{3h} symmetric force probe. This demonstrates that the particle in a box model is too simplistic to describe the changes in the electronic excitation spectra occurring during mechanical deformation, at least in the cases considered here.

To investigate the time-dependence of the influence of an external force on the geometry and the excitation energies of the D_{3h} symmetric force probe, BOMD calculations and subsequent calculations of the excitation energies into the five lowest singlet states for every fifth time step were carried out (Figure 5.3). The structural oscillations featured in
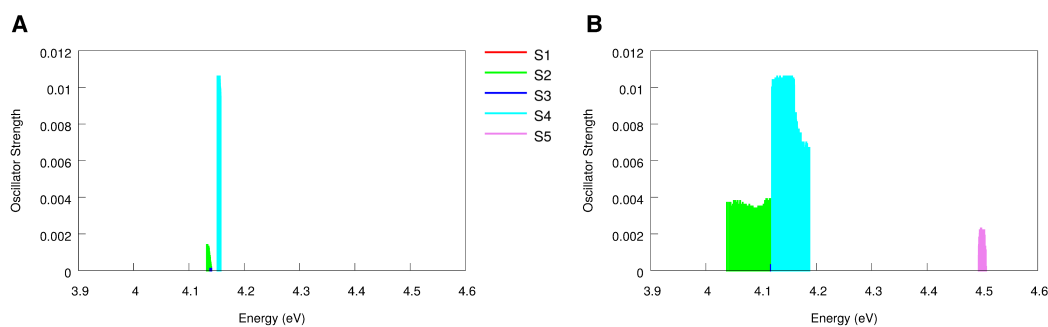
FIGURE 5.3: Absorption spectra including the five lowest excited singlet states of the D_{3h} symmetric force probe under external forces of A) 50 pN and B) 500 pN during BOMD simulations.

BOMD trajectories give rise to peak broadening of the absorption spectra. If a constant stretching force of 50 pN is applied to the ethinyl groups, the distance between the carbon atoms oscillates around an average value of 6.88 Å (6.85 Å in the equilibrium) with an amplitude of 0.05 Å. Therefore, the peak broadening is relatively weak and the average energies of the S_2 and S_4 states are 4.13 eV and 4.15 eV, respectively. If a force of 500 pN is applied, the distance between the ethinyl carbon atoms oscillates around an average value of 7.05 Å with an amplitude of approximately 0.35 Å, which causes pronounced peak broadenings with the average energies of the S_2, S_4 and S_5 states amounting to 4.09 eV, 4.14 eV and 4.50 eV, respectively. The significant peak broadening that arises from external forces and the increase in the oscillator strengths of the S_2 and S_5 states with increasing forces are beneficial properties of the D_{3h} symmetric force probes. These effects can be exploited in the interpretation of experimental spectra obtained with the use of the molecule as a force probe.

5.1.2 Infrared and Raman spectra

In addition to the electronic excitation spectra, IR and Raman spectra also change as a result of tensile stress and the reduction of point group symmetry is again identified as a beneficial feature (Figure 5.4). Moreover, IR and Raman spectra are more sensitive to mechanical deformation than electronic excitation spectra. Imposing only minor tensile stress on the D_{3h} symmetric force probe via the EFEI approach causes a pronounced shift of IR and Raman intensities. In the IR spectra, a number of different phenomena are observed as a result of tensile stress. The signal at 2232 cm^{-1}, for example, which is
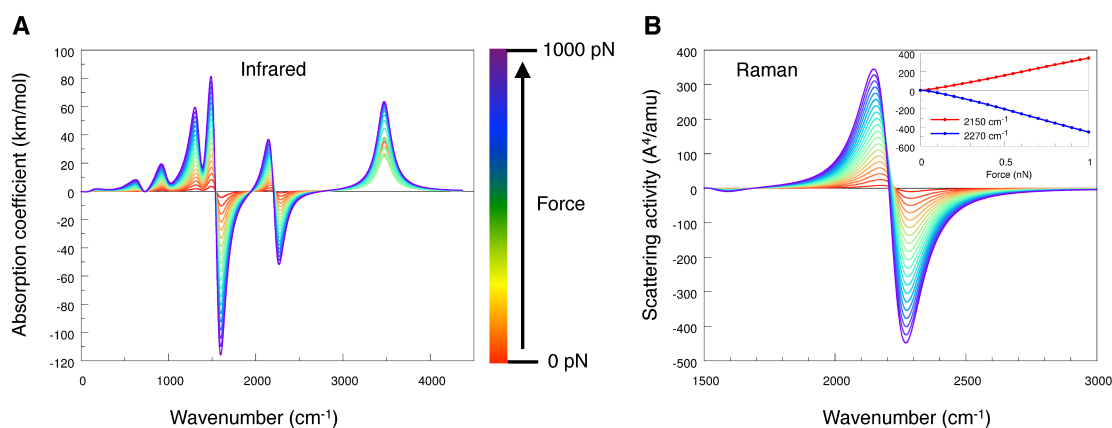
FIGURE 5.4: A) Infrared and B) Raman difference spectra of the D_{3h} symmetric force probe under an external force (with Lorentzian fitting). At each point of the stretching coordinate, the spectrum at the equilibrium geometry was subtracted. The relative Raman scattering activities at 2150 cm^{-1} and 2270 cm^{-1} are shown as a function of force (inset of B).

degenerate in the force-free equilibrium geometry and is characterized by asymmetric stretching motions of the ethinyl moieties, splits up and moves into the direction of smaller wavenumbers as soon as minor tensile stress is applied. Hence, in the region above 2232 cm^{-1}, the contribution of this signal to the overall Lorentzian spectrum is negative, whereas a positive contribution is found below 2232 cm^{-1}.

The force-induced changes in the Raman spectra are even more pronounced than in the case of the IR spectra. The only significant contribution is made by the signal 2232 cm^{-1} (see above), which is strongly Raman active. While the splitting of this signal causes the same qualitative results as in the IR spectra, the shift in intensities is much more pronounced. This profitable feature makes the D_{3h} symmetric force probe particularly promising for experimental studies. Incorporating the molecule into polymers or proteins in folding and unfolding experiments allows to tune a laser to 2150 cm^{-1} and monitor the distinct linear increase in intensity in real-time as soon as minor forces impose tensile stress on the force probe (Figure 5.4B, inset).

In summary, a unique ansatz for the combination of mechanochemistry and optical spectroscopy was introduced by proposing a novel kind of molecular force probe that makes use of the change of spectroscopic properties as a result of mechanical deformation. The changes in electronic excitation energies as well as IR and Raman spectra is brought about by the reduction of point group symmetry. The theoretical methodology described

here paves the way for the rational design of new kinds of molecular force probes, which can potentially be used in Single-Molecule Force Spectroscopy (SMFS) experiments. These kinds of experiments can be applied in order to gather information on the forces acting in specific regions of biomolecules, e.g. during folding processes in living cells, which is only possible because of the high sensitivity of the force probes. The relevant forces occurring in biological systems are in the magnitude of several hundred pN[2] and the D_{3h} symmetric test molecule delivers pronounced spectroscopic responses in this regime. Approaches to identify the direction of the external force and efforts to incorporate force probes into macromolecules without disturbing their natural fold are described in the following Chapter.

5.2   Protein force probes

Protein folding is the process in which proteins spontaneously transition from a disordered geometry to a well-defined tertiary structure.[326–335] This enables them to fulfil a plethora of tasks in biological systems. Despite its fundamental role in biology, our insights into the underlying principles of protein folding are still limited. During the past few decades, however, it has become apparent that forces play a major role in both folding and unfolding events.[11,17,157,336–342] Nevertheless, a comprehensive theory linking the propagation of mechanical force through proteins to real-time folding and unfolding events is unavailable to the present day. To gain insights into the mechanism of protein folding and unfolding and to fully understand the role of mechanical forces in these processes, detailed information on the magnitudes and directions of forces acting in different regions of proteins during structural transitions is required.

One way to acquire such information is to incorporate FRET sensors into proteins. Upon deformation, changes in the separation between donor and acceptor lead to spectroscopic signals that yield insights into mechanical stress within the molecules.[343–347] However, FRET sensors are large and typically distort the protein structure significantly, so that measurements on the protein in its native state are impossible. Therefore, smaller, less invasive force probes have been developed, which can be incorporated into larger

molecules and allow real-time spectroscopic monitoring of forces acting in these systems (see also Chapter 5.1).[324,325,348,349]

In the case of proteins, a number of requirements have to be fulfilled so that a molecule can be used as a force probe: (1) The application of mechanical force to the force probe should lead to pronounced changes in its spectroscopic properties, i.e. absorption wavelengths and peak intensities. (2) These changes should depend on the direction of the external force. Hence, the force probe should best be part of the protein backbone, so that forces both along the backbone and perpendicular to it can be detected. (3) The spectroscopic signal of the force probe should be visible in the presence of the entire protein spectrum, i.e. it should not be overlapped and thereby hidden by other strong signals. (4) The incorporation of the force probe into the protein should not affect the secondary and tertiary structure of the protein and, ideally, the folding pathway should remain unchanged. Hence, small molecules are preferred that, if possible, preserve the number of hydrogen bonds between neighboring strands. Considering these goals, it becomes apparent that molecular force probes should preferably be incorporated into the protein backbone of β-sheet domains. α-helices, in contrast, are less suitable for the incorporation of force probes, since these secondary structure elements consist of very densely packed amino acids and any substitution of an amino acid by a force probe would inescapably lead to a loss of secondary structure.

Based on these considerations, two non-natural amino acids (Figure 5.5A) are proposed that can be used as force probes when they are incorporated into the backbone of a β-sheet in a protein.[350] Each of these force probes replaces two arbitrary amino acids in the protein backbone. Spontaneous unfolding is prevented by stabilization through hydrogen bonds (Figure 5.5B and C). In the following, it is shown that application of force leads to pronounced changes in the infrared and Raman spectra of the force probes. The spectroscopic signals of the force probes can be further intensified and shifted to a transparent window in the protein spectrum by isotopic substitution to make the changes in the spectrum of the force probe observable. Please note that parts of this Chapter have already been published by Marvin T. Hoffmann, Prof. Dr. Andreas Dreuw and myself in *ChemPhysChem* **2016**, *17*, 1486-1492.
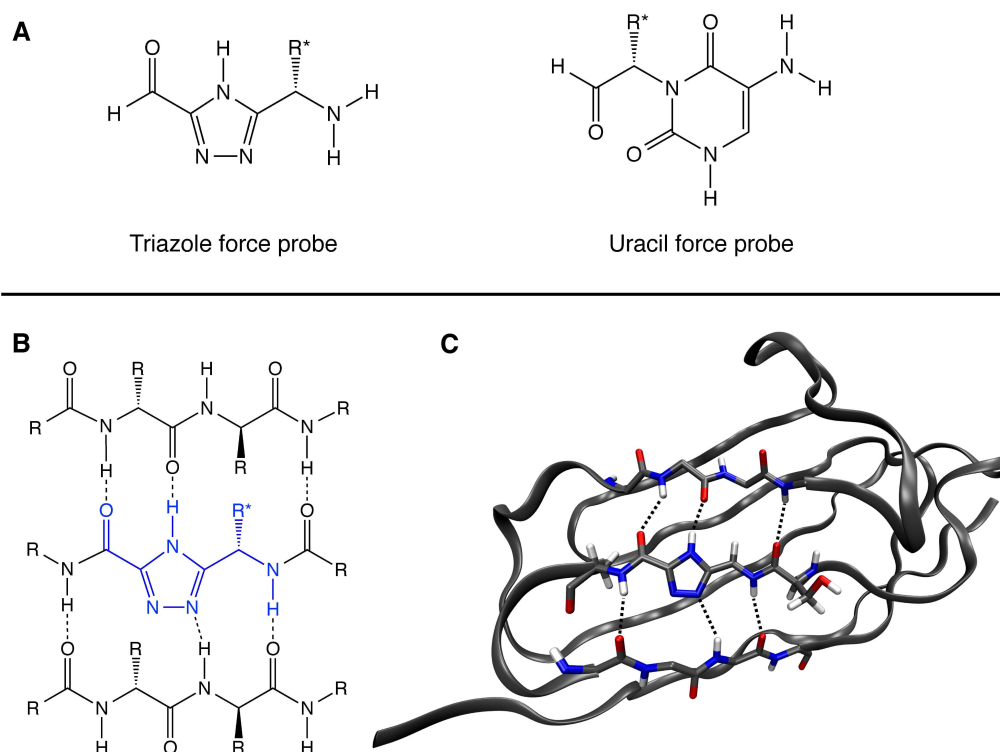
FIGURE 5.5: A) Two molecular force probes based on triazole and uracil are proposed. B) Incorporating the triazole force probe into a β-sheet preserves the number of hydrogen bonds between the strands, which is a favorable factor for the stability of the protein. C) Graphical representation of the triazole force probe mutant of immunoglobulin Ig27 from the giant muscle protein titin (PDB code: 1TIT.pdb). Most amino acid side chains are omitted for clarity.

For a first proof-of-principle, the force probes are incorporated into the representative immunoglobulin module Ig27 from the I-band of the highly repetitive muscle protein titin (PDB code: 1TIT.pdb, Fig. 5.5C).[351,352] The immunoglobulin modules play a crucial role in the elasticity and extensibility of muscles.[353–355] Ig27 consists of two packed β-sheets and has been used previously to detect forces in proteins during unfolding.[17,157,339,341] The triazole force probe replaces phenylalanine F72 and glutamine Q73 (R* = benzyl, Fig. 5.5A) and the uracil force probe replaces leucine L58 and isoleucine I59 (R* = hydrocarbon side chain of ILE). This demonstrates that the force probes can be inserted at different places in a protein, as long as they are part of the backbone of a β-sheet.

MD simulations of the Ig27 force probe mutants were conducted to assess their stability. All MD simulations were conducted with the GROMACS 4.5.5[356] program package. The force field parameters for the force probes are available in the AMBER03

force field[357–359] and were processed with the antechamber[360] and ACPYPE[361] tools. The native proteins and the mutants were placed in a cubic box with at least 1 nm distance between the protein and the edge of the box. Periodic boundary conditions were used in all cases. The proteins were solvated in water (SPC/E) with a concentration of 100 mM NaCl. Prior to production simulations, energy minimizations of the proteins in solution were conducted with the steepest descent algorithm and an energy minimization tolerance of 1000 kJ/mol/nm. Furthermore, equilibration runs under NVT and NPT ensembles were carried out with the leap-frog integrator for 100 ps each with a step size of 2 fs. A temperature of 300 K was adjusted with the modified Berendsen thermostat. In the NPT ensemble, Parrinello-Rahman pressure coupling (1 bar) was applied. The production MD simulations were run for 12 ns. The leap-frog integrator with a step size of 0.5 fs was used. In all simulations, oscillations of the hydrogen atoms were suppressed to allow larger step sizes and longer simulation times. The same temperature and pressure coupling parameters as in the NPT equilibration runs were used.

Moreover, model systems of the force probes were developed (Figure 5.6), which allow the application of forces in different directions via the quantum chemical EFEI approach. The corresponding infrared and Raman spectra along the stretching coordinates were calculated. All calculated stick spectra were convoluted with a Lorentzian function with a HWHM of 100 cm^{-1}. All DFT calculations were carried out at the B3LYP[66,67]/aug-cc-pVDZ[68,77] level of theory as implemented in the Q-Chem 4.0.1 program package.[253] This method was chosen because it delivered reliable results in a benchmark against experimental infrared spectra.[362] With the EFEI method, different forces were applied along various stretching coordinates in the force probe model systems. For stretching the force probes along the backbone, forces up to 1000 pN were applied to the methyl groups next to the force probes with a step size of 50 pN (atoms 3 and 6 in triazole, uracil and the unsubstituted system, Figure 5.6). For stretching the hydrogen bond in triazole, atoms 8 and 9 were pulled apart until rupture with a step size of 10 pN. In uracil, forces were imposed on atoms 7 and 10 and simultaneously on the atoms 8 and 9. Since the forces on the hydrogen bonds are additive, the step size amounts to 20 pN. With these stretching coordinates, the application of forces to the hydrogen atoms was avoided and instead the backbones were pulled apart.
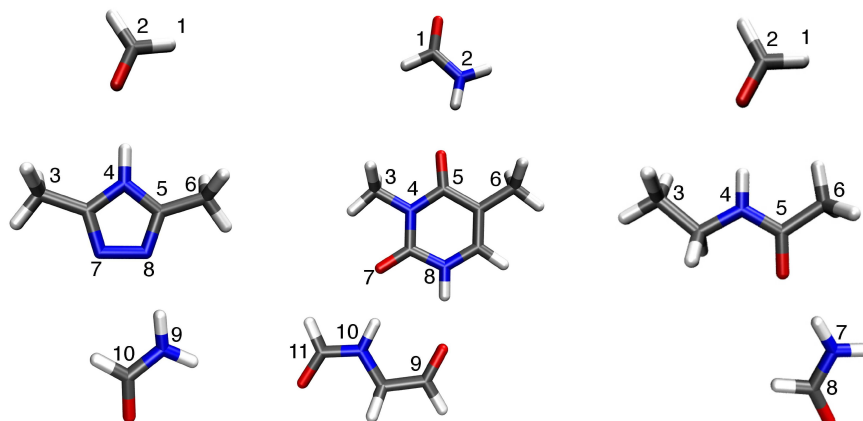
FIGURE 5.6: Numbering scheme of the force probe (left and middle) and unsubstituted (right) model systems used for defining the stretching coordinates and the torsional constraints.

In all DFT calculations, additional constraints were imposed to keep the model systems planar to better simulate the β-sheet environment. In the case of triazole, the dihedral angle of the atoms 1, 2, 4 and 5 were fixed at $0°$. In addition, the dihedral angle of the atoms 7, 8, 9 and 10 was set to $0°$. In the uracil model system, the dihedral angle of the atoms 1, 2, 5 and 4 was fixed at $0°$ and the dihedral angle of the atoms 3, 4, 10 and 11 was set to $0°$. In the unsubstituted system, the dihedral angle of the atoms 1, 2, 4 and 5 was fixed at $0°$ and the dihedral angle of the atoms 4, 5, 7 and 8 was set to $0°$.

5.2.1 Molecular Dynamics simulations

Since the force probes are incorporated into a β-sheet and hydrogen bonds are formed between the strands, the secondary structure elements of the native protein are preserved and the protein remains in its folded form. In the course of the MD simulation, the RMSD quickly reaches a plateau for both the native protein and the force probe mutants and remains largely constant throughout the rest of the simulation, revealing only minor structural fluctuations of the protein (Figure 5.7A). This view is supported by the temporal progression of the radius of gyration, which measures the distance between the protein's center of mass and its termini (Figure 5.7B). The radius of gyration stays practically constant during the simulation, thus indicating structural stability. Moreover,
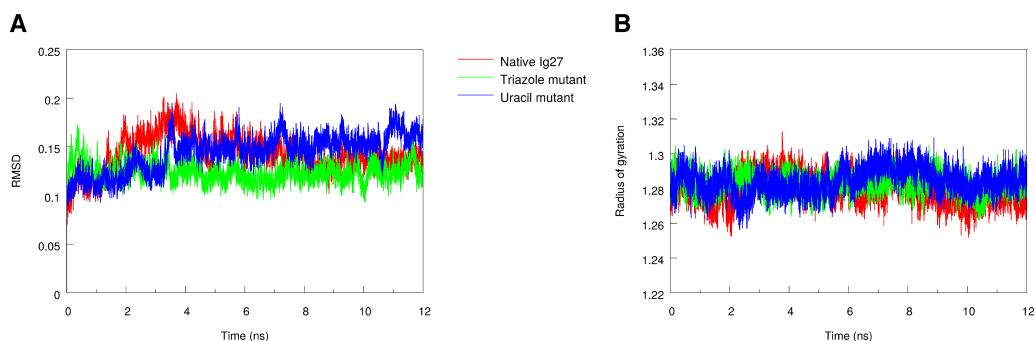
FIGURE 5.7: A) Temporal progression of the RMSD in the course of the MD simulation for the native protein and the force probe mutants. B) Temporal progression of the radius of gyration, which is a measure of the distance between the protein's center of mass and its termini, during the same trajectories.

the levels of structural compaction are similar for the native protein and for the force probe mutants, because the values for the radii of gyration are of the same magnitude. Clearly, these MD simulations cannot shed light on the question whether the folding pathways remain unchanged upon incorporation of the force probes. Nevertheless, this discussion demonstrates that the incorporation of the triazole or uracil force probe in the backbone of a β-sheet domain does not impair the structural stability of a protein.

5.2.2   The triazole force probe

To assess the spectroscopic changes that occur when mechanical force is applied to the force probes, molecular model systems that can be treated quantum chemically were developed (Figure 5.8A). Despite this drastic reduction of system size, which is necessary for accurate calculations of the stretching coordinates and the IR and Raman spectra, all hydrogen bonds that connect the force probes to neighboring strands in the β-sheet are retained in the model systems. In contrast to the work reported in Chapter 5.1, no significant changes in the UV/VIS absorption spectra can be observed, which can at least partly be explained by the fact that mechanical deformation does not lead to a reduction of point group symmetry. Hence, the further discussion focuses on the calculation of infrared and Raman difference spectra.

When the triazole force probe model system is stretched along the backbone, significant changes in the IR and Raman spectra are observable (Figure 5.8B). It is convenient
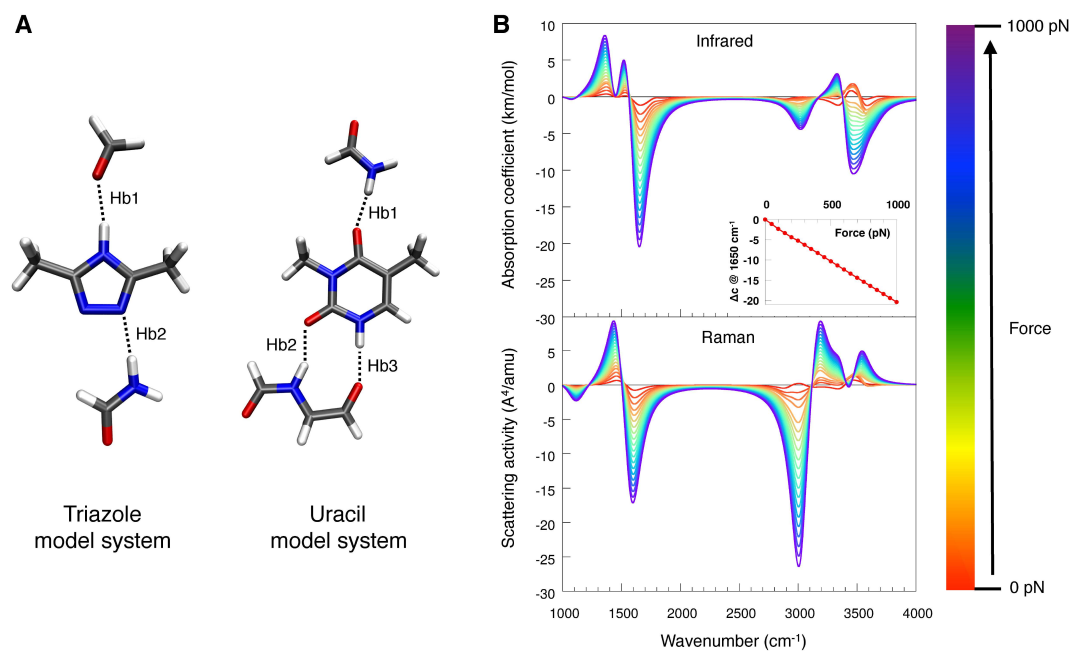
FIGURE 5.8: A) Model systems of the triazole and uracil force probes used in the quantum chemical calculations of the EFEI stretching coordinates and the IR and Raman spectra (Hb = hydrogen bond). B) Changes in the IR and Raman spectra of the triazole model system upon stretching along the backbone. In each point of the EFEI coordinate, the spectrum at the equilibrium structure is subtracted. The calculated stick spectra are superimposed with a Lorentzian function with a HWHM of 100 cm^{-1}. Inset: The infrared absorption coefficients at 1650 cm^{-1} decrease linearly with increasing pulling force.

to discuss changes in the IR absorption coefficients rather than the intensities of particular vibrational transitions, since the former quantities are independent of the experimental setup, i.e. the intensity of the incident light, the concentration of the sample and the length of the sample cell.[363] The differences in these absorption coefficients are generated by subtracting the convoluted spectrum of the equilibrium structure from the spectrum at each point along the stretching coordinate. As can be seen in Fig. 5.8B, these quantities change linearly with the external force. At 1650 cm^{-1} in the IR spectrum, for example, the convoluted absorption coefficients decrease linearly with increasing force. Remarkably, it is not the absorption coefficients themselves that show a linear decreasing behavior, but rather the energies of the transitions in this region (e.g. the symmetric C=N stretching in the ring or the C−N−H angle bending in the ring, cf. Figure 5.9). The reason is that, within the harmonic approximation, the energy is proportional to the restoring force. As a result, the corresponding peaks move to the left with increasing force and a decrease in the absorption coefficients can be observed. Hence, the triazole force probe
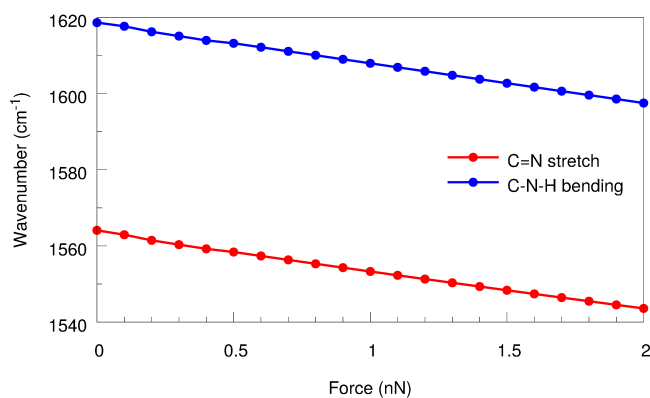
FIGURE 5.9: Wavenumbers of characteristic vibrations in the triazole model system upon stretching along the backbone.

can act as a "force ruler". This effect can prove advantageous in experiments, since a laser can be tuned to 1650 cm^{-1} and the forces acting in the region where the force probe is incorporated can be monitored in real-time. Analogous effects can be observed for the uracil force probe.

Changes in absorption coefficients upon stretching along the hydrogen bonds that connect the force probe to the other strands in the β-sheet are particularly pronounced. Pulling the different strands in the triazole model system apart along, e.g., hydrogen bond 2 (Figure 5.8A) leads to considerable changes in absorption coefficients in the region around 3400 cm^{-1} (Figure 5.10A). Prior to rupture of the hydrogen bonds at forces larger than 250 pN, the absorption coefficients change almost linearly with external force. These changes can be attributed to the elongation and the "weakening" of the hydrogen bonds.

The changes in the absorption coefficients can be intensified by substituting the nitrogen atom in the triazole ring that is involved in hydrogen bond 2 by ^{15}N (Figure 5.10B). This effect can be explained by an increase in the absorption coefficients of the vibrational mode located at approximately 3400 cm^{-1}, which consists of the ^{14}N$-$H stretching motion in the neighboring backbone chain that forms a hydrogen bond to the ^{15}N atom in the triazole ring. Intensifying the absorbances of vibrational transitions in this manner is a useful approach for experiments, since the measurements are facilitated by the improved signal-to-noise-ratio. It is noted in passing that stretching the triazole model system along hydrogen bond 1 also leads to pronounced spectroscopic changes.
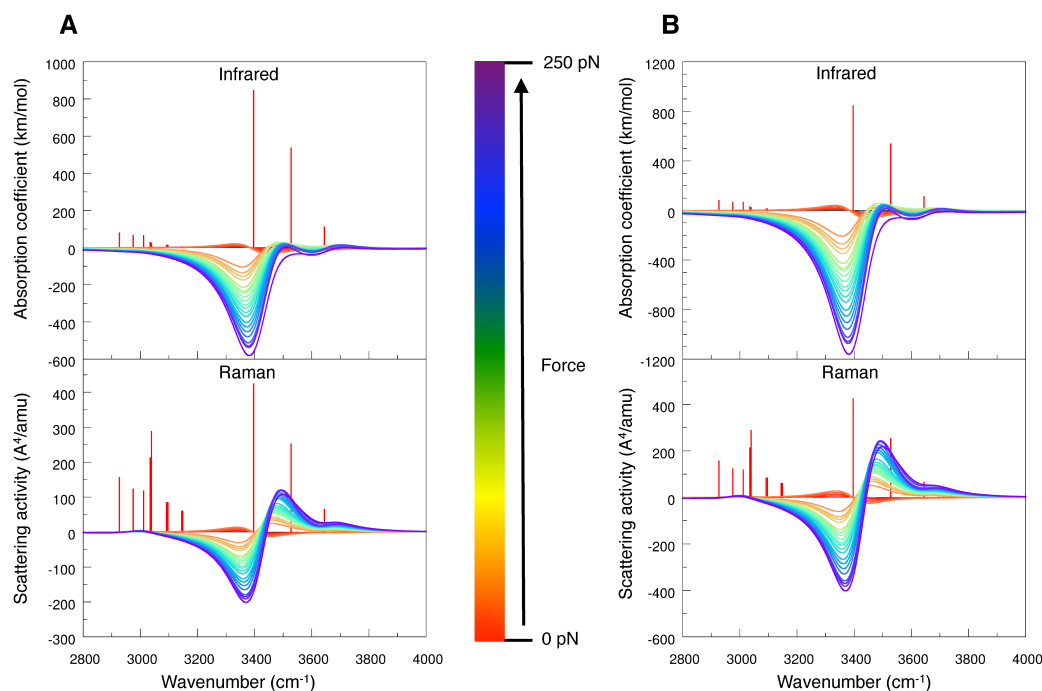
FIGURE 5.10: A) IR and Raman spectra of the triazole model system upon stretching perpendicular to the backbone along hydrogen bond 2. B) IR and Raman spectra of the triazole model system in which the nitrogen atom in the triazole ring involved in hydrogen bond 2 is substituted by ^{15}N, along the same stretching coordinate. The mid-IR region is not shown, since force-induced spectroscopic changes are not particularly pronounced in this region. Red bars correspond to the spectrum in the absence of external force.

5.2.3   The uracil force probe

The uracil force probe has some useful features that suggest its use in experiments. Changes in the vibrational spectra are even more pronounced than in the case of the triazole force probe (Figure 5.11A). If stretching forces are applied to hydrogen bonds 2 and 3 (Figure 5.8A), the decrease in intensity around 3400 cm^{-1} in the IR and Raman spectra is amplified by a factor of 2 in comparison to the triazole force probe, which can partly be attributed to the very strong absorbance of the uracil ring. The absorption coefficients of the vibrations around 3400 cm^{-1} are very high, so that changes in the absorbances and wavenumbers lead to immense changes in the convoluted intensities. Again, these changes are proportional to the external force. Furthermore, higher forces (>440 pN) than in the case of the triazole force probe are needed to detach neighboring strands from each other, since two hydrogen bonds need to be broken. As a result, the range of forces that can be detected with the uracil force probe is larger than in the case
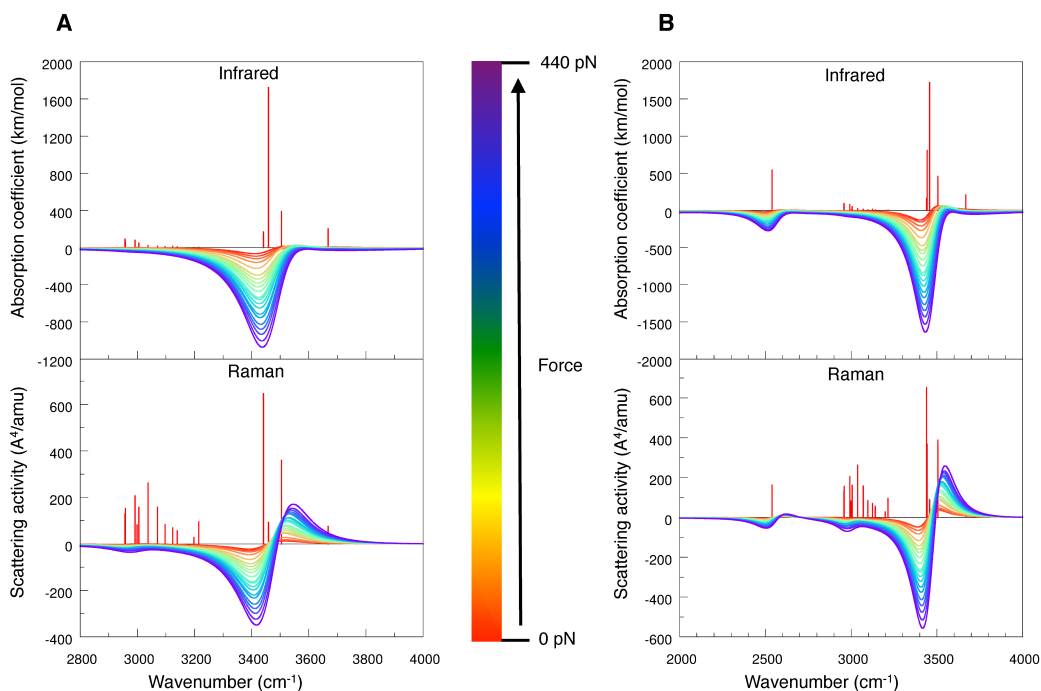
FIGURE 5.11: IR and Raman spectra of the uracil model system upon stretching perpendicular to the backbone along hydrogen bonds 2 and 3. B) IR and Raman spectra of the uracil model system, in which the hydrogen atom in the uracil ring involved in hydrogen bond 3 is substituted by a deuterium atom, along the same stretching coordinate. Red bars correspond to the spectrum in the absence of external force.

of the triazole force probe. It has to be kept in mind that the uracil force probe is larger than the triazole force probe, which has, however, not impaired the protein's stability in the MD simulations.

Upon deuteration of the amine in the uracil ring that is involved in hydrogen bond 3, an amplification of the decrease in absorbance comparable to the one discussed for the spectra of the triazole force probe is observable (Figure 5.11B). Additionally, the N−H stretching vibration in the uracil ring is downshifted from approximately 3450 cm^{-1} to around 2500 cm^{-1} due to the increased reduced mass of the vibration. The latter region is a transparent window in the protein spectrum due to the lack of protein signals that potentially overlap the signal from the deuterated uracil force probe. As an exception, cysteine S−H stretching vibrations in H_2O (but not in ^2H_2O) absorb in the same region and could potentially overlap the signal.[364] Deuteration is a useful tool to make the changes in absorbance largely orthogonal to the signals of the rest of the protein. Furthermore, it can be assumed that, in analogy to amide protons, the
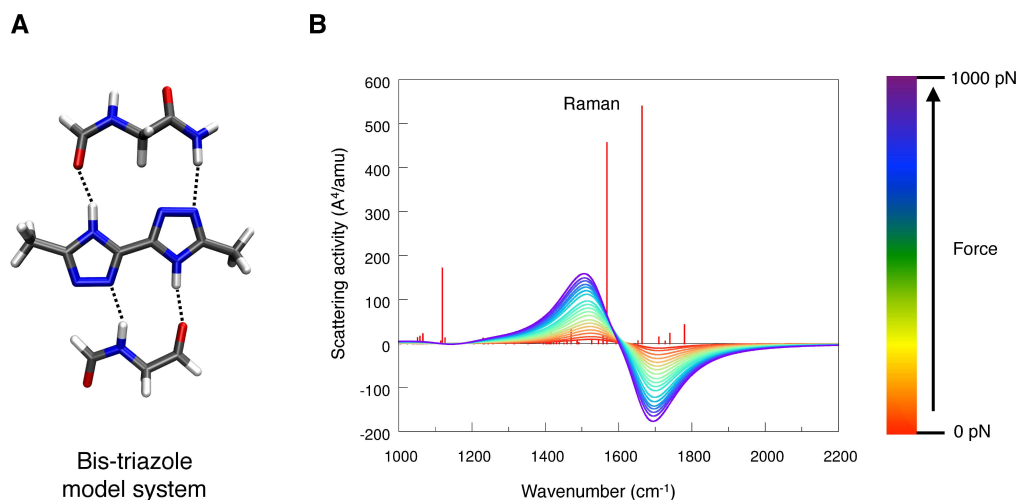
FIGURE 5.12: A) Model system employed in the quantum chemical calculations of the EFEI stretching coordinates and the vibrational spectra of the bis-triazole force probe. B) Raman spectrum of the bis-triazole model system upon stretching along the backbone. Red bars correspond to the spectrum in the absence of external force.

deuterium atom in uracil is somewhat protected from exchange with the solvent due to its incorporation in a hydrogen bond.

5.2.4   The bis-triazole force probe

The triazole force probe can be extended by placing another triazole moiety in the backbone next to the first one (Figure 5.12A). This approach has the advantage that changes in absorption coefficients upon stretching along the backbone, especially in the Raman spectrum, are intensified tremendously, which enhances experimental detectability by improving the signal-to-noise-ratio (Figure 5.12B). Again, these changes are largely proportional to the external force and the bis-triazole force probe can act as a force ruler. Profitably, the number of hydrogen bonds is retained and the secondary and tertiary structure remains unaffected (Figure 5.13). Preliminary calculations suggest that, in combination with deuteration, the extension of the triazole force probe presents an interesting perspective for future developments to identify the direction of the external force uniquely.
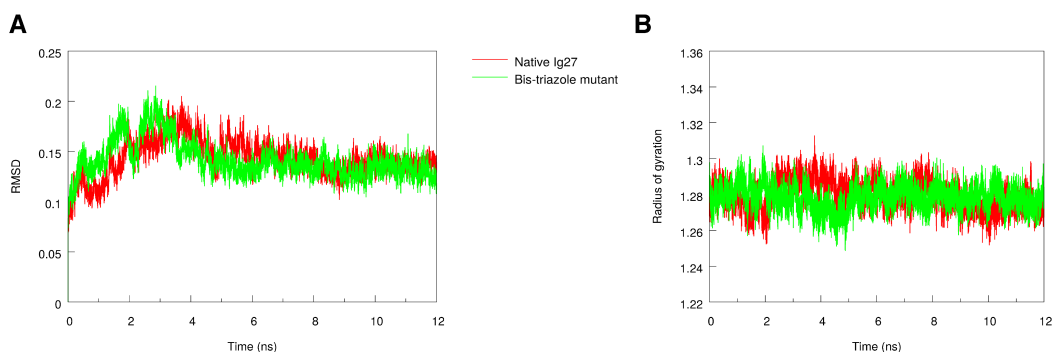
FIGURE 5.13: A) RMSD and B) radius of gyration during the MD simulation of the bis-triazole force probe mutant.

5.2.5   Comparison to the native protein

It is important to note that all spectroscopic changes in the force probe model systems described above are more pronounced than in the case of an unsubstituted, "native" reference system that is used for comparison (Figure 5.14). Moreover, the spectroscopic changes reported above for the force probe model systems are proportional to the external force, which is not true for all coordinates of the unsubstituted model system. These effects can be attributed to the contributions of the rings in the force probes, which demonstrates that the suggested force probes indeed lead to a significantly enhanced spectroscopic force-dependence and that they can be used in experiments to monitor the mechanical forces in real-time. An exception is the region around 1500 cm^{-1} of the backbone stretching coordinate, where the unsubstituted model system shows spectroscopic changes that are proportional to the external force. The reason is that the backbone can be deformed more easily if no ring is involved.

In summary, it was demonstrated that molecular force probes can be used to monitor mechanical forces in β-sheet domains of proteins in a noninvasive manner via their spectroscopic response. At characteristic positions in the spectrum, the changes in absorption coefficients are proportional to the restoring force and can be intensified and shifted to a transparent window in the protein spectrum by isotopic substitution. Due to the formation of hydrogen bonds between the force probes and neighboring strands, the secondary and tertiary structure is preserved and the protein remains stable. However, the incorporation of the suggested force probes in proteins constitutes a considerable challenge for experimentalists. A possible synthetic route is provided by chemical protein
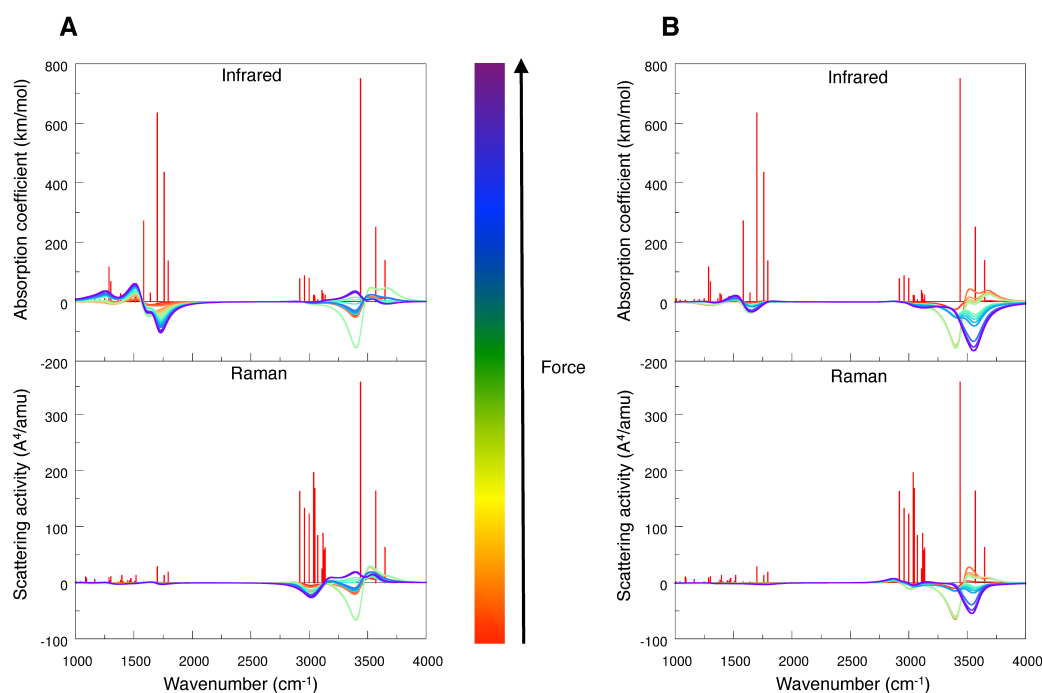
FIGURE 5.14: Convoluted IR and Raman difference spectra of the unsubstituted model system upon (A) stretching along the backbone, shown for forces between 0 and 1000 pN, and (B) stretching along hydrogen bond 1 (atoms 5 and 7, Figure 5.6), shown for forces between 0 and 280 pN. Red bars correspond to the spectrum in the absence of external force.

synthesis, which is limited small proteins. Nevertheless, spectroscopic studies on small proteins can certainly provide valuable insights into the mechanical forces acting in these systems during structural transitions. Moreover, future developments in protein synthesis will presumably extend the applicability of the suggested force probes to larger proteins.

In the future, further possibilities of identifying the direction of the external force uniquely should be elaborated on, e.g. through further calculations on deuterated force probes and on bis- or tris-triazole force probes. Furthermore, a promising perspective is the development of fluorescence force probes that can be incorporated into the protein backbone, since the sensitivity of fluorescence spectroscopy makes this method ideal for real-time measurements of forces acting in proteins. Additionally, dynamic IR and Raman spectra during folding and unfolding events of proteins should be calculated in the future. This will allow to estimate the influence of other factors like hydrogen bonding, conformational changes and thermal oscillations of the force probes on the spectra, which cannot be assessed by the static quantum chemical calculations presented here. However, calculations of dynamic spectra are not straightforward, since state-of-the-art

quantum chemical methods typically require the structure to be in a potential minimum to accurately calculate IR and Raman spectra, but during a trajectory this is almost never the case. An alternative is provided by MD studies, in which autocorrelation functions can be used to calculate vibrational spectra. However, the Fourier transforms applied in these analyses constitute transformations from the time domain to the frequency domain. Hence, the result is typically one spectrum for an entire trajectory, but the calculation of one spectrum for each snapshot of a trajectory is much more interesting in the present case. One obvious way to circumvent this problem is to conduct constrained quantum chemical geometry optimizations at certain snapshots of an MD trajectory, in which, e.g., the hydrogen bond lengths are fixed. As was shown in Chapter 2.2, this approach mimics the application of an external force, so that force-dependent vibrational spectra in each point of an MD trajectory can be calculated.

Chapter 6

Conclusions and Outlook

In this thesis I have presented the JEDI (**J**udgement of **E**nergy **DI**stribution) analysis, which is a quantum chemical analysis tool for the distribution of mechanical stress energy in deformed molecules. In the electronic ground state, it allows the identification of the mechanically relevant degrees of freedom in a molecule. Thus, the JEDI analysis contributes to a fundamental understanding of diverse mechanochemical processes. In the electronically excited state, the JEDI analysis can be used to quantify the energy released during the relaxation of every internal mode of the molecule on the excited state PES. The excited state JEDI analysis allows the calculation of the mechanochemical efficiency of a photoswitch. In addition to the discussion of the theoretical background and various applications of the JEDI analysis in the electronic ground and excited state, I presented several molecular force probes, which can be used to measure forces in macromolecules. The changes in spectroscopic properties upon mechanical deformation of the force probes allows the monitoring of forces occurring, for example, during structural transitions of proteins.

As was shown in Chapters 3 and 4, the JEDI analysis provides valuable insights into mechanochemical processes and contributes to the understanding of mechanochemistry at the molecular level. The JEDI analysis was used to investigate the mechanochemical behavior of polymers that are tangled into knots. The fundamental observations that covalent bonds do not need to be excessively stretched to be ruptured and that

torsions can act as work funnels that precondition bonds for rupture could lead to new perspectives in mechanochemical synthesis. The discussion of polymer knots was limited to a model system of polyethylene. Hence, it would be very interesting to investigate the mechanochemical properties of other polymers with the JEDI analysis. Polyamides, for example, are valued for their remarkable mechanical resistance, so that it would be particularly insightful to identify the point of bond rupture in a knotted polyamide chain and to quantify the various energy contributions in this process using the JEDI analysis.

Moreover, the JEDI analysis was used to investigate various methods for the mechanical stabilization of strained hydrocarbons. It was found that suitable coupling of angle-strained cycloalkynes and strained cyclophanes with short bridges significantly reduces the strain in both hydrocarbon subunits. Experimental validation of these findings is highly desirable. If coupling schemes that exert strong forces on the molecules were realized experimentally, highly strained hydrocarbons would become available as intermediates in organic synthesis.

Sonochemistry and ball milling techniques are promising branches of mechanochemistry, since they offer cheap and energy efficient synthetic routes that can be conducted at moderate ambient temperatures. Due to the lack of understanding of the underlying processes at the molecular level, however, the applicability of these experimental methods is limited and a systematic optimization of the syntheses is not possible. No successful attempt to predict the outcome of a chemical synthesis in a ball mill by computational methods has been documented in literature. In the future, the applicability of the JEDI analysis in the context of sonochemistry or ball milling techniques should be assessed. The inherent multiscale character and the plethora of effects that play a role in these experiments, however, constitutes a serious challenge for any quantum mechanochemical method, including the JEDI analysis.

As the JEDI analysis is based on the harmonic approximation, errors increase with increasing bond lengths. Therefore, the results of JEDI analyses of pulling setups in which bonds are overstretched have to be interpreted with great care. The EFEI method is particularly well-suited to provide the geometry of the mechanically deformed molecule, because with this method bond stretching can only be simulated until the bond rupture force is reached. This value coincides with the inflection point of the

Morse potential, where, in most cases, the harmonic approximation is still reasonable. Torsion flips, however, represent a considerable challenge for the JEDI analysis. Although most torsions can reasonably well be modeled by the harmonic approximation around their equilibrium, the transition of torsions to another local minimum is possible in mechanochemical processes that are calculated with the EFEI method. In these cases, the JEDI analysis yields unphysically high energies, since the displacement of these torsions is extremely large. Hence, the inclusion of anharmonic effects in the JEDI analysis is desirable. This anharmonic extension of the JEDI analysis, however, would inevitably lead to a drastic complication of the method and to a tremendous increase in computational cost. Moreover, it is not clear whether the transformation of the energy distribution from delocalized internal to redundant internal coordinates would still be exact if anharmonic effects were included.

In its present state, the ground state JEDI analysis requires three pieces of input: (1) The geometry of the relaxed molecule, (2) the geometry of the deformed molecule and (3) the Hessian at the relaxed geometry. In all calculations reported in this thesis, the geometry of the deformed molecule was calculated with quantum mechanochemical tools, e.g. with the EFEI method, and mechanical deformation was simulated. However, all that is required for the JEDI analysis is a Hessian and a difference in geometries. Hence, it is likely that the JEDI analysis can be used in a more general sense, e.g. for quantifying the energy contributions in each internal mode when a molecule transitions from the gas phase to the solid state. This process is accompanied by a distortion of the molecular geometry, and it would be interesting to test the applicability of the JEDI analysis in this context.

In addition, the JEDI analysis can be used to monitor the propagation of stress in deformed molecules during Born-Oppenheimer Molecular Dynamics (BOMD) simulations. The dynamic JEDI analysis has proven useful in the investigation of the mechanochemical behaviors of knotted polymer strands and the cyclobutene molecule. However, it has to be considered that only the potential energy contributions are quantified in the JEDI analysis. The kinetic energy, on the other hand, is omitted in the treatment, although it contributes to the total energy in most points of the trajectory. Hence, an extension of the dynamic JEDI analysis, which quantifies also the kinetic energy, is highly desirable.

Although the calculation of kinetic energy in a redundant coordinate system is highly problematic, it is possible that a transformation from delocalized to internal coordinates, in analogy to the static JEDI analysis, is available for the kinetic energy.

The JEDI analysis is not limited to the electronic ground state. In its excited state variant, the JEDI analysis can be used to quantify the energy contributions in every internal coordinate during relaxation on the excited state PES. This procedure allows the calculation of the mechanical efficiency of a photoswitch. It was found that, for example, the forces generated by the stiff-stilbene photoswitch during photochemical $cis \rightarrow trans$-isomerization are much too low to initiate bond rupture in cyclobutene. This process is rather initiated by efficient local heating of the macrocycle in which stiff-stilbene and cyclobutene are coupled, which of course accelerates the rupture of a thermally labile bond in cyclobutene. The excited state JEDI analysis can be used to develop more efficient photoswitches that are "strong" enough to rupture bonds mechanically. For this, a library of possible photoswitches can be calculated and the substitution patterns as well as the chemical composition and the attachment points of the linkers can be optimized. Such a procedure is also profitable in the development of molecular motors and nanomechanical devices, where the maximization of the mechanical output of a photoswitch is critical.

The harmonic approximation, on which the JEDI analysis is based, is more problematic in the electronically excited state than in the ground state. While the JEDI analysis typically describes mechanochemical processes in the ground state with reasonable accuracy until bond rupture, excited state PESs can be approximated as harmonic in far fewer cases. Often, only the relevant PES of the initial step of the excited state isomerization can be approximated as harmonic. Excited state PESs that are linear, dissociative or decay through a conical intersection without a barrier cannot be described by the excited state JEDI analysis. Preliminary calculations on 10-hydroxybenzo[h]quinoline (10-HBQ), for example, suggest that the excited state intramolecular proton transfer coordinate can be described by a linear potential rather than by a harmonic one. Hence, the excited state JEDI analysis delivers unreasonably high energies for the proton transfer. A straightforward approach to carry out a mechanochemical force analysis of this process is to calculate the gradient in the excited state and multiply it with the displacement

of the hydrogen bond length coordinate, which yields the correct energy. However, this remarkably simple and intuitive approach is problematic, because forces cannot be distributed uniquely among a redundant set of coordinates.

In addition to the JEDI analysis, I presented several molecular force probes that can be used to measure forces in macromolecules. In polymers, force probes can be used to study the wear and tear of materials as well as crack propagation. Generally, two design principles of molecular force probes can be conceived. First, different intra- or intermolecular interactions (covalent or hydrogen bonds, dispersive interactions etc.) can be ruptured by mechanical force, which leads to changes in the spectroscopic properties. Such binary force probes have the advantage that spectroscopic signals occur at a well-defined force. Second, the force probe may be sensitive enough so that pronounced spectroscopic signals can be observed at forces that are much lower than the bond rupture force. This approach has the advantage that the force probe reacts to mechanical stress well before the material fails. In this context, the reduction of point group symmetry upon mechanical deformation was found to be a profitable feature, because the spectroscopic signal of the force probe is intensified tremendously. In all cases, a maximization of the sensitivity of the force probes is highly desirable. A promising perspective is the development of fluorescence force probes, which respond to mechanical stress by changes in fluorescence intensity, wavelength and/or lifetime. The outstanding sensitivity of fluorescence spectroscopy makes this approach ideal for the real-time detection of forces in macromolecules.

Several force probes that can be incorporated into proteins were introduced in this thesis. These molecules allow the measurement of forces during folding and unfolding of proteins without impairing their natural fold. The force probes based on triazole and uracil were shown to be sensitive to forces acting in different directions in a β-sheet of a protein. Profitably, the spectroscopic signals of the force probes depend linearly on the external force and can be shifted to a transparent window in the protein spectrum by isotopic substitution. Experimental validation of these findings is highly desirable, since suitable experiments on force probe mutants potentially allow the monitoring of forces in proteins during structural transitions in an IR spectrometer. To further elaborate on the spectroscopic response of the force probe mutants, vibrational spectra during

MD simulations of folding and unfolding events should be calculated. For this, QM/MM approaches could prove useful, in which the unfolding is simulated via MD simulations and the vibrational spectra of force probe model systems are calculated via quantum chemical methods in every time step.

Bibliography

[1] Takacs, L. The historical development of mechanochemistry. *Chemical Society Reviews* **2013**, *42*, 7649–7659.

[2] Beyer, M. K.; Clausen-Schaumann, H. Mechanochemistry: The Mechanical Activation of Covalent Bonds. *Chemical Reviews* **2005**, *105*, 2921–2948.

[3] Fischer, F.; Emmerling, F. Synthesen in der Kugelmühle. *Nachrichten aus der Chemie* **2016**, *64*, 509–513.

[4] Ostwald, W. *Handbuch der Allgemeinen Chemie*, 1st ed.; Akademische Verlagsgesellschaft mbH: Leipzig, 1919.

[5] James, S. L.; Adams, C. J.; Bolm, C.; Braga, D.; Collier, P.; Friscic, T.; Grepioni, F.; Harris, K. D. M.; Hyett, G.; Jones, W.; Krebs, A.; Mack, J.; Maini, L.; Orpen, A. G.; Parkin, I. P.; Shearouse, W. C.; Steed, J. W.; Waddell, D. C. Mechanochemistry: Opportunities for New and Cleaner Synthesis. *Chemical Society Reviews* **2012**, *41*, 413–447.

[6] Heinz, W. F.; Hoh, J. H. Spatially resolved force spectroscopy of biological surfaces using the atomic force microscope. *Trends in Biotechnology* **1999**, *17*, 143–150.

[7] Clausen-Schaumann, H.; Seitz, M.; Krautbauer, R.; Gaub, H. E. Force spectroscopy with single bio-molecules. *Current Opinion in Chemical Biology* **2000**, *4*, 524–530.

[8] Zlatanova, J.; Lindsay, S. M.; Leuba, S. H. Single molecule force spectroscopy in biology using the atomic force microscope. *Progress in Biophysics & Molecular Biology* **2000**, *74*, 37–61.

[9] Evans, E. Probing the Relation Between Force - Lifetime - and Chemistry in Single Molecular Bonds. *Annual Review of Biophysics and Biomolecular Structure* **2001**, *30*, 105–128.

[10] Zhang, W.; Zhang, X. Single molecule mechanochemistry of macromolecules. *Progress in Polymer Science* **2003**, *28*, 1271–1295.

[11] Carrion-Vazquez, M.; Oberhauser, A. F.; Fisher, T. E.; Marszalek, P. E.; Li, H.; Fernandez, J. M. Mechanical design of proteins studied by single-molecule force spectroscopy and protein engineering. *Progress in Biophysics & Molecular Biology* **2000**, *74*, 63–91.

[12] Sotomayor, M.; Schulten, K. Single-Molecule Experiments in Vitro and in Silico. *Science* **2007**, *316*, 1144–1148.

[13] Neuman, K. C.; Nagy, A. Single-molecule force spectroscopy: optical tweezers, magnetic tweezers and atomic force microscopy. *Nature Methods* **2008**, *5*, 491–505.

[14] Marszalek, P. E.; Dufrêne, Y. F. Stretching single polysaccharides and proteins using atomic force microscopy. *Chemical Society Reviews* **2012**, *41*, 3523–3534.

[15] Hoffmann, T.; Dougan, L. Single molecule force spectroscopy using polyproteins. *Chemical Society Reviews* **2012**, *41*, 4781–4796.

[16] Zocher, M.; Bippes, C. A.; Zhang, C.; Müller, D. J. Single-molecule force spectroscopy of G-protein-coupled receptors. *Chemical Society Reviews* **2013**, *42*, 7801–7815.

[17] Rief, M.; Gautel, M.; Oesterhelt, F.; Fernandez, J. M.; Gaub, H. E. Reversible Unfolding of Individual Titin Immunoglobulin Domains by AFM. *Science* **1997**, *276*, 1109–1112.

[18] Makarov, D. E.; Wang, Z.; Thompson, J. B.; Hansma, H. G. On the interpretation of force extension curves of single protein molecules. *Journal of Chemical Physics* **2002**, *116*, 7760–7765.

[19] Cravotto, G.; Gaudino, E. C.; Cintas, P. On the mechanochemical activation by ultrasound. *Chemical Society Reviews* **2013**, *42*, 7521–7534.

[20] Cintas, P.; Cravotto, G.; Barge, A.; Martina, K. Interplay Between Mechanochemistry and Sonochemistry. *Topics in Current Chemistry* **2014**, *11*.

[21] Suslick, K. S. Sonochemistry. *Science* **1990**, *247*, 1439–1445.

[22] Ashokkumar, M.; Lee, J.; Kentish, S.; Grieser, F. Bubbles in an acoustic field: An overview. *Ultrasonics Sonochemistry* **2007**, *14*, 470–475.

[23] Ashokkumar, M. The characterization of acoustic cavitation bubbles - An overview. *Ultrasonics Sonochemistry* **2011**, *18*, 864–872.

[24] Henglein, A. Chemical effects of continuous and pulsed ultrasound in aqueous solutions. *Ultrasonics Sonochemistry* **1995**, *2*, 115–121.

[25] Ando, T.; Sumi, S.; Kawate, T.; Ichihara (née Yamawaki), J.; Hanafusa, T. Sonochemical Switching of Reaction Pathways in Solid-Liquid Two-phase Reactions. *Journal of the Chemical Society, Chemical Communications* **1984**, 439–440.

[26] Hickenboth, C. R.; Moore, J. S.; White, S. R.; Sottos, N. R.; Baudry, J.; Wilson, S. R. Biasing reaction pathways with mechanical force. *Nature* **2007**, *446*, 423–427.

[27] Lenhardt, J. M.; Ong, M. T.; Choe, R.; Evenhuis, C. R.; Martínez, T. J.; Craig, S. L. Trapping a Diradical Transition State by Mechanochemical Polymer Extension. *Science* **2010**, *329*, 1057–1060.

[28] Krupička, M.; Sander, W.; Marx, D. Mechanical Manipulation of Chemical Reactions: Reactivity Switching of Bergman Cyclizations. *The Journal of Physical Chemistry Letters* **2014**, *5*, 905–909.

[29] Fritze, U. F.; von Delius, M. Dynamic disulfide metathesis induced by ultrasound. *Chemical Communications* **2016**, *52*, 6363–6366.

[30] Mason, T. J. Ultrasound in synthetic organic chemistry. *Chemical Society Reviews* **1997**, *26*, 443–451.

[31] Cravotto, G.; Cintas, P. Power ultrasound in organic synthesis: moving cavitational chemistry from academia to innovative and large-scale applications. *Chemical Society Reviews* **2006**, *35*, 180–196.

[32] Cravotto, G.; Cintas, P. Forcing and Controlling Chemical Reactions with Ultrasound. *Angewandte Chemie International Edition* **2007**, *46*, 5476–5478.

[33] Kean, Z. S.; Craig, S. L. Mechanochemical remodeling of synthetic polymers. *Polymer* **2012**, *53*, 1035–1048.

[34] Brantley, J. N.; Wiggins, K. M.; Bielawski, C. W. Polymer mechanochemistry: The design and study of mechanophores. *Polymer International* **2013**, *62*, 2–12.

[35] Wiggins, K. M.; Brantley, J. N.; Bielawski, C. W. Methods for activating and characterizing mechanically responsive polymers. *Chemical Society Reviews* **2013**, *42*, 7130–7147.

[36] Shy, H.; Mackin, P.; Orvieto, A. S.; Gharbharan, D.; Peterson, G. R.; Bampos, N.; Hamilton, T. D. The two-step mechanochemical synthesis of porphyrins. *Faraday Discussions* **2014**, *170*, 59–69.

[37] Boldyreva, E. Mechanochemistry of inorganic and organic systems: what is similar, what is different? *Chemical Society Reviews* **2013**, *42*, 7719–7738.

[38] Baláž, P.; Achimovičová, M.; Baláž, M.; Billik, P.; Cherkezova-Zheleva, Z.; Criado, J. M.; Delogu, F.; Dutková, E.; Gaffet, E.; Gotor, F. J.; Kumar, R.; Mitov, I.; Rojac, T.; Senna, M.; Streletskii, A.; Wieczorek-Ciurowa, K. Hallmarks of mechanochemistry: from nanoparticles to technology. *Chemical Society Reviews* **2013**, *42*, 7571–7637.

[39] Friščić, T.; James, S. L.; Boldyreva, E. V.; Bolm, C.; Jones, W.; Mack, J.; Steed, J. W.; Suslick, K. S. Highlights from Faraday Discussion 170: Challenges and opportunities of modern mechanochemistry, Montreal, Canada, 2014. *Chemical Communications* **2015**, *51*, 6248–6256.

[40] Hugel, T.; Holland, N. B.; Cattani, A.; Moroder, L.; Seitz, M.; Gaub, H. E. Single-Molecule Optomechanical Cycle. *Science* **2002**, *296*, 1103–1106.

[41] Barrett, C. J.; Mamiya, J.-i.; Yager, K. G.; Ikeda, T. Photo-mechanical effects in azobenzene-containing soft materials. *Soft Matter* **2007**, *3*, 1249–1261.

[42] Bandara, H. M. D.; Burdette, S. C. Photoisomerization in different classes of azobenzene. *Chemical Society Reviews* **2012**, *41*, 1809–1825.

[43] Koumura, N.; Zijlstra, R. W.; van Delden, R. A.; Harada, N.; Feringa, B. L. Light-driven monodirectional molecular rotor. *Nature* **1999**, *401*, 152–155.

[44] Leigh, D. A.; Wong, J. K. Y.; Dehez, F.; Zerbetto, F. Unidirectional rotation in a mechanically interlocked molecular rotor. *Nature* **2003**, *424*, 174–179.

[45] Beharry, A. A.; Woolley, G. A. Azobenzene photoswitches for biomolecules. *Chemical Society Reviews* **2011**, *40*, 4422–4437.

[46] Spörlein, S.; Carstens, H.; Satzger, H.; Renner, C.; Behrendt, R.; Moroder, L.; Tavan, P.; Zinth, W.; Wachtveitl, J. Ultrafast spectroscopy reveals subnanosecond peptide conformational dynamics and validates molecular dynamics simulation. *Proceedings of the National Academy of Sciences of the United States of America* **2002**, *99*, 7998–8002.

[47] Bredenbeck, J.; Helbing, J.; Sieg, A.; Schrader, T.; Zinth, W.; Renner, C.; Behrendt, R.; Moroder, L.; Wachtveitl, J.; Hamm, P. Picosecond conformational transition and equilibration of a cyclic peptide. *Proceedings of the National Academy of Sciences of the United States of America* **2003**, *100*, 6452–6457.

[48] Wachtveitl, J.; Spörlein, S.; Satzger, H.; Fonrobert, B.; Renner, C.; Behrendt, R.; Oesterhelt, D.; Moroder, L.; Zinth, W. Ultrafast Conformational Dynamics in Cyclic Azobenzene Peptides of Increased Flexibility. *Biophysical Journal* **2004**, *86*, 2350–2362.

[49] Kusebauch, U.; Cadamuro, S. A.; Musiol, H.-J.; Lenz, M. O.; Wachtveitl, J.; Moroder, L.; Renner, C. Photocontrolled Folding and Unfolding of a Collagen Triple Helix. *Angewandte Chemie International Edition* **2006**, *45*, 7015–7018.

[50] Kusebauch, U.; Cadamuro, S. A.; Musiol, H.-J.; Lenz, M. O.; Wachtveitl, J.; Moroder, L.; Renner, C. Lichtgesteuerte Faltung und Entfaltung einer Collagen-Tripelhelix. *Angewandte Chemie* **2006**, *118*, 7170–7173.

[51] Nguyen, P. H.; Stock, G. Nonequilibrium molecular dynamics simulation of a photoswitchable peptide. *Chemical Physics* **2006**, *323*, 36–44.

[52] Kobus, M.; Lieder, M.; Nguyen, P. H.; Stock, G. Simulation of transient infrared spectra of a photoswitchable peptide. *The Journal of Chemical Physics* **2011**, *135*, 225102.

[53] Buchenberg, S.; Knecht, V.; Walser, R.; Hamm, P.; Stock, G. Long-Range Conformational Transition of a Photoswitchable Allosteric Protein: Molecular Dynamics Simulation Study. *The Journal of Physical Chemistry B* **2014**, *118*, 13468–13476.

[54] Tanaka, F.; Mochizuki, T.; Liang, X.; Asanuma, H.; Tanaka, S.; Suzuki, K.; Kitamura, S. I.; Nishikawa, A.; Ui-Tei, K.; Hagiya, M. Robust and Photocontrollable DNA Capsules Using Azobenzenes. *Nano Letters* **2010**, *10*, 3560–3565.

[55] McCullagh, M.; Franco, I.; Ratner, M. A.; Schatz, G. C. DNA-Based Optomechanical Molecular Motor. *Journal of the American Chemical Society* **2011**, *133*, 3452–3459.

[56] Nishioka, H.; Liang, X.; Kato, T.; Asanuma, H. A Photon-Fueled DNA Nanodevice that Contains Two Different Photoswitches. *Angewandte Chemie International Edition* **2012**, *51*, 1165–1168.

[57] Khan, A.; Kaiser, C.; Hecht, S. Prototype of a Photoswitchable Foldamer. *Angewandte Chemie International Edition* **2006**, *45*, 1878–1881.

[58] Khan, A.; Kaiser, C.; Hecht, S. Prototyp eines photoschaltbaren Foldamers. *Angewandte Chemie* **2006**, *118*, 1912–1915.

[59] Braun, S.; Böckmann, M.; Marx, D. Unfolding a Photoswitchable Azo-Foldamer Reveals a Non-Covalent Reaction Mechanism. *ChemPhysChem* **2012**, *13*, 1440–1443.

[60] Lee, C. K.; Beiermann, B. A.; Silberstein, M. N.; Wang, J.; Moore, J. S.; Sottos, N. R.; Braun, P. V. Exploiting Force Sensitive Spiropyrans as Molecular Level Probes. *Macromolecules* **2013**, *46*, 3746–3752.

[61] Özçoban, C.; Halbritter, T.; Steinwand, S.; Herzig, L.-M.; Kohl-Landgraf, J.; Askari, N.; Groher, F.; Fürtig, B.; Richter, C.; Schwalbe, H.; Suess, B.; Wachtveitl, J.; Heckel, A. Water-soluble Py-BIPS Spiropyrans as Photoswitches for Biological Applications. *Organic Letters* **2015**, *17*, 1517–1520.

[62] Kauzmann, W.; Eyring, H. The Viscous Flow of Large Molecules. *Journal of the American Chemical Society* **1940**, *62*, 3113–3125.

[63] Beyer, M. K. The mechanical strength of a covalent bond calculated by density functional theory. *The Journal of Chemical Physics* **2000**, *112*, 7307–7312.

[64] Freund, L. B. Characterizing the resistance generated by a molecular bond as it is forcibly separated. *Proceedings of the National Academy of Sciences of the United States of America* **2009**, *106*, 8818–8823.

[65] Marszalek, P. E.; Oberhauser, A. F.; Pang, Y.-P.; Fernandez, J. M. Polysaccharide elasticity governed by chair-boat transitions of the glucopyranose ring. *Nature* **1998**, *396*, 661–664.

[66] Lee, C.; Yang, W.; Parr, R. G. Development of the Colle-Salvetti correlation-energy formula into a functional of the electron density. *Physical Review B* **1988**, *37*, 785–789.

[67] Becke, A. D. A new mixing of Hartree-Fock and local density-functional theories. *The Journal of Chemical Physics* **1993**, *98*, 1372–1377.

[68] Dunning, T. H. Gaussian basis sets for use in correlated molecular calculations. I. The atoms boron through neon and hydrogen. *The Journal of Chemical Physics* **1989**, *90*, 1007–1023.

[69] Dunning Jr., T. H. In *Methods of Electronic Structure Theory*, 3rd ed.; Schaefer III, H. F., Ed.; Springer US: New York, 1977; pp 1–27.

[70] Iozzi, M. F.; Helgaker, T.; Uggerud, E. Assessment of theoretical methods for the determination of the mechanochemical strength of covalent bonds. *Molecular Physics* **2009**, *107*, 2537–2546.

[71] Hohenberg, P.; Kohn, W. Inhomogeneous Electron Gas. *Physical Review* **1964**, *136*, 864–871.

[72] Kohn, W.; Sham, L. J. Self-Consistent Equations Including Exchange and Correlation Effects. *Physical Review* **1965**, *140*, 1133–1138.

[73] Lee, T. J.; Taylor, P. R. A Diagnostic for Determining the Quality of Single-Reference Electron Correlation Methods. *International Journal of Quantum Chemistry* **1989**, *23*, 199–207.

[74] Coester, F.; Kümmel, H. Short-Range Correlations in Nuclear Wave Functions. *Nuclear Physics* **1960**, *17*, 477–485.

[75] Purvis III, G. D.; Bartlett, R. J. A full coupled-cluster singles and doubles model: The inclusion of disconnected triples. *The Journal of Chemical Physics* **1982**, *76*, 1910–1918.

[76] Raghavachari, K.; Trucks, G. W.; Pople, J. A.; Head-Gordon, M. A fifth-order perturbation comparison of electron correlation theories. *Chemical Physics Letters* **1989**, *157*, 479–483.

[77] Kendall, R. A.; Jr., Dunnin, T. A.; Harrison, R. J. Electron affinities of the first-row atoms revisited. Systematic basis sets and wave functions. *The Journal of Chemical Physics* **1992**, *96*, 6796–6806.

[78] Angeli, C.; Cimiraglia, R.; Evangelisti, S.; Leininger, T.; Malrieu, J.-P. Introduction of n-electron valence states for multireference perturbation theory. *Journal of Chemical Physics* **2001**, *114*, 10252–10264.

[79] Schapiro, I.; Sivalingam, K.; Neese, F. Assessment of nElectron Valence State Perturbation Theory for Vertical Excitation Energies. *Journal of Chemical Theory and Computation* **2013**, *9*, 3567–3580.

[80] Perdew, J. P.; Burke, K.; Ernzerhof, M. Generalized Gradient Approximation Made Simple. *Physical Review Letters* **1996**, *77*, 3865–3868.

[81] Perdew, J. P.; Burke, K.; Ernzerhof, M. Generalized Gradient Approximation Made Simple- ERRATA. *Physical Review Letters* **1997**, *78*, 1396.

[82] Becke, A. D. Correlation energy of an inhomogeneous electron gas: A coordinate-space model. *The Journal of Chemical Physics* **1988**, *88*, 1053–1062.

[83] Yanai, T.; Tew, D. P.; Handy, N. C. A new hybrid exchange-correlation functional using the Coulomb-attenuating method (CAM-B3LYP). *Chemical Physics Letters* **2004**, *393*, 51–57.

[84] Kedziora, G. S.; Barr, S. A.; Berry, R.; Moller, J. C.; Breitzman, T. D. Bond breaking in stretched molecules: multi-reference methods versus density functional theory. *Theoretical Chemistry Accounts* **2016**, *135*, 79.

[85] Grimme, S. Semiempirical hybrid density functional with perturbative second-order correlation. *The Journal of Chemical Physics* **2006**, *124*, 034108.

[86] Peverati, R.; Truhlar, D. G. Exchange-correlation functional with good accuracy for both structural and energetic properties while depending only on the density and its gradient. *Journal of Chemical Theory and Computation* **2012**, *8*, 2310–2319.

[87] Handy, N. C.; Cohen, A. J. Left-right correlation energy. *Molecular Physics* **2001**, *99*, 403–412.

[88] Curtiss, L. A.; Redfern, P. C.; Raghavachari, K. Gaussian-4 theory. *The Journal of Chemical Physics* **2007**, *126*, 084108.

[89] Ribas-Arino, J.; Shiga, M.; Marx, D. Understanding Covalent Mechanochemistry. *Angewandte Chemie International Edition* **2009**, *48*, 4190–4193.

[90] Pill, M. F.; Kersch, A.; Clausen-Schaumann, H.; Beyer, M. K. Force dependence of the infrared spectra of polypropylene calculated with density functional theory. *Polymer Degradation and Stability* **2016**, *128*, 294–299.

[91] Krupička, M.; Marx, D. Disfavoring Mechanochemical Reactions by Stress-Induced Steric Hindrance. *Journal of Chemical Theory and Computation* **2015**, *11*, 841–846.

[92] TURBOMOLE, a development of University of Karlsruhe and Forschungszentrum Karlsruhe GmbH, 1989-2007, TURBOMOLE GmbH, since 2007; available from http://www.turbomole.com.

[93] Frisch, M. J.; Trucks, G. W.; Schlegel, H. B.; Scuseria, G. E.; Robb, M. A.; Cheeseman, J. R.; Scalmani, G.; Barone, V.; Mennucci, B.; Petersson, G. A.; Nakatsuji, H.; Caricato, M.; Li, X.; Hratchian, H. P.; Izmaylov, A. F.; Bloino, J.; Zheng, G.; Sonnenberg, J. L.; Hada, M.; Ehara, M.; Toyota, K.; Fukuda, R.; Hasegawa, J.; Ishida, M.; Nakajima, T.; Honda, Y.; Kitao, O.; Nakai, H.; Vreven, T.; Montgomery Jr., J. A.; Peralta, J. E.; Ogliaro, F.; Bearpark, M.; Heyd, J. J.; Brothers, E.; Kudin, K. N.; Staroverov, V. N.; Kobayashi, R.; Normand, J.; Raghavachari, K.; Rendell, A.; Burant, J. C.; Iyengar, S. S.; Tomasi, J.; Cossi, M.; Rega, N.; Millam, J. M.; Klene, M.; Knox, J. E.; Cross, J. B.; Bakken, V.; Adamo, C.; Jaramillo, J.; Gomperts, R.; Stratmann, R. E.; Yazyev, O.; Austin, A. J.; Cammi, R.; Pomelli, C.; Ochterski, J. W.; Martin, R. L.; Morokuma, K.; Zakrzewski, V. G.; Voth, G. A.; Salvador, P.; Dannenberg, J. J.; Dapprich, S.; Daniels, A. D.; Farkas, Ö.; Foresman, J. B.; Ortiz, J. V.; Cioslowski, J.; Fox, D. J. Gaussian 09.

[94] Shao, Y.; Gan, Z.; Epifanovsky, E.; Gilbert, A. T. B.; Wormit, M.; Kussmann, J.; Lange, A. W.; Behn, A.; Deng, J.; Feng, X.; Ghosh, D.; Goldey, M.; Horn, P. R.; Jacobson, L. D.; Kaliman, I.; Khaliullin, R. Z.; Kuś, T.; Landau, A.; Liu, J.; Proynov, E. I.; Rhee, Y. M.; Richard, R. M.; Rohrdanz, M. A.; Steele, R. P.; Sundstrom, E. J.; Woodcock, H. L.; Zimmerman, P. M.; Zuev, D.; Albrecht, B.; Alguire, E.; Austin, B.; Beran, G. J. O.; Bernard, Y. A.; Berquist, E.; Brandhorst, K.; Bravaya, K. B.; Brown, S. T.; Casanova, D.; Chang, C.-M.; Chen, Y.; Chien, S. H.; Closser, K. D.; Crittenden, D. L.; Diedenhofen, M.; DiStasio, R. A.; Do, H.; Dutoi, A. D.; Edgar, R. G.; Fatehi, S.; Fusti-Molnar, L.; Ghysels, A.; Golubeva-Zadorozhnaya, A.; Gomes, J.; Hanson-Heine, M. W. D.; Harbach, P. H. P.; Hauser, A. W.; Hohenstein, E. G.; Holden, Z. C.; Jagau, T.-C.; Ji, H.; Kaduk, B.; Khistyaev, K.; Kim, J.; Kim, J.; King, R. A.; Klunzinger, P.; Kosenkov, D.; Kowalczyk, T.; Krauter, C. M.; Lao, K. U.; Laurent, A. D.; Lawler, K. V.; Levchenko, S. V.; Lin, C. Y.; Liu, F.; Livshits, E.; Lochan, R. C.; Luenser, A.; Manohar, P.; Manzer, S. F.; Mao, S.-P.; Mardirossian, N.; Marenich, A. V.; Maurer, S. A.; Mayhall, N. J.; Neuscamman, E.; Oana, C. M.; Olivares-Amaya, R.; O'Neill, D. P.; Parkhill, J. A.; Perrine, T. M.; Peverati, R.; Prociuk, A.; Rehn, D. R.; Rosta, E.; Russ, N. J.; Sharada, S. M.; Sharma, S.; Small, D. W.; Sodt, A.; Stein, T.; Stück, D.; Su, Y.-C.; Thom, A. J. W.; Tsuchimochi, T.; Vanovschi, V.; Vogt, L.; Vydrov, O.; Wang, T.; Watson, M. A.; Wenzel, J.; White, A.; Williams, C. F.;

Yang, J.; Yeganeh, S.; Yost, S. R.; You, Z.-Q.; Zhang, I. Y.; Zhang, X.; Zhao, Y.; Brooks, B. R.; Chan, G. K. L.; Chipman, D. M.; Cramer, C. J.; Goddard, W. A.; Gordon, M. S.; Hehre, W. J.; Klamt, A.; Schaefer, H. F.; Schmidt, M. W.; Sherrill, C. D.; Truhlar, D. G.; Warshel, A.; Xu, X.; Aspuru-Guzik, A.; Baer, R.; Bell, A. T.; Besley, N. A.; Chai, J.-D.; Dreuw, A.; Dunietz, B. D.; Furlani, T. R.; Gwaltney, S. R.; Hsu, C.-P.; Jung, Y.; Kong, J.; Lambrecht, D. S.; Liang, W.; Ochsenfeld, C.; Rassolov, V. A.; Slipchenko, L. V.; Subotnik, J. E.; Van Voorhis, T.; Herbert, J. M.; Krylov, A. I.; Gill, P. M. W.; Head-Gordon, M. Advances in molecular quantum chemistry contained in the Q-Chem 4 program package. *Molecular Physics* **2014**, *113*, 184–215.

[95] Avdoshenko, S. M.; Makarov, D. E. Reaction Coordinates and Pathways of Mechanochemical Transformations. *The Journal of Physical Chemistry B* **2016**, *120*, 1537–1545.

[96] Wolinski, K.; Baker, J. Theoretical predictions of enforced structural changes in molecules. *Molecular Physics* **2009**, *107*, 2403–2417.

[97] Wolinski, K.; Baker, J. Geometry optimization in the presence of external forces: a theoretical model for enforced structural changes in molecules. *Molecular Physics* **2010**, *108*, 1845–1856.

[98] Baker, J.; Wolinski, K. Isomerization of Stilbene Using Enforced Geometry Optimization. *Journal of Computational Chemistry* **2010**, *32*, 43–53.

[99] Bader, R. F. W. Atomic force microscope as an open system and the Ehrenfest force. *Physical Review B* **2000**, *61*, 7795–7802.

[100] Ong, M. T.; Leiding, J.; Tao, H.; Virshup, A. M.; Martínez, T. J. First Principles Dynamics and Minimum Energy Pathways for Mechanochemical Ring Opening of Cyclobutene. *Journal of the American Chemical Society* **2009**, *131*, 6377–6379.

[101] Kochhar, G. S.; Heverly-Coulson, G. S.; Mosey, N. J. Theoretical Approaches for Understanding the Interplay Between Stress and Chemical Reactivity. *Topics in Current Chemistry* **2015**, *August*, 1–60.

[102] Woodward, R. B.; Hoffmann, R. The Conservation of Orbital Symmetry. *Angewandte Chemie International Edition* **1969**, *8*, 781–853.

[103] Woodward, R. B.; Hoffmann, R. Stereochemistry of Electrocyclic Reactions. *Journal of the American Chemical Society* **1965**, *87*, 395–397.

[104] Hoffmann, R.; Woodward, R. B. Selection Rules for Concerted Cycloaddition Reactions. *Journal of the American Chemical Society* **1965**, *87*, 2046–2048.

[105] Avdoshenko, S. M.; Makarov, D. E. Finding mechanochemical pathways and barriers without transition state search. *The Journal of Chemical Physics* **2015**, *142*, 174106.

[106] Subramanian, G.; Mathew, N.; Leiding, J. A generalized force-modified potential energy surface for mechanochemical simulations. *The Journal of Chemical Physics* **2015**, *143*, 134109.

[107] Lo, Y. S.; Simons, J.; Beebe, T. P. Temperature Dependence of the Biotin-Avidin Bond-Rupture Force Studied by Atomic Force Microscopy. *Journal of Physical Chemistry B* **2002**, *106*, 9847–9852.

[108] Schumakovitch, I.; Grange, W.; Strunz, T.; Bertoncini, P.; Güntherodt, H.-J.; Hegner, M. Temperature Dependence of Unbinding Forces between Complementary DNA Strands. *Biophysical Journal* **2002**, *82*, 517–521.

[109] Car, R.; Parrinello, M. Unified Approach for Molecular Dynamics and Density-Functional Theory. *Physical Review Letters* **1985**, *55*, 2471–2474.

[110] Krüger, D.; Fuchs, H.; Rousseau, R.; Marx, D.; Parrinello, M. Pulling Monatomic Gold Wires with Single Molecules: An Ab Initio Simulation. *Physical Review Letters* **2002**, *89*, 186402.

[111] Rubio-Bollinger, G.; Bahn, S. R.; Agraït, N.; Jacobsen, K. W.; Vieira, S. Mechanical Properties and Formation Mechanisms of a Wire of Single Gold Atoms. *Physical Review Letters* **2001**, *87*, 026101.

[112] Konôpka, M.; Turanský, R.; Reichert, J.; Fuchs, H.; Marx, D.; Štich, I. Mechanochemistry and Thermochemistry are Different: Stress-Induced Strengthening of Chemical Bonds. *Physical Review Letters* **2008**, *100*, 115503.

[113] Marx, D.; Hutter, J. *Ab Initio Molecular Dynamics. Basic Theory and Advanced Methods*, 1st ed.; Cambridge University Press: Cambridge, UK, 2009.

[114] Ribas-Arino, J.; Marx, D. Covalent Mechanochemistry: Theoretical Concepts and Computational Tools with Applications to Molecular Nanomechanics. *Chemical Reviews* **2012**, *112*, 5412–5487.

[115] Dopieralski, P.; Latajka, Z. In *Practical Aspects of Computational Chemistry IV*, 1st ed.; Leszczynski, J., Shukla, M. K., Eds.; Springer US: New York, 2016; pp 233–243.

[116] Bell, G. I. Models for the Specific Adhesion of Cells to Cells. *Science* **1978**, *200*, 618–627.

[117] Tian, Y.; Boulatov, R. Comparison of the predictive performance of the Bell-Evans, Taylor-expansion and statistical-mechanics models of mechanochemistry. *Chemical Communications* **2013**, *49*, 4187–4189.

[118] Kucharski, T. J.; Yang, Q.-Z.; Tian, Y.; Boulatov, R. Strain-Dependent Acceleration of a Paradigmatic SN2 Reaction Accurately Predicted by the Force Formalism. *The Journal of Physical Chemistry Letters* **2010**, *1*, 2820–2825.

[119] Hyeon, C.; Thirumalai, D. Measuring the energy landscape roughness and the transition state location of biomolecules using single molecule mechanical unfolding experiments. *Journal of Physics: Condensed Matter* **2007**, *19*, 113101.

[120] Hermes, M.; Boulatov, R. The Entropic and Enthalpic Contributions to Force-Dependent Dissociation Kinetics of the Pyrophosphate Bond. *Journal of the American Chemical Society* **2011**, *133*, 20044–20047.

[121] Wu, D.; Lenhardt, J. M.; Black, A. L.; Akhremitchev, B. B.; Craig, S. L. Molecular Stress Relief through a Force-Induced Irreversible Extension in Polymer Contour Length. *Journal of the American Chemical Society* **2010**, *132*, 15936–15938.

[122] Konda, S. S. M.; Brantley, J. N.; Bielawski, C. W.; Makarov, D. E. Chemical reactions modulated by mechanical stress: Extended Bell theory. *The Journal of Chemical Physics* **2011**, *135*, 164103.

[123] Bailey, A.; Mosey, N. J. Prediction of reaction barriers and force-induced instabilities under mechanochemical conditions with an approximate model: A case study of the ring opening of 1,3-cyclohexadiene. *The Journal of Chemical Physics* **2012**, *136*, 044102.

[124] Jones, L. H.; Swanson, B. I. Interpretation of Potential Constants: Application to Study of Bonding Forces in Metal Cyanide Complexes and Metal Carbonyls. *Accounts of Chemical Research* **1976**, *9*, 128–134.

[125] Grunenberg, J.; Streubel, R.; von Frantzius, G.; Marten, W. The strongest bond in the universe? Accurate calculation of compliance matrices for the ions N2H+, HCO+, and HOC+. *Journal of Chemical Physics* **2003**, *119*, 165–169.

[126] Konda, S. S. M.; Avdoshenko, S. M.; Makarov, D. E. Exploring the topography of the stress-modified energy landscapes of mechanosensitive molecules. *The Journal of Chemical Physics* **2014**, *140*, 104114.

[127] Wales, D. J. A Microscopic Basis for the Global Appearance of Energy Landscapes. *Science* **2001**, *293*, 2067–2070.

[128] Akbulatov, S.; Tian, Y.; Kapustin, E.; Boulatov, R. Model Studies of the Kinetics of Ester Hydrolysis under Stretching Force. *Angewandte Chemie International Edition* **2013**, *52*, 6992–6995.

[129] Prezhdo, O. V.; Pereverzev, Y. V. Theoretical Aspects of the Biological Catch Bond. *Accounts of Chemical Research* **2009**, *42*, 693–703.

[130] Konda, S. S. M.; Brantley, J. N.; Varghese, B. T.; Wiggins, K. M.; Bielawski, C. W.; Makarov, D. E. Molecular Catch Bonds and the Anti-Hammond Effect in Polymer Mechanochemistry. *Journal of the American Chemical Society* **2013**, *135*, 12722–12729.

[131] Groote, R.; Szyja, B. M.; Leibfarth, F. A.; Hawker, C. J.; Doltsinis, N. L.; Sijbesma, R. P. Strain-Induced Strengthening of the Weakest Link: The Importance of Intermediate Geometry for the Outcome of Mechanochemical Reactions. *Macromolecules* **2014**, *47*, 1187–1192.

[132] Taft, R. W. Polar and Steric Substituent Constants for Aliphatic and o-Benzoate Groups from Rates of Esterification and Hydrolysis of Esters. *Journal of the American Chemical Society* **1952**, *74*, 3120–3128.

[133] Taft, R. W. Linear Steric Energy Relationships. *Journal of the American Chemical Society* **1953**, *75*, 4538–4539.

[134] Makarov, D. E. The effect of a mechanical force on quantum reaction rate: Quantum Bell formula. *The Journal of Chemical Physics* **2011**, *135*, 194112.

[135] Koo, B.; Chattopadhyay, A.; Dai, L. Atomistic modeling framework for a cyclobutane-based mechanophore-embedded nanocomposite for damage precursor detection. *Computational Materials Science* **2016**, *120*, 135–141.

[136] Halgren, T. A. Merck Molecular Force Field. I. Basis, Form, Scope, Parameterization, and Performance of MMFF94. *Journal of Computational Chemistry* **1996**, *17*, 490–519.

[137] Zoete, V.; Cuendet, M. A.; Grosdidier, A.; Michielin, O. SwissParam: A Fast Force Field Generation Tool for Small Organic Molecules. *Journal of Computational Chemistry* **2011**, *32*, 2359–2368.

[138] Singh, S. K.; Srinivasan, S. G.; Neek-Amal, M.; Costamagna, S.; van Duin, A. C. T.; Peeters, F. M. Thermal properties of fluorinated graphene. *Physical Review B* **2013**, *87*, 104114.

[139] Huang, Z.; Yang, Q.-Z.; Khvostichenko, D.; Kucharski, T. J.; Chen, J.; Boulatov, R. Method to Derive Restoring Forces of Strained Molecules from Kinetic Measurements. *Journal of the American Chemical Society* **2009**, *131*, 1407–1409.

[140] Akbulatov, S.; Tian, Y.; Boulatov, R. Force Reactivity Property of a Single Monomer Is Sufficient To Predict the Micromechanical Behavior of Its Polymer. *Journal of the American Chemical Society* **2012**, *134*, 7620–7623.

[141] Godet, J.; Giustino, F.; Pasquarello, A. Proton-Induced Fixed Positive Charge at the Si(100)-SiO2 Interface. *Physical Review Letters* **2007**, *99*, 126102.

[142] Hilton, C. L.; Crowfoot, J. M.; Rempala, P.; King, B. T. 18,18'Dihexyl[9,9']biphenanthro[9,10-b]triphenylene: Construction and Consequences of a Profoundly Hindered Aryl-Aryl Single Bond. *Journal of the American Chemical Society* **2008**, *130*, 13392–13399.

[143] Makarov, D. E. Perspective: Mechanochemistry of biological and synthetic molecules. *The Journal of Chemical Physics* **2016**, *144*, 030901.

[144] Yang, Q.-Z.; Huang, Z.; Kucharski, T. J.; Khvostichenko, D.; Chen, J.; Boulatov, R. A molecular force probe. *Nature Nanotechnology* **2009**, *4*, 302–306.

[145] Kucharski, T. J.; Huang, Z.; Yang, Q.-Z.; Tian, Y.; Rubin, N. C.; Concepcion, C. D.; Boulatov, R. Kinetics of Thiol/Disulfide Exchange Correlate Weakly with the Restoring Force in the Disulfide Moiety. *Angewandte Chemie International Edition* **2009**, *48*, 7040–7043.

[146] Kucharski, T. J.; Boulatov, R. The physical chemistry of mechanoresponsive polymers. *Journal of Materials Chemistry* **2011**, *21*, 8237–8255.

[147] Avdoshenko, S. M.; Konda, S. S. M.; Makarov, D. E. On the calculation of internal forces in mechanically stressed polyatomic molecules. *The Journal of Chemical Physics* **2014**, *141*, 134115.

[148] Brandhorst, K.; Grunenberg, J. How strong is it? The interpretation of force and compliance constants as bond strength descriptors. *Chemical Society Reviews* **2008**, *37*, 1558–1567.

[149] Carter, E. A.; Goddard, W. Relation between Singlet-Triplet Gaps and Bond Energies. *The Journal of Physical Chemistry* **1986**, *90*, 998–1001.

[150] Jacob, C. R.; Reiher, M. Localizing normal modes in large molecules. *Journal of Chemical Physics* **2009**, *130*, 084106.

[151] Vicharelli, P. A. Generalized Approach to Relaxed Force Constants. *Spectroscopy Letters* **1978**, *11*, 701–705.

[152] Cyvin, S. J.; Slater, N. B. Invariance of Molecular 'Inverse' Force-constants. *Nature* **1960**, *188*, 485.

[153] Decius, J. C. Compliance Matrix and Molecular Vibrations. *The Journal of Chemical Physics* **1963**, *38*, 241–248.

[154] Brandhorst, K.; Grunenberg, J. Characterizing Chemical Bond Strengths Using Generalized Compliance Constants. *ChemPhysChem* **2007**, *8*, 1151–1156.

[155] Cotton, F. A.; Cowley, A. H.; Feng, X. The Use of Density Functional Theory To Understand and Predict Structures and Bonding in Main Group Compounds with Multiple Bonds. *Journal of the American Chemical Society* **1998**, *120*, 1795–1799.

[156] Brandhorst, K.; Grunenberg, J. Efficient computation of compliance matrices in redundant internal coordinates from Cartesian Hessians for nonstationary points. *The Journal of Chemical Physics* **2010**, *132*, 184101.

[157] Stacklies, W.; Vega, M. C.; Wilmanns, M.; Gräter, F. Mechanical Network in Titin Immunoglobulin from Force Distribution Analysis. *PLoS Computational Biology* **2009**, *5*, e1000306.

[158] Stacklies, W.; Seifert, C.; Gräter, F. Implementation of force distribution analysis for molecular dynamics simulations. *BMC Bioinformatics* **2011**, *12*, 101.

[159] Eom, K.; Li, P.-C.; Makarov, D. E.; Rodin, G. J. Relationship between the Mechanical Properties and Topology of Cross-Linked Polymer Molecules: Parallel Strands Maximize the Strength of Model Polymers and Protein Domains. *Journal of Physical Chemistry B* **2003**, *107*, 8730–8733.

[160] Xiao, S.; Stacklies, W.; Debes, C.; Gräter, F. Force distribution determines optimal length of β-sheet crystals for mechanical robustness. *Soft Matter* **2011**, *7*, 1308–1311.

[161] Stacklies, W.; Xia, F.; Gräter, F. Dynamic Allostery in the Methionine Repressor Revealed by Force Distribution Analysis. *PLoS Computational Biology* **2009**, *5*, e1000574.

[162] Seifert, C.; Gräter, F. Force Distribution Reveals Signal Transduction in E. coli Hsp90. *Biophysical Journal* **2012**, *103*, 2195–2202.

[163] Palmai, Z.; Seifert, C.; Gräter, F.; Balog, E. An Allosteric Signaling Pathway of Human 3-Phosphoglycerate Kinase from Force Distribution Analysis. *PLoS Computational Biology* **2014**, *10*, e1003444.

[164] Zhou, B.; Baldus, I. B.; Li, W.; Edwards, S. A.; Gräter, F. Identification of Allosteric Disulfides from Prestress Analysis. *Biophysical Journal* **2014**, *107*, 672–681.

[165] Louet, M.; Seifert, C.; Hensen, U.; Gräter, F. Dynamic Allostery of the Catabolite Activator Protein Revealed by Interatomic Forces. *PLoS Computational Biology* **2015**, *11*, 1–17.

[166] Zhou, J.; Bronowska, A.; Le Coq, J.; Lietha, D.; Gräter, F. Allosteric Regulation of Focal Adhesion Kinase by PIP2 and ATP. *Biophysical Journal* **2015**, *108*, 698–705.

[167] Baldauf, C.; Schneppenheim, R.; Stacklies, W.; Obser, T.; Pieconka, A.; Schneppenheim, S.; Budde, U.; Zhou, J.; Gräter, F. Shear-induced unfolding activates von Willebrand factor A2 domain for proteolysis. *Journal of Thrombosis and Haemostasis* **2009**, *7*, 2096–2105.

[168] Edwards, S. A.; Wagner, J.; Gräter, F. Dynamic prestress in a globular protein. *PLoS Computational Biology* **2012**, *8*, e1002509.

[169] Wang, B.; Xiao, S.; Edwards, S. A.; Gräter, F. Isopeptide Bonds Mechanically Stabilize Spy0128 in Bacterial Pili. *Biophysical Journal* **2013**, *104*, 2051–2057.

[170] Xiao, S.; Stacklies, W.; Cetinkaya, M.; Markert, B.; Gräter, F. Mechanical response of silk crystalline units from force-distribution analysis. *Biophysical Journal* **2009**, *96*, 3997–4005.

[171] Cetinkaya, M.; Xiao, S.; Markert, B.; Stacklies, W.; Gräter, F. Silk Fiber Mechanics from Multiscale Force Distribution Analysis. *Biophysical Journal* **2011**, *100*, 1298–1305.

[172] Young, H. T.; Edwards, S. A.; Gräter, F. How Fast Does a Signal Propagate through Proteins? *PLoS ONE* **2013**, *8*, e64746.

[173] Costescu, B. I.; Gräter, F. Time-resolved force distribution analysis. *BMC Biophysics* **2013**, *6*, 5.

[174] Costescu, B. I.; Gräter, F. Graphene mechanics: II. Atomic stress distribution during indentation until rupture. *Physical Chemistry Chemical Physics* **2014**, *16*, 12582–12590.

[175] Zhou, J.; Aponte-Santamaría, C.; Sturm, S.; Bullerjahn, J. T.; Bronowska, A.; Gräter, F. Mechanism of Focal Adhesion Kinase Mechanosensing. *PLoS Computational Biology* **2015**, *11*, 1–16.

[176] Grimme, S. A General Quantum Mechanically Derived Force Field (QMDFF) for Molecules and Condensed Phase Simulations. *Journal of Chemical Theory and Computation* **2014**, *10*, 4497–4514.

[177] Hartke, B.; Grimme, S. Reactive force fields made simple. *Physical Chemistry Chemical Physics* **2015**, *17*, 16715–16718.

[178] Warshel, A.; Weiss, R. M. An Empirical Valence Bond Approach for Comparing Reactions in Solutions and in Enzymes. *Journal of the American Chemical Society* **1980**, *102*, 6218–6226.

[179] Saitta, A. M.; Soper, P. D.; Wasserman, E.; Klein, M. L. Influence of a knot on the strength of a polymer strand. *Nature* **1999**, *399*, 46–48.

[180] Smalø, H. S.; Uggerud, E. Breaking covalent bonds using mechanical force, which bond breaks? *Molecular Physics* **2013**, *111*, 1563–1573.

[181] Smalø, H. S.; Rybkin, V. V.; Klopper, W.; Helgaker, T.; Uggerud, E. Mechanochemistry: The Effect of Dynamics. *The Journal of Physical Chemistry A* **2014**, *118*, 7683–7694.

[182] Wang, Y.; Zhang, C.; Zhou, E.; Sun, C.; Hinkley, J.; Gates, T. S.; Su, J. Atomistic finite elements applicable to solid polymers. *Computational Materials Science* **2006**, *36*, 292–302.

[183] Quapp, W.; Bofill, J. M. A contribution to a theory of mechanochemical pathways by means of Newton trajectories. *Theoretical Chemistry Accounts* **2016**, *135*, 113.

[184] Stauch, T.; Dreuw, A. A quantitative quantum-chemical analysis tool for the distribution of mechanical force in molecules. *The Journal of Chemical Physics* **2014**, *140*, 134107.

[185] Stauch, T.; Dreuw, A. On the use of different coordinate systems in mechanochemical force analyses. *The Journal of Chemical Physics* **2015**, *143*, 074118.

[186] Stauch, T.; Dreuw, A. Predicting the Efficiency of Photoswitches Using Force Analysis. *The Journal of Physical Chemistry Letters* **2016**, *7*, 1298–1302.

[187] Wilson, E. B.; Decius, J. C.; Cross, P. C. *Molecular Vibrations. The Theory of Infrared and Raman Vibrational Spectra*, 1st ed.; Dover Publications Inc: Mineola, New York, 1955.

[188] Baker, J.; Kessi, A.; Delley, B. The generation and use of delocalized internal coordinates in geometry optimization. *The Journal of Chemical Physics* **1996**, *105*, 192–212.

[189] Pulay, P.; Fogarasi, G.; Pang, F.; Boggs, J. E. Systematic ab Initio Gradient Calculation of Molecular Geometries, Force Constants, and Dipole Moment Derivatives. *Journal of the American Chemical Society* **1979**, *101*, 2550–2560.

[190] Bakken, V.; Helgaker, T. The efficient optimization of molecular geometries using redundant internal coordinates. *The Journal of Chemical Physics* **2002**, *117*, 9160–9174.

[191] Abadir, K. M.; Magnus, J. R. *Matrix Algebra*; Cambridge University Press: Cambridge, 2005.

[192] Hehre, W. J.; Ditchfield, R.; Pople, J. A. SelfConsistent Molecular Orbital Methods. XII. Further Extensions of GaussianType Basis Sets for Use in Molecular Orbital Studies of Organic Molecules. *The Journal of Chemical Physics* **1972**, *56*, 2257–2261.

[193] Møller, C.; Plesset, M. S. Note on an Approximation Treatment for Many-Electron Systems. *Physical Review* **1934**, *46*, 618–622.

[194] Weigend, F.; Häser, M. RI-MP2: first derivatives and global consistency. *Theoretical Chemistry Accounts* **1997**, *97*, 331–340.

[195] Hättig, C.; Weigend, F. CC2 excitation energy calculations on large molecules using the resolution of the identity approximation. *The Journal of Chemical Physics* **2000**, *113*, 5154–5161.

[196] Weigend, F. A fully direct RI-HF algorithm: Implementation, optimised auxiliary basis sets, demonstration of accuracy and efficiency. *Physical Chemistry Chemical Physics* **2002**, *4*, 4285–4291.

[197] Weigend, F.; Köhn, A.; Hättig, C. Efficient use of the correlation consistent basis sets in resolution of the identity MP2 calculations. *The Journal of Chemical Physics* **2002**, *116*, 3175–3183.

[198] Harada, N.; Koumura, N.; Feringa, B. L. Chemistry of Unique Chiral Olefins. 3. Synthesis and Absolute Stereochemistry of trans- and cis-1,1',2,2',3,3',4,4'-Octahydro-3,3'-dimethyl-4,4'- biphenanthrylidenes. *Journal of the American Chemical Society* **1997**, *119*, 7256–7264.

[199] Grimm, S.; Bräuchle, C.; Frank, I. Light-Driven Unidirectional Rotation in a Molecule: ROKS Simulation. *ChemPhysChem* **2005**, *6*, 1943–1947.

[200] Browne, W. R.; Feringa, B. L. Making molecular machines work. *Nature Nanotechnology* **2006**, *1*, 25–35.

[201] Kay, E. R.; Leigh, D. A.; Zerbetto, F. Synthetic Molecular Motors and Mechanical Machines. *Angewandte Chemie International Edition* **2007**, *46*, 72–191.

[202] Spruell, J. M.; Hawker, C. J. Triggered structural and property changes in polymeric nanomaterials. *Chemical Science* **2011**, *2*, 18–26.

[203] Boyle, M. M.; Smaldone, R. A.; Whalley, A. C.; Ambrogio, M. W.; Botros, Y. Y.; Stoddart, J. F. Mechanised materials. *Chemical Science* **2011**, *2*, 204–210.

[204] Nikiforov, A.; Gamez, J. A.; Thiel, W.; Filatov, M. Computational Design of a Family of Light Driven Rotary Molecular Motors with Improved Quantum Efficiency. *The Journal of Physical Chemistry Letters* **2016**, *7*, 105–110.

[205] Bléger, D.; Yu, Z.; Hecht, S. Toward optomechanics: Maximizing the photodeformation of individual molecules. *Chemical Communications* **2011**, *47*, 12260–12266.

[206] Huang, Z.; Boulatov, R. Chemomechanics with molecular force probes. *Pure and Applied Chemistry* **2010**, *82*, 931–951.

[207] Huang, Z.; Boulatov, R. Chemomechanics: chemical kinetics for multiscale phenomena. *Chemical Society Reviews* **2011**, *40*, 2359–2384.

[208] Stauch, T.; Dreuw, A. Knots "Choke Off" Polymers upon Stretching. *Angewandte Chemie International Edition* **2016**, *55*, 811–814.

[209] Stauch, T.; Dreuw, A. Polymere werden beim Strecken durch Knoten abgeschnürt. *Angewandte Chemie* **2016**, *128*, 822–825.

[210] Bauernschmitt, R.; Ahlrichs, R. Treatment of electronic excitations within the adiabatic approximation of time dependent density functional theory. *Chemical Physics Letters* **1996**, *256*, 454–464.

[211] Mulliken, R. S. The lower excited states of some simple molecules. *Canadian Journal of Chemistry* **1958**, *36*, 10–23.

[212] O'Neil, S. V.; Schaefer III, H. F. Valence-Excited States of Carbon Monoxide. *The Journal of Chemical Physics* **1970**, *53*, 3994–4004.

[213] Dugave, C.; Demange, L. Cis-Trans Isomerization of Organic Molecules and Biomolecules: Implications and Applications. *Chemical Reviews* **2003**, *103*, 2475–2532.

[214] Hoff, W. D.; Düx, P.; Hård, K.; Devreese, B.; Nugteren-Roodzant, I. M.; Crielaard, W.; Boelens, R.; Kaptein, R.; van Beeumen, J.; Hellingwerf, K. J. Thiol Ester-Linked p-Coumaric Acid as a New Photoactive Prosthetic Group in a Protein with Rhodopsin-Like Photochemistry. *Biochemistry* **1994**, *33*, 13959–13962.

[215] van Brederode, M. E.; Gensch, T.; Hoff, W. D.; Hellingwerf, K. J.; Braslavsky, S. E. Photoinduced Volume Change and Energy Storage Associated with the Early Transformations of the Photoactive Yellow Protein from Ectothiorhodospira halophila. *Biophysical Journal* **1995**, *68*, 1101–1109.

[216] Kort, R.; Vonk, H.; Xu, X.; Hoff, W. D.; Crielaard, W.; Hellingwerf, K. J. Evidence for trans-cis isomerization of the p-coumaric acid chromophore as the photochemical basis of the photocycle of photoactive yellow protein. *FEBS Letters* **1996**, *382*, 73–78.

[217] Perman, B.; Šrajer, V.; Ren, Z.; Teng, T.-y.; Pradervand, C.; Ursby, T.; Bourgeois, D.; Schotte, F.; Wulff, M.; Kort, R.; Hellingwerf, K.; Moffat, K. Energy Transduction on the Nanosecond Time Scale: Early Structural Events in a Xanthopsin Photocycle. *Science* **1998**, *279*, 1946–1950.

[218] Takeshita, K.; Hirota, N.; Terazima, M. Enthalpy changes and reaction volumes of photoisomerization reactions in solution: azobenzene and p-coumaric acid. *Journal of Photochemistry and Photobiology A: Chemistry* **2000**, *134*, 103–109.

[219] Ryan, W. L.; Gordon, D. J.; Levy, D. H. Gas-Phase Photochemistry of the Photoactive Yellow Protein Chromophore trans-p-Coumaric Acid. *Journal of the American Chemical Society* **2002**, *124*, 6194–6201.

[220] Schotte, F.; Cho, H. S.; Kaila, V. R. I.; Kamikubo, H.; Dashdorj, N.; Henry, E. R.; Graber, T. J.; Henning, R.; Wulff, M.; Hummer, G.; Kataoka, M.; Anfinrud, P. A. Watching a signaling protein function in real time via 100-ps time-resolved Laue crystallography. *Proceedings of the National Academy of Sciences of the United States of America* **2012**, *109*, 19256–19261.

[221] Kundu, P. K.; Lerner, A.; Kučanda, K.; Leitus, G.; Klajn, R. Cyclic Kinetics during Thermal Equilibration of an Axially Chiral Bis-Spiropyran. *Journal of the American Chemical Society* **2014**, *136*, 11276–11279.

[222] Wang, J.; Lv, Y.; Wan, W.; Wang, X.; Li, A. D. Q.; Tian, Z. Photoswitching Near-Infrared Fluorescence from Polymer Nanoparticles Catapults Signals over the Region of Noises and Interferences for Enhanced Sensitivity. *ACS Applied Materials & Interfaces* **2016**, *8*, 4399–4406.

[223] Humphrey, W.; Dalke, A.; Schulten, K. VMD: Visual Molecular Dynamics. *Journal of Molecular Graphics* **1996**, *14*, 33–38.

[224] Frisch, H. J.; Wasserman, E. Chemical Topology. *Chemical Topology* **1961**, *83*, 3789–3795.

[225] Michels, J. P. J.; Wiegel, F. W. Probability of Knots in a Polymer Ring. *Physics Letters A* **1982**, *90A*, 381–384.

[226] Mansfield, M. L. Knots in Hamilton Cycles. *Macromolecules* **1994**, *27*, 5924–5926.

[227] Virnau, P.; Kantor, Y.; Kardar, M. Knots in Globule and Coil Phases of a Model Polyethylene Peter. *Journal of the American Chemical Society* **2005**, *127*, 15102–15106.

[228] van Rensburg, E. J. J.; Sumners, D. A. W.; Wasserman, E.; Whittington, S. G. Entanglement complexity of self-avoiding walks. *Journal of Physics A: Mathematical and General* **1992**, *25*, 6557–6566.

[229] Huang, L.; Makarov, D. E. Langevin Dynamics Simulations of the Diffusion of Molecular Knots in Tensioned Polymer Chains. *Journal of Physical Chemistry A* **2007**, *111*, 10338–10344.

[230] Kirmizialtin, S.; Makarov, D. E. Simulations of the untying of molecular friction knots between individual polymer strands. *The Journal of Chemical Physics* **2008**, *128*, 094901.

[231] Mansfield, M. L. Fit to be tied. *Nature Structural Biology* **1997**, *4*, 166–167.

[232] Taylor, W. R. A deeply knotted protein structure and how it might fold. *Nature* **2000**, *406*, 916–919.

[233] Mallam, A. L.; Jackson, S. E. Folding Studies on a Knotted Protein. *Journal of Molecular Biology* **2005**, *346*, 1409–1421.

[234] Mallam, A. L.; Jackson, S. E. Probing Nature's Knots: The Folding Pathway of a Knotted Homodimeric Protein. *Journal of Molecular Biology* **2006**, *359*, 1420–1436.

[235] Mallam, A. L.; Jackson, S. E. A Comparison of the Folding of Two Knotted Proteins: YbeA and YibK. *Journal of Molecular Biology* **2007**, *366*, 650–665.

[236] Mallam, A. L.; Jackson, S. E. The Dimerization of an α/β-Knotted Protein Is Essential for Structure and Function. *Structure* **2007**, *15*, 111–122.

[237] Wallin, S.; Zeldovich, K. B.; Shakhnovich, E. I. The Folding Mechanics of a Knotted Protein. *Journal of Molecular Biology* **2007**, *368*, 884–893.

[238] Sułkowska, J. I.; Sułkowski, P.; Szymczak, P.; Cieplak, M. Tightening of Knots in Proteins. *Physical Review Letters* **2008**, *100*, 058106.

[239] Huang, L.; Makarov, D. E. Translocation of a knotted polypeptide through a pore. *Journal of Chemical Physics* **2008**, *129*, 121107.

[240] Lim, N. C. H.; Jackson, S. E. Mechanistic Insights into the Folding of Knotted Proteins In Vitro and In Vivo. *Journal of Molecular Biology* **2015**, *427*, 248–258.

[241] Schmid, F. X. How Proteins Knot Their Ties. *Journal of Molecular Biology* **2015**, *427*, 225–227.

[242] Rawdon, E. J.; Millett, K. C.; Stasiak, A. Subknots in ideal knots, random knots, and knotted proteins. *Scientific Reports* **2015**, *5*, 8928.

[243] Frank-Kamenetskii, M. D.; Lukashin, A. V.; Vologodskii, A. V. Statistical mechanics and topology of polymer chains. *Nature* **1975**, *258*, 398–402.

[244] Wasserman, S. A.; Cozzarelli, N. R. Biochemical Topology: Applications to DNA Recombination and Replication. *Science* **1986**, *232*, 951–960.

[245] Schlick, T.; Olson, W. K. Trefoil Knotting Revealed by Molecular Dynamics Simulations of Supercoiled DNA. *Science* **1992**, *257*, 1110–1115.

[246] Shaw, S. Y.; Wang, J. C. Knotting of a DNA Chain During Ring Closure. *Science* **1993**, *260*, 533–536.

[247] Arai, Y.; Yasuda, R.; Akashi, K.-i.; Harada, Y.; Miyata, H.; Kinosita, K.; Itoh, H. Tying a molecular knot with optical tweezers. *Nature* **1999**, *399*, 446–448.

[248] Ashley, C. W. *The Ashley Book of Knots*; Doubleday: New York, 1944.

[249] Saitta, A. M.; Klein, M. L. Polyethylene under tensile load: strain energy storage and breaking of linear and knotted alkanes probed by first-principles molecular dynamics calculations. *Journal of Chemical Physics* **1999**, *111*, 9434–9440.

[250] Saitta, A. M.; Klein, M. L. Evolution of Fragments Formed at the Rupture of a Knotted Alkane Molecule. *Journal of the American Chemical Society* **1999**, *121*, 11827–11830.

[251] Siepmann, J. I.; Karaboni, S.; Smit, B. Simulating the critical behavior of complex fluids. *Nature* **1993**, *365*, 330–332.

[252] Mundy, C. J.; Balasubramanian, S.; Bagchi, K.; Siepmann, J. I.; Klein, M. L. Equilibrium and non-equilibrium simulation studies of fluid alkanes in bulk and at interfaces. *Faraday Discussions* **1996**, *104*, 17–36.

[253] Shao, Y.; Molnar, L. F.; Jung, Y.; Kussmann, J.; Ochsenfeld, C.; Brown, S. T.; Gilbert, A. T. B.; Slipchenko, L. V.; Levchenko, S. V.; O'Neill, D. P.; DiStasio, R. A.; Lochan, R. C.; Wang, T.; Beran, G. J. O.; Besley, N. A.; Herbert, J. M.; Lin, C. Y.; van Voorhis, T.; Chien, S. H.; Sodt, A.; Steele, R. P.; Rassolov, V. A.; Maslen, P. E.; Korambath, P. P.; Adamson, R. D.; Austin, B.; Baker, J.; Byrd, E. F. C.; Dachsel, H.; Doerksen, R. J.; Dreuw, A.; Dunietz, B. D.; Dutoi, A. D.; Furlani, T. R.; Gwaltney, S. R.; Heyden, A.; Hirata, S.; Hsu, C.-P.; Kedziora, G.; Khalliulin, R. Z.; Klunzinger, P.; Lee, A. M.; Lee, M. S.; Liang, W.; Lotan, I.; Nair, N.; Peters, B.; Proynov, E. I.; Pieniazek, P. A.; Rhee, Y. M.;

Ritchie, J.; Rosta, E.; Sherrill, C. D.; Simmonett, A. C.; Subotnik, J. E.; Woodcock, H. L.; Zhang, W.; Bell, A. T.; Chakraborty, A. K.; Chipman, D. M.; Keil, F. J.; Warshel, A.; Hehre, W. J.; Schaefer, H. F.; Kong, J.; Krylov, A. I.; Gill, P. M. W.; Head-Gordon, M. Advances in methods and algorithms in a modern quantum chemistry program package. *Physical Chemistry Chemical Physics* **2006**, 3172–3191.

[254] Saitta, A. M.; Klein, M. L. First-Principles Molecular Dynamics Study of the Rupture Processes of a Bulklike Polyethylene. *The Journal of Physical Chemistry B* **2001**, *105*, 6495–6499.

[255] Bernasconi, M.; Parrinello, M.; Chiarotti, G.; Focher, P.; Tosatti, E. Anisotropic a-C:H from Compression of Polyacetylene. *Physical Review Letters* **1996**, *76*, 2081–2084.

[256] Miao, M. S.; van Camp, P. E.; van Doren, V. E.; Ladik, J. J.; Mintmire, J. W. Conformation and electronic structure of polyethylene: A density-functional approach. *Physical Review B* **1996**, *54*, 10430–10435.

[257] Bernasconi, M.; Chiarotti, G.; Focher, P.; Parrinello, M.; Tosatti, E. Solid-State Polymerization of Acetylene under Pressure: Ab Initio Simulation. *Physical Review Letters* **1997**, *78*, 2008–2011.

[258] Borrmann, A.; Montanari, B.; Jones, R. O. Density functional study of polypropylene and its submolecules. *The Journal of Chemical Physics* **1997**, *106*, 8545–8551.

[259] Montanari, B.; Jones, R. O. Density functional study of crystalline polyethylene. *Chemical Physics Letters* **1997**, *272*, 347–352.

[260] Lourderaj, U.; McAfee, J. L.; Hase, W. L. Potential energy surface and unimolecular dynamics of stretched n-butane. *The Journal of Chemical Physics* **2008**, *129*, 094701.

[261] Dopieralski, P.; Anjukandi, P.; Rückert, M.; Shiga, M.; Ribas-Arino, J.; Marx, D. On the role of polymer chains in transducing external mechanical forces to benzocyclobutene mechanophores. *Journal of Materials Chemistry* **2011**, *21*, 8309–8316.

[262] Stauch, T.; Dreuw, A. Stiff-stilbene photoswitch ruptures bonds not by pulling but by local heating. *Physical Chemistry Chemical Physics* **2016**, *18*, 15848–15853.

[263] Hayes, R.; Ingham, S.; Saengchantara, S. T.; Wallace, T. W. Thermal Electrocyclic Ring-Opening of Cyclobutenes: Substituents with Complementary Conrotatory Preferences Induce High Stereoselectivity. *Tetrahedron Letters* **1991**, *32*, 2953–2954.

[264] Binns, F.; Hayes, R.; Ingham, S.; Saengchantara, S. T.; Turner, R. W.; Wallace, T. W. Thermal electrocyclic ring-opening of cyclobutenes: stereoselective routes to functionalised conjugated (Z,E)- and (E,E)-2,4-dienals. *Tetrahedron* **1992**, *48*, 515–530.

[265] Binns, F.; Hayes, R.; Hodgetts, K. J.; Saengchantara, S. T.; Wallace, T. W.; Wallis, C. J. The Preparation and Electrocyclic Ring-opening of Cyclobutenes: Stereocontrolled Approaches to Substituted Conjugated Dienes and Trienes. *Tetrahedron* **1996**, *52*, 3631–3658.

[266] Murakami, M.; Hasegawa, M.; Igawa, H. Theoretical and Experimental Studies on the Thermal Ring-Opening Reaction of Cyclobutene Having a Stannyl Substitutent at the 3-Position. *The Journal of Organic Chemistry* **2004**, *69*, 587–590.

[267] Murakami, M.; Hasegawa, M. Synthesis and Thermal Ring Opening of trans-3,4-Disilylcyclobutene. *Angewandte Chemie International Edition* **2004**, *43*, 4874–4876.

[268] Hasegawa, M.; Murakami, M. Studies on the Thermal Ring-Opening Reactions of cis-3,4-Bis(organosilyl)cyclobutenes. *The Journal of Organic Chemistry* **2007**, *72*, 3764–3769.

[269] Nava, P.; Carissan, Y. On the ring-opening of substituted cyclobutene to benzocyclobutene: analysis of π delocalization, hyperconjugation, and ring strain. *Physical Chemistry Chemical Physics* **2014**, *16*, 16196–16203.

[270] Doany, F. E.; Heilweil, E. J.; Moore, R.; Hochstrasser, R. M. Picosecond study of an intermediate in the trans to cis isomerization pathway of stiff stilbene. *The Journal of Chemical Physics* **1984**, *80*, 201–206.

[271] Schneider, S.; Brem, B.; Jäger, W.; Rehaber, H.; Lenoir, D.; Frank, R. Influence of solvent viscosity on the photoisomerization of a novel trans-stilbene derivative with hindered single bond torsion. *Chemical Physics Letters* **1999**, *308*, 211–217.

[272] Hohlneicher, G.; Wrzal, R.; Lenoir, D.; Frank, R. Two-Photon Spectra of Stiff Stilbenes: A Contribution to the Assignment of the Low Lying Electronically Excited States of the Stilbene System. *Journal of Physical Chemistry A* **1999**, *103*, 8969–8975.

[273] Improta, R.; Santoro, F. Excited-State Behavior of trans and cis Isomers of Stilbene and Stiff Stilbene: A TD-DFT Study. *The Journal of Physical Chemistry A* **2005**, *109*, 10058–10067.

[274] Liu, F.; Morokuma, K. Computational Study on the Working Mechanism of a Stilbene Light-Driven Molecular Rotary Motor: Sloped Minimal Energy Path and Unidirectional Nonadiabatic Photoisomerization. *Journal of the American Chemical Society* **2012**, *134*, 4864–4876.

[275] Quick, M.; Berndt, F.; Dobryakov, A. L.; Ioffe, I. N.; Granovsky, A. A.; Knie, C.; Mahrwald, R.; Lenoir, D.; Ernsting, N. P.; Kovalenko, S. A. Photoisomerization Dynamics of Stiff-Stilbene in Solution. *The Journal of Physical Chemistry B* **2014**, *118*, 1389–1402.

[276] Plasser, F.; Wormit, M.; Dreuw, A. New tools for the systematic analysis and visualization of electronic excitations. I. Formalism. *The Journal of Chemical Physics* **2014**, *141*, 024106.

[277] Plasser, F.; Bäppler, S. A.; Wormit, M.; Dreuw, A. New tools for the systematic analysis and visualization of electronic excitations. II. Applications. *The Journal of Chemical Physics* **2014**, *141*, 024107.

[278] Plasser, F.; Thomitzni, B.; Bäppler, S. A.; Wenzel, J.; Rehn, D. R.; Wormit, M.; Dreuw, A. Statistical Analysis of Electronic Excitation Processes: Spatial Location, Compactness, Charge Transfer, and Electron-Hole Correlation. *Journal of Computational Chemistry* **2015**, *36*, 1609–1620.

[279] Schirmer, J. Beyond the random-phase approximation: A new approximation scheme for the polarization propagator. *Physical Review A* **1982**, *26*, 2395–2416.

[280] Trofimov, A. B.; Stelter, G.; Schirmer, J. A consistent third-order propagator method for electronic excitation. *Journal of Chemical Physics* **1999**, *111*, 9982–9999.

[281] Schirmer, J.; Trofimov, A. B. Intermediate state representation approach to physical properties of electronically excited molecules. *Journal of Chemical Physics* **2004**, *120*, 11449–11464.

[282] Dreuw, A.; Wormit, M. The algebraic diagrammatic construction scheme for the polarization propagator for the calculation of excited states. *Wiley Interdisciplinary Reviews: Computational Molecular Science* **2015**, *5*, 82–95.

[283] Jmol: an open-source Java viewer for chemical structures in 3D. http://www.jmol.org/.

[284] Schmidt, S. W.; Kersch, A.; Beyer, M. K.; Clausen-Schaumann, H. Mechanically activated rupture of single covalent bonds: evidence of force induced bond hydrolysis. *Physical Chemistry Chemical Physics* **2011**, *13*, 5994–5999.

[285] Genick, U. K.; Soltis, S. M.; Kuhn, P.; Canestrelli, I. L.; Getzoff, E. D. Structure at 0.85 A resolution of an early protein photocycle intermediate. *Nature* **1998**, *392*, 206–209.

[286] Lamb, T. D. Gain and kinetics of activation in the G-protein cascade of photo-transduction. *Proceedings of the National Academy of Sciences of the United States of America* **1996**, *93*, 566–570.

[287] Yawo, H.; Kandori, H.; Koizumi, A. *Optogenetics*, 1st ed.; Springer Japan, 2015; pp 3–16.

[288] Martinez, M. L.; Cooper, W. C.; Chou, P.-T. A novel excited-state intramolecular proton transfer molecule, 10-hydroxybenzo[h]quinoline. *Chemical Physics Letters* **1992**, *193*, 151–154.

[289] Deperasińska, I.; Gryko, D. T.; Karpiuk, E.; Kozankiewicz, B.; Makarewicz, A.; Piechowska, J. Low-Temperature Spectra of the Analogues of 10-Hydroxybenzo[h]quinoline as an Indication of Barrierless ESIPT. *The Journal of Physical Chemistry A* **2012**, *116*, 12049–12055.

[290] Bredt, J. Über sterische Hinderung in Brückenringen (Bredtsche Regel) und über die meso-trans-Stellung in kondensierten Ringsystemen des Hexamethylens. *Justus Liebigs's Annalen der Chemie* **1924**, *437*, 1–13.

[291] Shea, K. J. Recent developments in the synthesis, structure and chemistry of bridgehead alkenes. *Tetrahedron* **1980**, *36*, 1683–1715.

[292] Maier, W. F.; von Ragué Schleyer, P. Evaluation and Prediction of the Stability of Bridgehead Olefins. *Journal of the American Chemical Society* **1981**, *103*, 1891–1900.

[293] Warner, P. M. Strained Bridgehead Double Bonds. *Chemical Reviews* **1989**, *89*, 1067–1093.

[294] Johnson, R. P. Strained Cyclic Cumulenes. *Chemical Reviews* **1989**, *89*, 1111–1124.

[295] Hoffmann, R.; Hopf, H. Learning from Molecules in Distress. *Angewandte Chemie International Edition* **2008**, *47*, 4474–4481.

[296] Dodziuk, H. *Strained Hydrocarbons: Beyond the van't Hoff and Le Bel Hypothesis*, 1st ed.; Wiley-VCH: Weinheim, 2009.

[297] Typke, V.; Haase, J.; Krebs, A. The Molecular Structure of Cyclononyne: A Gas Phase Electron Diffraction Investigation. *Journal of Molecular Structure* **1979**, *56*, 77–86.

[298] Trætteberg, M.; Lüttke, W.; Machinek, R.; Krebs, A.; Hohlt, H. J. Cyclooctyne - a sterically strained molecule with an unusual CC triple bond geometry. *Journal of Molecular Structure* **1985**, *128*, 217–232.

[299] Johnson, R. P.; Daoust, K. J. Interconversions of Cyclobutyne, Cyclopentyne, Cyclohexyne, and Their Corresponding Cycloalkylidenecarbenes. *Journal of the American Chemical Society* **1995**, *117*, 362–367.

[300] Hopf, H.; Grunenberg, J. In *Strained Hydrocarbons: Beyond the van't Hoff and Le Bel Hypothesis*, 1st ed.; Dodziuk, H., Ed.; Wiley-VCH: Weinheim, 2009; pp 375–397.

[301] Willey, F. G. Photolysis of 1-Tosylamino-1,2,3-triazole Anions; A New Synthesis of Alkynes. *Angewandte Chemie International Edition* **1964**, *3*, 138.

[302] Willey, F. G. Die Photolyse von 1-Tosylamino-1.2.3-triazol-Anionen - eine neue Synthese von Alkinen. *Angewandte Chemie* **1964**, *76*, 144.

[303] Wittig, G.; Meske-Schüller, J. Bildung und Verhalten von Cycloheptin. *Liebigs Annalen der Chemie* **1968**, *711*, 65–75.

[304] Krebs, A.; Kimling, H. 3,3,7,7-Tetramethylcycloheptin, ein isolierbares carbocyclisches Siebenring-Alkin. *Angewandte Chemie* **1971**, *83*, 540–541.

[305] Allinger, N. L.; Meyer, A. Y. Conformational Analysis - CIX. Applications of Molecular Mechanics to the Structures and Energies of Alkynes. *Tetrahedron* **1975**, *31*, 1807–1811.

[306] Krebs, A.; Cholcha, W.; Müller, M.; Eicher, T.; Pielartzik, H.; Schnöckel, H. Erzeugung von Sieben- und Sechsring-Alkinen durch Photolyse und Thermolyse von Cyclopropenonen. *Tetrahedron Letters* **1984**, *25*, 5027–5030.

[307] Fujita, M.; Sakanishi, Y.; Nishii, M.; Okuyama, T. Cycloheptyne Intermediate in the Reaction of Chiral Cyclohexylidenemethyliodonium Salt with Sulfonates. *Journal of Organic Chemistry* **2002**, *67*, 8138–8146.

[308] Haase, J.; Krebs, A. Die Molekülstruktur des 3.3.6.6-Tetramethyl-1-thiacycloheptins. *Zeitschrift für Naturforschung Teil A* **1972**, *27a*, 624–627.

[309] Haase, J.; Krebs, A. Die Molekülstruktur des Cyclooctins. *Zeitschrift für Natur-forschung Teil A* **1971**, *26a*, 1190–1193.

[310] Daoust, K. J.; Hernandez, S. M.; Konrad, K. M.; Mackie, I. D.; Winstanley, J.; Johnson, R. P. Strain Estimates for Small-Ring Cyclic Allenes and Butatrienes. *The Journal of Organic Chemistry* **2006**, *71*, 5708–5714.

[311] Potisek, S. L.; Davis, D. A.; Sottos, N. R.; White, S. R.; Moore, J. S. Mechanophore-Linked Addition Polymers. *Journal of the American Chemical Society* **2007**, *129*, 13808–13809.

[312] May, P. A.; Moore, J. S. Polymer mechanochemistry: techniques to generate molecular force via elongational flows. *Chemical Society Reviews* **2013**, *42*, 7497–7506.

[313] Davis, D. A.; Hamilton, A.; Yang, J.; Cremar, L. D.; van Gough, D.; Potisek, S. L.; Ong, M. T.; Braun, P. V.; Martínez, T. J.; White, S. R.; Moore, J. S.; Sottos, N. R. Force-induced activation of covalent bonds in mechanoresponsive polymeric materials. *Nature* **2009**, *459*, 68–72.

[314] Lenhardt, J. M.; Black Ramirez, A. L.; Lee, B.; Kouznetsova, T. B.; Craig, S. L. Mechanistic Insights into the Sonochemical Activation of Multimechanophore Cyclopropanated Polybutadiene Polymers. *Macromolecules* **2015**, *48*, 6396–6403.

[315] Caruso, M. M.; Davis, D. A.; Shen, Q.; Odom, S. A.; Sottos, N. R.; White, S. R.; Moore, J. S. Mechanically-Induced Chemical Changes in Polymeric Materials. *Chemical Reviews* **2009**, *109*, 5755–5798.

[316] Brantley, J. N.; Konda, S. S. M.; Makarov, D. E.; Bielawski, C. W. Regiochemical Effects on Molecular Stability: A Mechanochemical Evaluation of 1,4- and 1,5-Disubstituted Triazoles. *Journal of the American Chemical Society* **2012**, *134*, 9882–9885.

[317] Wool, R. P.; Statton, W. O. Dynamic Polarized Infrared Studies of Stress Relaxation and Creep in Polypropylene. *Journal of Polymer Science Part B: Polymer Physics* **1974**, *12*, 1575–1586.

[318] Ciezak, J. A.; Jenkins, T. A.; Liu, Z.; Hemley, R. J. High-Pressure Vibrational Spectroscopy of Energetic Materials: Hexahydro-1,3,5-trinitro-1,3,5-triazine. *Journal of Physical Chemistry A* **2007**, *111*, 59–63.

[319] Dreger, Z. A.; Gupta, Y. M. Raman Spectroscopy of High-Pressure-High-Temperature Polymorph of Hexahydro-1,3,5-trinitro-1,3,5-triazine (ϵ-RDX). *Journal of Physical Chemistry A* **2010**, *114*, 7038–7047.

[320] Zheng, X.; Zhao, J.; Tan, D.; Liu, C.; Song, Y.; Yang, Y. High-Pressure Vibrational Spectroscopy of Hexahydro-1,3,5-Trinitro-1,3,5-Triazine (RDX). *Propellants, Explosives, Pyrotechnics* **2011**, *36*, 22–27.

[321] Pereverzev, A.; Sewell, T. D.; Thompson, D. L. Molecular dynamics study of the pressure-dependent terahertz infrared absorption spectrum of α- and γ-RDX. *The Journal of Chemical Physics* **2013**, *139*, 044108.

[322] Röhrig, U. F.; Troppmann, U.; Frank, I. Organic chromophores under tensile stress. *Chemical Physics* **2003**, *289*, 381–388.

[323] Marawske, S.; Dörr, D.; Schmitz, D.; Koslowski, A.; Lu, Y.; Ritter, H.; Thiel, W.; Seidel, C. A. M.; Kühnemuth, R. Fluorophores as Optical Sensors for Local Forces. *ChemPhysChem* **2009**, *10*, 2041–2048.

[324] Stauch, T.; Dreuw, A. Force-Spectrum Relations for Molecular Optical Force Probes. *Angewandte Chemie International Edition* **2014**, *53*, 2759–2761.

[325] Stauch, T.; Dreuw, A. Kraft-Spektrum-Beziehungen molekularer optischer Kraftsonden. *Angewandte Chemie* **2014**, *126*, 2797–2800.

[326] Levinthal, C. Are There Pathways for Protein Folding? *Extrait du Journal de Chimie Physique* **1968**, *65*, 44–45.

[327] Anfinsen, C. B. The Formation and Stabilization of Protein Structure. *Biochemical Journal* **1972**, *128*, 737–749.

[328] Anfinsen, C. B. Principles that Govern the Folding of Protein Chains. *Science* **1973**, *181*, 223–230.

[329] Kim, P. S. Intermediates In The Folding Reactions Of Small Proteins. *Annual Review of Biochemistry* **1990**, *59*, 631–660.

[330] Leopold, P. E.; Montal, M.; Onuchic, J. N. Protein folding funnels: A kinetic approach to the sequence-structure relationship. *Proceedings of the National Academy of Sciences of the United States of America* **1992**, *89*, 8721–8725.

[331] Shortle, D. The denatured state (the other half of the folding equation) and its role in protein stability. *The FASEB Journal* **1996**, *10*, 27–34.

[332] Deechongkit, S.; Nguyen, H.; Powers, E. T.; Dawson, P. E.; Gruebele, M.; Kelly, J. W. Context-dependent contributions of backbone hydrogen bonding to beta-sheet folding energetics. *Nature* **2004**, *430*, 101–105.

[333] Onuchic, J. N.; Wolynes, P. G. Theory of protein folding. *Current Opinion in Structural Biology* **2004**, *14*, 70–75.

[334] Rose, G. D.; Fleming, P. J.; Banavar, J. R.; Maritan, A. A backbone-based theory of protein folding. *Proceedings of the National Academy of Sciences of the United States of America* **2006**, *103*, 16623–16633.

[335] Compiani, M.; Capriotti, E. Computational and Theoretical Methods for Protein Folding. *Biochemistry* **2013**, *52*, 8601–8624.

[336] Dill, K. A. Dominant Forces in Protein Folding. *Biochemistry* **1990**, *29*, 7133–7155.

[337] Pace, C. N.; Shirley, B. A.; McNutt, M.; Gajiwala, K. Forces contributing to the conformational stability of proteins. *The FASEB Journal* **1996**, *10*, 75–83.

[338] Nölting, B.; Salimi, N.; Guth, U. Protein folding forces. *Journal of Theoretical Biology* **2008**, *251*, 331–347.

[339] Rief, M.; Gautel, M.; Schemmel, A.; Gaub, H. E. The Mechanical Stability of Immunoglobulin and Fibronectin III Domains in the Muscle Protein Titin Measured by Atomic Force Microscopy. *Biophysical Journal* **1998**, *75*, 3008–3014.

[340] Rief, M.; Pascual, J.; Saraste, M.; Gaub, H. E. Single Molecule Force Spectroscopy of Spectrin Repeats: Low Unfolding Forces in Helix Bundles. *Journal of Molecular Biology* **1999**, *286*, 553–561.

[341] Carrion-Vazquez, M.; Oberhauser, A. F.; Fowler, S. B.; Marszalek, P. E.; Broedel, S. E.; Clarke, J.; Fernandez, J. M. Mechanical and chemical unfolding of a single protein: A comparison. *Proceedings of the National Academy of Sciences of the United States of America* **1999**, *96*, 3694–3699.

[342] Lenne, P.-F.; Raae, A. J.; Altmann, S. M.; Saraste, M.; Hörber, J. K. H. States and transitions during forced unfolding of a single spectrin repeat. *FEBS Letters* **2000**, *476*, 124–128.

[343] Meng, F.; Suchyna, T. M.; Sachs, F. A fluorescence energy transfer-based mechanical stress sensor for specific proteins in situ. *FEBS Journal* **2008**, *275*, 3072–3087.

[344] Grashoff, C.; Hoffman, B. D.; Brenner, M. D.; Zhou, R.; Parsons, M.; Yang, M. T.; McLean, M. A.; Sligar, S. G.; Chen, C. S.; Ha, T.; Schwartz, M. A. Measuring mechanical tension across vinculin reveals regulation of focal adhesion dynamics. *Nature* **2010**, *466*, 263–266.

[345] Meng, F.; Sachs, F. Visualizing dynamic cytoplasmic forces with a compliance-matched FRET sensor. *Journal of Cell Science* **2011**, *124*, 261–269.

[346] Meng, F.; Suchyna, T. M.; Lazakovitch, E.; Gronostajski, R. M.; Sachs, F. Real Time FRET Based Detection of Mechanical Stress in Cytoskeletal and Extracellular Matrix Proteins. *Cellular and Molecular Bioengineering* **2011**, *4*, 148–159.

[347] Meng, F.; Sachs, F. Orientation-based FRET sensor for real-time imaging of cellular forces. *Journal of Cell Science* **2012**, *125*, 743–750.

[348] Black, A. L.; Lenhardt, J. M.; Craig, S. L. From molecular mechanochemistry to stress-responsive materials. *Journal of Materials Chemistry* **2011**, *21*, 1655–1663.

[349] Ciardelli, F.; Ruggeri, G.; Pucci, A. Dye-containing polymers: methods for preparation of mechanochromic materials. *Chemical Society Reviews* **2013**, *42*, 857–870.

[350] Stauch, T.; Hoffmann, M. T.; Dreuw, A. Spectroscopic Monitoring of Mechanical Forces during Protein Folding by using Molecular Force Probes. *ChemPhysChem* **2016**, *17*, 1486–1492.

[351] Improta, S.; Politou, A. S.; Pastore, A. Immunoglobulin-like modules from titin I-band: extensible components of muscle elasticity. *Structure* **1996**, *4*, 323–337.

[352] Nave, R.; Fürst, D. O.; Weber, K. Visualization of the Polarity of Isolated Titin Molecules: A Single Globular Head on a Long Thin Rod As the M Band Anchoring Domain? *The Journal of Cell Biology* **1989**, *109*, 2177–2187.

[353] Maruyama, K. Connectin, an elastic protein of striated muscle. *Biophysical Chemistry* **1994**, *50*, 73–85.

[354] Trinick, J. Titin and nebulin: Protein rulers in muscle? *Trends in Biochemical Sciences* **1994**, *19*, 405–409.

[355] Keller III, T. C. Structure and function of titin and nebulin. *Current Opinion in Cell Biology* **1995**, *7*, 32–38.

[356] Hess, B.; Kutzner, C.; Van Der Spoel, D.; Lindahl, E. GROMACS 4: Algorithms for Highly Efficient, Load-Balanced, and Scalable Molecular Simulation. *Journal of Chemical Theory and Computation* **2008**, *4*, 435–447.

[357] Ponder, J. W.; Case, D. A. Force Fields for Protein Simulations. *Advances in Protein Chemistry* **2003**, *66*, 27–85.

[358] Wang, J.; Wolf, R. M.; Caldwell, J. W.; Kollman, P. A.; Case, D. A. Development and Testing of a General Amber Force Field. *Journal of Computational Chemistry* **2004**, *25*, 1157–1174.

[359] Case, D. A.; Cheatham III, T. E.; Darden, T.; Gohlke, H.; Luo, R.; Merz, K. M.; Onufriev, A.; Simmerling, C.; Wang, B.; Woods, R. J. The Amber biomolecular simulation programs. *Journal of Computational Chemistry* **2005**, *26*, 1668–1688.

[360] Wang, J.; Wang, W.; Kollman, P. A.; Case, D. A. Automatic atom type and bond type perception in molecular mechanical calculations. *Journal of Molecular Graphics and Modelling* **2006**, *25*, 247–260.

[361] Sousa da Silva, A. W.; Vranken, W. F. ACPYPE - AnteChamber PYthon Parser interfacE. *BMC Research Notes* **2012**, *5*, 367.

[362] Colarusso, P.; Zhang, K.; Guo, B.; Bernath, P. F. The infrared spectra of uracil, thymine, and adenine in the gas phase. *Chemical Physics Letters* **1997**, *269*, 39–48.

[363] Neugebauer, J.; Reiher, M.; Kind, C.; Hess, B. A. Quantum Chemical Calculation of Vibrational Spectra of Large Molecules - Raman and IR Spectra for Buckminsterfullerene. *Journal of Computational Chemistry* **2002**, *23*, 895–910.

[364] Barth, A. Infrared spectroscopy of proteins. *Biochimica et Biophysica Acta* **2007**, *1767*, 1073–1101.

Publication List

1. a) <u>Stauch, T.</u>; Dreuw, A. Force-Spectrum Relations for Molecular Optical Force Probes. *Angewandte Chemie International Edition* **2014**, *53*, 2759-2761. b) <u>Stauch, T.</u>; Dreuw, A. Kraft-Spektrum-Beziehungen molekularer optischer Kraftsonden. *Angewandte Chemie* **2014**, *126*, 2797-2800.

2. <u>Stauch, T.</u>; Dreuw, A. A quantitative quantum-chemical analysis tool for the distribution of mechanical force in molecules. *The Journal of Chemical Physics* **2014**, *140*, 134107.

3. <u>Stauch, T.</u>; Dreuw, A. On the use of different coordinate systems in mechanochemical force analyses. *The Journal of Chemical Physics* **2015**, *143*, 074118.

4. a) <u>Stauch, T.</u>; Dreuw, A. Knots "Choke Off" Polymers upon Stretching. *Angewandte Chemie International Edition* **2016**, *55*, 811-814. b) <u>Stauch, T.</u>; Dreuw, A. Polymere werden beim Strecken durch Knoten abgeschnürt. *Angewandte Chemie* **2016**, *128*, 822-825.

5. <u>Stauch, T.</u>; Dreuw, A. Predicting the Efficiency of Photoswitches Using Force Analysis. *The Journal of Chemical Physics Letters* **2016**, *7*, 1298-1302.

6. <u>Stauch, T.</u>; Scholtes, J. F.; Dreuw, A. Rational design of improved dienophiles for in vivo tetrazine-trans-cyclooctene ligation. *Chemical Physics Letters* **2016**, *654*, 6-8.

7. <u>Stauch, T.</u>; Hoffmann, M. T.; Dreuw, A. Spectroscopic Monitoring of Mechanical Forces during Protein Folding by using Molecular Force Probes. *ChemPhysChem* **2016**, *17*, 1486-1492.

8. Stauch, T.; Dreuw, A. Stiff-stilbene photoswitch ruptures bonds not by pulling but by local heating. *Physical Chemistry Chemical Physics* **2016**, *18*, 15848-15853.

9. Stauch, T.; Günther, B.; Dreuw, A. Can Strained Hydrocarbons Be "Forced" to Be Stable? *The Journal of Physical Chemistry A*, in revision

10. Stauch, T., Dreuw, A. Advances in Quantum Mechanochemistry: Electronic Structure Methods and Force Analysis. *Chemical Reviews*, invited review, submitted for publication

List of Figures

List of Tables

Danksagung

Mein Dank gilt zuallererst Prof. Dr. Andreas Dreuw, der mich seit meiner Bachelorarbeit konsequent unterstützt hat und in den vergangenen Jahren mehr als nur ein Doktorvater für mich war. Ich bedanke mich für die Bereitstellung dieses faszinierenden Themas, für die vielen Diskussionen und interessanten Fragen, die dabei aufgekommen sind und nicht zuletzt für die Schaffung einer Atmosphäre, in der die Arbeit in dieser Gruppe immer Spaß gemacht hat. Bei Dr. Markus Pernpointner bedanke ich mich herzlich für die Begutachtung meiner Doktorarbeit.

Mein besonderer Dank gilt meiner gesamten Familie, die mich in jedweder Hinsicht stets bedingungslos unterstützt hat. Meine Eltern, meine Großeltern und mein Bruder haben die Voraussetzung für diese Promotion geschaffen.

Ich möchte mich ferner bei der gesamten Arbeitsgruppe Dreuw für zahlreiche erkenntnisreiche Gespräche innerhalb und vielfältige Aktivitäten außerhalb des IWR bedanken. Max, Daniel, Daria, Manu, Stefan, Jan M., Steffi, Ben, Marvin, Jan W., Michael, Tobias, Chong, Jie, Jörg, Georg, Mary, Adrian sowie den ehemaligen Mitgliedern Dirk, Philipp, Katie, Shirin, Matze und Felix gilt mein Dank für die stetige Unterstützung in den vergangenen Jahren. Ich möchte mich außerdem bei Ellen Vogel und Manfred Trunk für die Minimierung des verwaltungstechnischen Aufwands sowie der Hard- und Softwareprobleme bedanken. Einen besonderen Dank möchte ich Dr. Michael Wormit aussprechen, dessen Beharrlichkeit mich stets dazu veranlasst hat, immer wieder neu über die JEDI Analyse nachzudenken.

Ich bedanke mich herzlich bei den Forschungspraktikanten sowie den Bachelor- und Masterstudenten, die auf dem Gebiet der Quanten-Mechanochemie mitgearbeitet haben. Marvin Hoffmann, Benjamin Günther, Kai Kohler und Dieter Faltermeier haben durch ihr konstantes Engagement und viele interessante Diskussionen einen wichtigen Beitrag zu dieser Arbeit geleistet.

Bei Dr. Jan Wenzel, Daniel Lefrancois und meinem Bruder Benjamin bedanke ich mich für das Korrekturlesen dieser Doktorarbeit.

Meinen Kommilitonen aus Frankfurt danke ich für die schöne Zeit, an die ich gerne zurückdenke, sowie für die konstante Unterstützung während des Chemiestudiums.

Ich möchte mich ferner bei allen meinen Freunden bedanken, die mich auf diesem Weg begleitet und zeitweise für die nötige Ablenkung gesorgt haben. Ich bedanke mich herzlich bei Dr. Björn Pospiech, meinem Meister und Schulleiter des Taekwon-Do Centers Heidelberg, sowie bei allen anderen Trainern und Mitgliedern für die Möglichkeit, meine Arbeit auch mal hinter mir zu lassen und mich nicht nur auf dem Weg der Theoretischen Chemie weiterzuentwickeln.

Abschließend möchte ich mich beim Verband der Chemischen Industrie für mein Chemiefonds-Stipendium und für die Finanzierung diverser Konferenzreisen bedanken. Der Heidelberg Graduate School of Mathematical and Computational Methods for the Sciences (HGS MathComp) sowie der Graduiertenakademie der Universität Heidelberg danke ich ebenso für die Finanzierung von Konferenzreisen sowie für die Gelegenheit, zahlreiche Kurse zu fachnahen und fachfremden Themen zu absolvieren.

Eidesstattliche Versicherung gemäß § 8 der Promotionsordnung der Naturwissenschaftlich-Mathematischen Gesamtfakultät der Universität Heidelberg

1. Bei der eingereichten Dissertation zu dem Thema
   "Development and Application of Quantum Chemical Methods for the Description of Molecules Under Mechanical Stress"
   handelt es sich um meine eigenständig erbrachte Leistung.

2. Ich habe nur die angegebenen Quellen und Hilfsmittel benutzt und mich keiner unzulässigen Hilfe Dritter bedient. Insbesondere habe ich wörtlich oder sinngemäß aus anderen Werken übernommene Inhalte als solche kenntlich gemacht.

3. Die Arbeit oder Teile davon habe ich bislang nicht an einer Hochschule des In- oder Auslands als Bestandteil einer Prüfungs- oder Qualifikationsleistung vorgelegt.

4. Die Richtigkeit der vorstehenden Erklärungen bestätige ich.

5. Die Bedeutung der eidesstattlichen Versicherung und die strafrechtlichen Folgen einer unrichtigen oder unvollständigen eidesstattlichen Versicherung sind mir bekannt.

Ich versichere an Eides statt, dass ich nach bestem Wissen die reine Wahrheit erklärt und nichts verschwiegen habe.

_____   _____

Ort/Datum   Unterschrift